



12-2002

Reproducibility and optimization in capillary electrophoresis

James P. Schaeper
University of Tennessee

Follow this and additional works at: https://trace.tennessee.edu/utk_graddiss

Recommended Citation

Schaeper, James P., "Reproducibility and optimization in capillary electrophoresis. " PhD diss., University of Tennessee, 2002.
https://trace.tennessee.edu/utk_graddiss/6302

This Dissertation is brought to you for free and open access by the Graduate School at TRACE: Tennessee Research and Creative Exchange. It has been accepted for inclusion in Doctoral Dissertations by an authorized administrator of TRACE: Tennessee Research and Creative Exchange. For more information, please contact trace@utk.edu.

To the Graduate Council:

I am submitting herewith a dissertation written by James P. Schaeper entitled "Reproducibility and optimization in capillary electrophoresis." I have examined the final electronic copy of this dissertation for form and content and recommend that it be accepted in partial fulfillment of the requirements for the degree of Doctor of Philosophy, with a major in Chemistry.

Michael Sepaniak, Major Professor

We have read this dissertation and recommend its acceptance:

Doug Gilman, Ben Xue, Cynthia Pereson

Accepted for the Council:


Carolyn R. Hodges

Vice Provost and Dean of the Graduate School

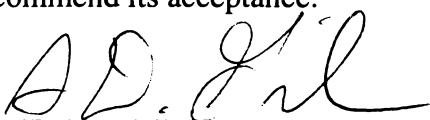
(Original signatures are on file with official student records.)

To the Graduate Council:

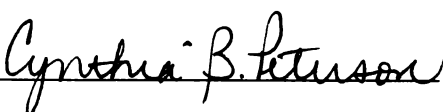
I am submitting a dissertation written by James Schaeper entitled "Reproducibility and Optimization in Capillary Electrophoresis." I have examined the paper copy of this dissertation for form and content and recommend that it be accepted in partial fulfillment of the requirements for the degree of Doctor of Philosophy, with a major in Chemistry.


Dr. Sepaniak, Major Professor


We have read this dissertation and recommend its acceptance:







Acceptance for the Council:


Vice Provost and Dean of
Graduate Studies

REPRODUCIBILITY AND OPTIMIZATION IN CAPILLARY ELECTROPHORESIS

A Dissertation
Presented for the
Doctor of Philosophy
Degree
The University of Tennessee, Knoxville

James Schaeper
December 2002

Thesis
2002b
, 832

Dedication

This work is dedicated to my family and to friends such as Ray Lietemeyer who have greatly impacted my life by their positive examples. It was their love and support that has enabled me to make it this far. I appreciate the many helpful discussions that I had with all of the Sepaniak group members. I was fortunate to have friends in the group such as Chris Tipple, Shannon Fox, Jeremy Headrick, Will Nirode, and Tim Gibson. It was also a pleasure to become friends with the newer Sepaniak group members. Finally, I would like to thank Dr. Sepaniak for his guidance and financial support over the years.

Acknowledgements

I wish to thank all of those who helped me complete a doctorate in analytical chemistry. I would like to thank Dr. Michael Sepaniak for his guidance and financial support over the years. I would also like to thank Dr. Doug Gilman, Dr. Ben Xue, and Dr. Cynthia Peterson for serving on my committee. Also, I am appreciative of all the discussions and helpful suggestions that I obtained from the members of the Sepaniak group. Finally, I thank my family for their love and encouragement that inspired me to complete this degree.

Abstract

It is well known that poor quantitative reproducibility substantially limits the practical implementation of capillary electrophoresis (CE) separations in chemical analysis. The principal sources of variance in observed peak areas are irreproducible flow rate which influences on-column detector response, and inconsistent injection volume or amount. In addition, current efforts in our laboratory to assess sources of quantitative variance for separations of dansylated amino acids using an automated CE system are presented and related when appropriate to the body of existing knowledge on this important topic. A comparison of different injection methods, the effect of random changes in electroosmotic flow (EOF), and choice of certain peak integration parameters in terms of peak area reproducibility are presented. An approach is presented to optimize conditions for capillary electrophoresis separations of multi-analyte enantiomeric-pairs (D- and L-Dansyl (Dns)-amino acids) that involves the rational use of combinations of cyclodextrins (CDs) as enantio-selective running buffer additives. Migration data is experimentally obtained for a range of concentrations for native CDs used individually and employed to determine inclusion constants for the Dns-amino acids of interest. Simplex methods are then employed for the first time to optimize conditions for the separation of amino acid enantiomers. The validity of this approach is demonstrated for separations of five Dns-amino acids enantiomers using γ - and β -CDs at various concentrations. Extending the dual-CD approach to other CDs and increasing the number of CDs beyond two should be possible. To this end, preliminary experiments are performed by using several available single-isomer, derivatized CDs (individually) to determine if they have potential for further studies. It was found that molecular mechanics modeling is useful in interpreting those cases where low inclusion constants likely contributed to the ineffectiveness of the CDs. Finally, it is important in CE to have solute identification capabilities for unknown mixtures and because of the variable electroosmotic flow, which causes irreproducible migration times. A counter flow arrangement for surface enhanced Raman Spectroscopy was developed for this purpose and colloidal silver is added externally since it can affect efficiency when inserted in the running buffer.

Table of Contents	Page
Chapter 1. Capillary Electrophoresis	1
1.0 Introduction and Capillary Electrophoresis Apparatus	1
1.1 Capillary Electrophoresis Separation Theory	3
1.1.2 Electroosmotic Flow	5
1.2 Analytical Considerations	11
1.2.1 Dispersion and Efficiency	11
1.2.2 Factors Affecting Efficiency	13
1.2.3 Resolution	16
1.2.4 Selection of the Running Buffer and Capillary Material	17
1.3 Background on Select Modes of Capillary Electrophoresis	17
1.3.1 Cyclodextrin Capillary Electrophoresis	18
1.3.2 Micellar Electrokinetic Chromatography	21
1.3.3 Cyclodextrin-Modified Micellar Electrokinetic Chromatography..	27
1.4 Injection in Capillary Electrophoresis	29
1.4.1 Hydrodynamic Injection	30
1.4.2 Electrokinetic Injection	30
1.5 Common Detection Techniques in Capillary Electrophoresis	32
1.5.1 Ultraviolet and Visible Absorption	33
1.5.2 Laser Induced Fluorescence	34
1.6 Reproducibility in Capillary Electrophoresis	36
1.6.1 Injection and Precision in Capillary Electrophoresis	36
1.6.2 Electroosmotic Flow Variation	37

1.6.3 Peak Integration and Precision	38
Chapter 2. Parameters Affecting Reproducibility in Capillary Electrophoresis	40
2.1 Introduction	40
2.2 Experimental	42
2.2.1 Materials	42
2.2.2 Apparatus and Methods	43
2.3 Results and Discussion	43
2.3.1 Pressure Injection Studies	43
2.3.2 Use of Multiple Sample Vials	47
2.3.3 Migration Time Reproducibility	48
2.3.4 Use of an Internal Standard	49
2.3.5 Electrokinetic Injection Studies	52
2.3.6 Effect of Slope Sensitivity on Reproducibility	55
2.3.7 Effect of Air Bubbles on Precision	59
2.4 Future Plans	64
2.5 Concluding Remarks	65
Chapter 3. Optimization Strategies and Modeling of Separations of Dansyl- Amino Acids by Cyclodextrin-Modified Capillary Electrophoresis	66
3.1 Introduction	66
3.2 Experimental	68
3.2.1 Materials	68

3.2.2 Apparatus and Methods	69
3.2.3 Molecular Modeling	70
3.2.4 Computational Methods	71
3.3 Results and Discussion	72
3.3.1 Mobility and K_c data	72
3.3.2 Use of the Simplex Method and CRF Values	78
3.3.3 Studies With Modified Single Isomer Cyclodextrins	82
3.3.4 Molecular Modeling of Various Cyclodextrins	87
3.4 Future Work	90
3.5 Concluding Remarks	92
Chapter 4. Raman Theory and Surface Enhanced Raman Spectroscopy with Capillary Electrophoresis	94
4.1 Raman Theory	94
4.2 Surface Enhanced Raman Spectroscopy	99
4.2.1 Background and Theory	99
4.2.2 SERS Substrates	104
4.3 Introduction to Surface Enhanced Raman Spectroscopy/Capillary Electrophoresis	107
4.4 Experimental	110
4.4.1 Materials	110
4.4.2 Silver Colloidal Solution Preparation	110
4.4.3 Capillary Preparation and Utilization	111
4.4.4 SERS/CE Apparatus	111

4.5 Results and Discussion	112
4.5.1 Effect of Sodium Chloride on SERS Intensity	114
4.5.2 Initial Optimization of Flow Rates	117
4.5.3 Alternative Approaches for SERS/CE	122
4.6 Concluding Remarks	124
References	125
Vita	136

List of Tables	Page
Table 2.1 A Comparison of High Pressure Injection Conditions to Low Pressure Injection Conditions	46
Table 2.2 Use of Dansyl-Asparagine as an Internal Standard for the Data in Table 2.1	51
Table 2.3 Electrokinetic Injection Study of High Voltage for a Short Time Versus Low Voltage for a Long Time	54
Table 2.4 Effect of the Zone of Bubbles on Precision	62
Table 3.1 Mobility and K_c Data for Amino Acids with Beta and Gamma CD	76
Table 3.2 Selected Data Points from the Simplex Method with mM CD Concentrations	80

List of Figures	Page
Figure 1.1 A Typical CE Instrument Arrangement	2
Figure 1.2 Electroosmotic Flow Development in Normal Polarity Mode	6
Figure 1.3 A Comparison of Flow Profiles	8
Figure 1.4 Differential Migration of the Solutes Superimposed on Electroosmotic Flow in CE for Normal Polarity Mode	10
Figure 1.5 Depiction of Alpha- and Beta-Cyclodextrin Molecules	19
Figure 1.6 Conception of an Anionic Micelle Associated with a Solute	23
Figure 1.7 Depiction of the Flow in MECC and Solute-Micelle Association	26
Figure 1.8 Depiction of the Process of a Neutral Molecule Partitioning in CD-MECC upon Application of Voltage	28
Figure 1.9 Illustration of Various Injection Modes in CE	31
Figure 2.1 Separation of Six Dansylated Amino Acids	45
Figure 2.2 Plot of RSD Versus Slope Sensitivity for Three Amino Acids	57
Figure 2.3 Electropherogram Depicting the Bubble Zone Within the Capillary as the Solute Passes the Detector	61
Figure 3.1 Separation of Five Dansylated Amino Acid Enantiomers	74
Figure 3.2 Plot of the Observed Mobility of Glutamic Acid Enantiomers Versus Molar Concentration of Beta-CD	75
Figure 3.3 Examination of the Simplex Predictions from Table 3.2	81
Figure 3.4 Depiction of Dns-Asp with the Dns Group Poised to Insert into the Cavity of Gamma-CD	84
Figure 3.5 Separations of Dansylated Amino Acids with Various CDs.....	85
Figure 3.6 Space Filled Model Depictions of the Open and Closed Cavity 16-me-Gamma-CD Conformations Used in Modeling Studies	89

Figure 4.1 Schematic of Raman Scattering in Which Incident Frequency Interacts with a Molecular System	96
Figure 4.2 Energy Level Diagram for Raman Scattering	98
Figure 4.3 Metal Nanospheres and the Production of Large Enhancements of Incident Fields	101
Figure 4.4 A Typical Arrangement for Raman Spectroscopy	103
Figure 4.5 Schematic of the Flow of Colloidal Silver Towards the Separation Capillary	113
Figure 4.6 Static SERS Spectra of the Solutes of Interest	115
Figure 4.7 The Effect of Sodium Chloride on Static SERS Intensity	116
Figure 4.8 Flow Profiles of the Separation Capillary with Various Syringe Pump Flow Rates	119
Figure 4.9 Comparison of the Intensity Change with Distance for Fluorescence and SERS	121

Chapter 1. Capillary Electrophoresis

1.0 Introduction and Capillary Electrophoresis Apparatus

Chromatography and electrophoresis are the two most common techniques utilized for the separation of mixtures into their individual components. In chromatography, the difference in free energy of distribution of solutes between two phases allows for a separation to occur. These two phases are the stationary phase (packed silica for example) and the mobile phase. In capillary electrophoresis (CE), separation occurs because of different migration rates of solutes in an electric field. CE can be used to separate cations and anions in a single analysis. The advantage of performing electrophoresis in capillaries was highlighted by the work of Jorgenson and Lukacs (1). Electrophoretic separations in capillaries offered the possibilities of automation, rapid analysis times, and on-line detection of the solutes. Heat generated inside the capillary was effectively dissipated through the walls of the capillary that allowed for high voltages to be used to achieve rapid, efficient separations.

A typical CE instrument configuration can be seen in Figure 1.1. The operation of a CE system involves application of a high voltage across a narrow bore capillary. The capillary is filled with buffer solution that conducts current through the inside of the capillary. The capillary ends are immersed into reservoirs filled with the running buffer. Phosphate and borate buffers are commonly employed in CE applications. Fused silica capillaries with an external polyimide protective coating are used in CE and typically have an inner diameter in the range of 25 to 100 μm . A small portion of this coating is removed to form a detection window. Capillaries are typically 25-60 cm long and are held in a housing device such as a cartridge to facilitate the insertion of the capillary into the

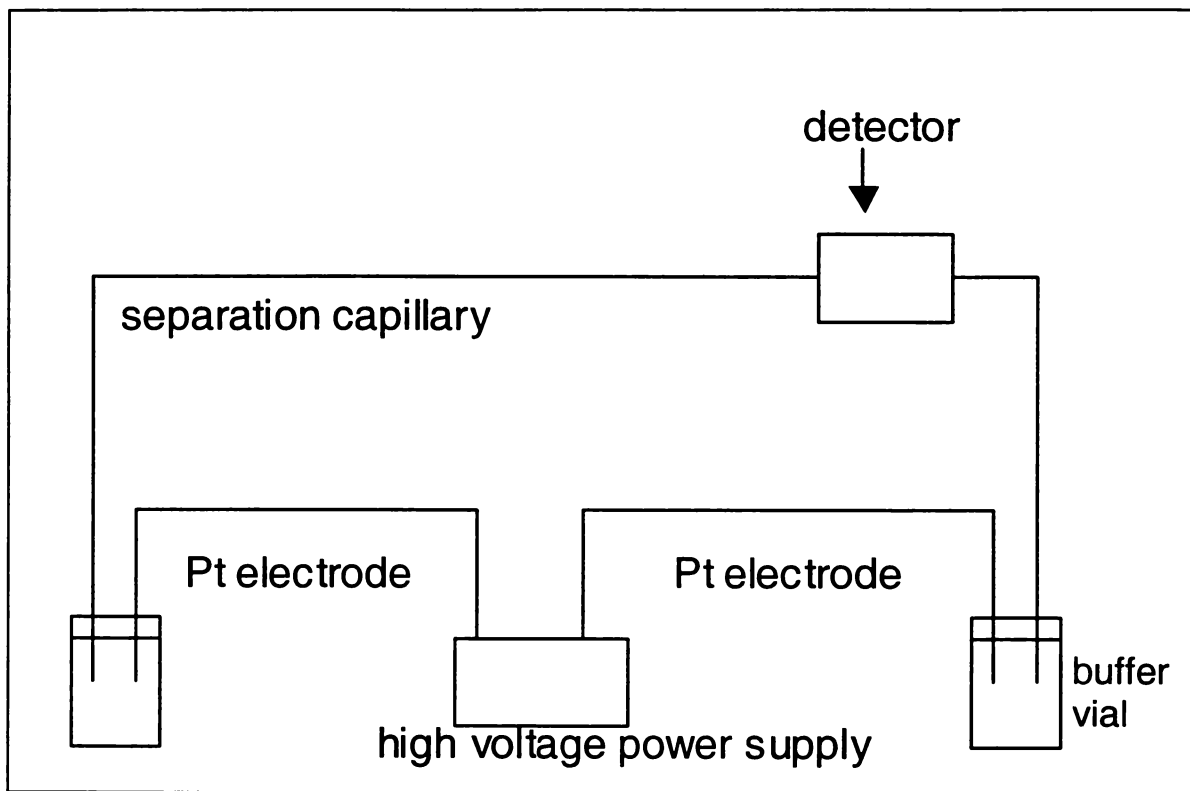


Figure 1.1 A typical CE instrument arrangement.

commercial CE instrument. Capillaries are sometimes chemically modified to alter the charge on the capillary wall or to reduce sample adsorption. Electrodes that are made of an inert material such as platinum are inserted into the running buffer reservoirs to complete the electrical circuit. A small volume of sample is injected into the capillary as a short plug and application of a voltage causes movement of the solute ions in zones. A high voltage power supply is required to apply the electric field during the separation. Generally, a voltage between 15-25 kV is applied in a CE separation which results in currents in the range of 10-100 μ A. The capillary passes through a detection zone at the opposite end of the capillary. The plot of detector response with time is generated which is called an electropherogram. CE is frequently used for the separation of biological molecules such as proteins, peptides, and nucleic acids. In our studies, CE was utilized for the separation of biological compounds such as amino acids.

1.1 Capillary Electrophoresis Separation Theory

Separations are obtained because of the differences in velocity of ions in an electric field (2). The movement of the ions is determined by the mobility of an ion (μ). This mobility is defined as the average velocity that an ion moves under the influence of an applied electric field. The velocity of an ion is given by equation 1.1.

$$(1.1) \quad v = \mu_e E$$

The ion velocity is v and μ_e is the electrophoretic mobility. For a certain ion and medium the mobility is a constant which is a characteristic of that ion. The electric field (E)

depends on the applied voltage and capillary length (volts/cm). The mobility depends on the electric force that the solute encounters, balanced by its frictional drag through that medium (2).

$$\mu_e \propto \frac{\text{Electric force (F}_E\text{)}}{\text{Frictional force (F}_F\text{)}}$$

The electric force (F_E) can be defined as

$$(1.2) \quad F_E = qE$$

and the frictional force (F_F) for a spherical ion is

$$(1.3) \quad F_F = 6\pi\eta rv$$

where charge of the ion is q, the solution viscosity is η , r is the ion radius, and v is the ion velocity. During electrophoresis an equilibrium condition occurs defined by the balance of these forces. At this time the forces are equal but opposite and

$$(1.4) \quad qE = 6\pi\eta rv$$

If equation 1.4 is solved for velocity and substitution of equation 1.1 is made, an equation for mobility can be obtained.

$$(1.5) \quad \mu_e = q/6\pi\eta r$$

From this equation it can be seen that mobility is directly proportional to the charge on the ion. The mobility is inversely proportional to the viscosity of the solvent and the radius of the ion. It is apparent that small, highly charged species have large mobilities.

1.1.2 Electroosmotic Flow

An important component of CE is the electroosmotic flow (EOF) occurring in the capillary. The EOF is the bulk flow of liquid in the capillary as a result of the surface charge on the interior capillary wall (2). The capillary is generally fused silica that contains numerous silanol groups (SiOH) that can exist in the anionic form (SiO⁻). Close to the interior of the capillary wall there are oriented dipoles of water molecules and the larger hydronium cations (3). Counterions that aggregate near the surface to maintain charge balance form an electric double layer defined by a zeta potential (2). Once the voltage is applied across the capillary the cations forming the double layer are attracted towards the cathode. The cations are solvated so their movement drags the bulk solution in the capillary toward the cathode, which results in electroosmotic flow. The development of electroosmotic flow is depicted in Figure 1.2 (2). An equation for EOF can be given in terms of velocity or mobility.

$$(1.6) \quad v_{\text{EOF}} = (\epsilon\zeta/\eta)E \quad \text{or} \quad \mu_{\text{EOF}} = (\epsilon\zeta/\eta)$$

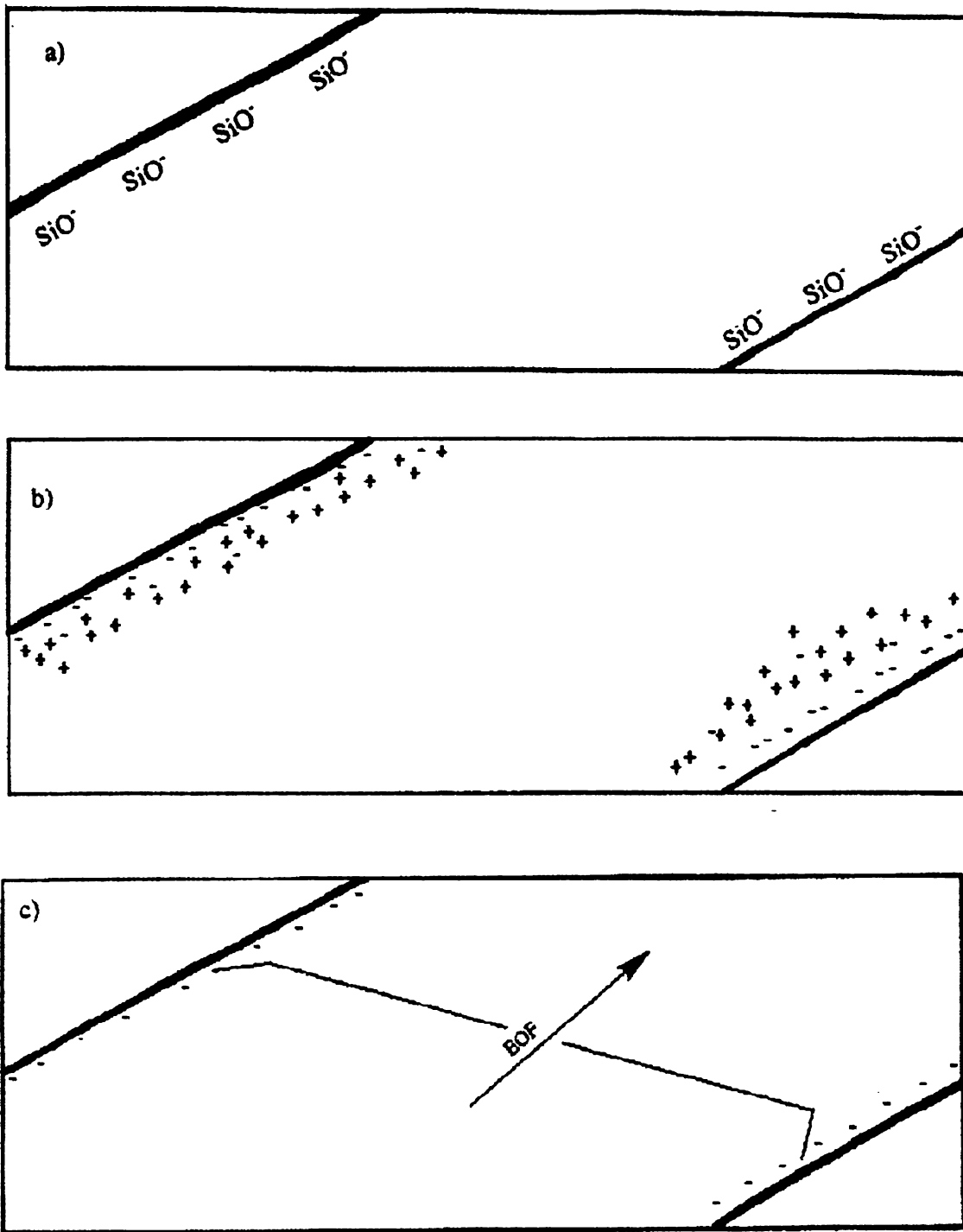


Figure 1.2 Electroosmotic flow development for normal polarity mode in which flow is from anode (+) to cathode (-). (a) The negatively charged surface SiO^- . (b) Aggregation of hydrated cations. (c) Application of separation voltage and subsequent electroosmotic flow.

The terms are as follows: v_{EOF} = velocity, μ_{EOF} = EOF mobility, ζ = zeta potential, and ϵ = dielectric constant. The zeta potential is dependent on the surface charge on the interior of the capillary wall. The surface charge is pH dependent and hence the EOF varies with pH. At high pH the silanol groups are mainly deprotonated whereas at low pH the silanol groups are protonated. Thus, at high pH the EOF is much greater than at low pH (4). The zeta potential is also dependent on the ionic strength of the running buffer (2). At higher ionic strength the effective charge at the wall is decreased and the double layer is compressed. This results in decreased zeta potential and reduced EOF.

A unique quality of the EOF is the flat flow profile that is produced (2). The driving force of the flow is uniformly distributed at the walls so there is no pressure drop in the capillary. This flat flow profile allows for increased separation efficiency since it does not directly add to the dispersion of solute zones. This is not the case with liquid chromatography in which an external pump generates parabolic flow due to the shear force at the wall. This is illustrated in Figure 1.3 (2). The flat flow profile in CE results in tighter solute bands and this leads to sharper peaks (less band spreading).

Another beneficial quality of the EOF is that it produces movement of all species in the same direction (2). When the normal CE conditions are used the flow is from anode to cathode. Anions are dragged to the cathode since the magnitude of the EOF is usually greater than their electrophoretic mobilities. Hence, cations, neutral molecules, and anions can be electrophoresed in one run since the direction of migration is the same.

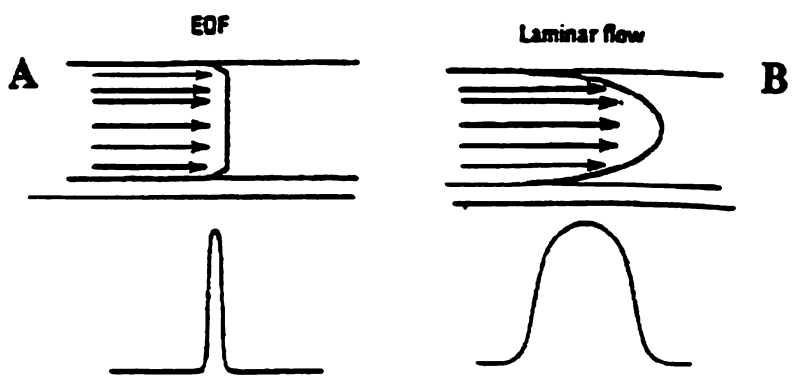


Figure 1.3 Flow profiles generated by electroosmotic flow (A) and pressure difference (B) with the resulting solute zone.

The resulting process is shown in Figure 1.4 (2). The cations move the fastest due to their attraction to the cathode and the EOF is in the same direction. Neutral molecules migrate at the velocity of the EOF and are not separated from one another. The neutral molecules are not separated because they lack a charge, hence their mobilities are all the same. Anions migrate the slowest since they are attracted to the anode.

The EOF can be controlled by various methods to optimize the separation. As mentioned before the EOF is dependent on the pH and ionic strength of the running buffer. Decreasing the pH or increasing the ionic strength of the buffer will reduce the EOF. The mobility of the ions are affected by pH. Increasing the pH of the running buffer will increase the EOF but the mobility will decrease if the ion becomes more negative due to the loss of an ionizable hydrogen. Another way of altering the EOF is by changing the applied electric field (2). Finally, the capillary wall can be modified by use of buffer additives or covalently attached coatings. It is important to control the EOF so as to obtain a good separation. At low to moderate pH the solute has a longer migration time due to a lower EOF and adsorption of cationic solutes to the negatively charged walls can occur.

Much care should be taken in deciding how to control the EOF due to the possible ramifications. The applied electric field can be changed but efficiency and resolution may decrease if the electric field is lowered (2). Also, the presence of joule heating could cause problems. Joule heat is the heat produced by the passage of electrical current. Joule heat is a problem because it can cause temperature gradients, variation of the local viscosity, and zone broadening. Control of the EOF by changing the pH of the buffer can affect the charge of the solute. Finally, increasing the ionic strength of the buffer can

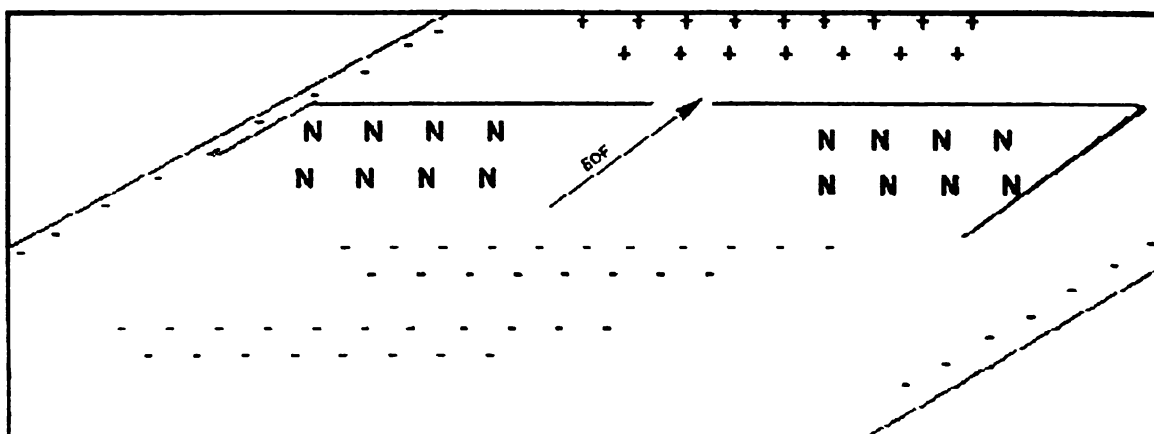


Figure 1.4 Differential migration of the analytes superimposed on electroosmotic flow in CE for normal polarity mode.

lead to joule heat generation and low ionic strength buffers may cause increased sample adsorption.

1.2 Analytical Considerations

1.2.1 Dispersion and Efficiency

The length of the solute zone is critical in determining whether a separation can be achieved. The lengths of the zones depend on dispersive processes that act on it (2). Dispersion needs to be controlled since it makes the zone length longer and it increases the mobility difference between solutes needed to obtain a separation. Dispersion arises from differences in solute velocity within that zone. For a gaussian peak, $w_b = 4\sigma$ where w_b is the baseline peak width and σ is the standard deviation of the peak in time (sec.), length (m), or volume (m^3). Next, the efficiency can be expressed by the number of theoretical plates (N).

$$(1.7) N = (l/\sigma)^2$$

The effective capillary length (distance from injection end to detector window) is l and the other variables were defined previously. An equation for the HETP (height equivalent to a theoretical plate) (H) is:

$$(1.8) H = l/N$$

Under optimum conditions the only contribution to solute zone broadening in CE is longitudinal diffusion. Resistance to mass transfer across the capillary diameter (radial diffusion) is not problematic in CE, as compared to HPLC, due to the plug flow profile in CE. Under conditions of limiting longitudinal diffusion, efficiency expressed by the variance (σ^2) is given by:

$$(1.9) \sigma^2 = 2Dt = 2DIL/\mu_e V$$

where D is the diffusion coefficient of the solute, L is the total capillary length, and V is the applied voltage. An important expression for plate number in CE is:

$$(1.10) N = \mu_e VI/2DL = \mu_e EI/2D$$

The reason for the application of high electric fields is apparent from the previous equation. The solute spends less time in the capillary and there is less time for longitudinal diffusion to occur. The number of theoretical plates can be calculated from an electropherogram with gaussian shaped peaks by:

$$(1.11) N = 5.54 (t/w_{1/2})^2$$

where t is the migration time and $w_{1/2}$ is the peak width at half height.

1.2.2 Factors Affecting Efficiency

There are other factors that may under certain conditions affect efficiency in addition to longitudinal diffusion (2). Some examples are solute wall adsorption, injection plug length, and temperature gradients as a result of joule heating. The total variance of the system σ_T^2 is determined by the sum of the contributing variances.

$$(1.12) \sigma_T^2 = \sigma_{DIF}^2 + \sigma_{INJ}^2 + \sigma_{TEMP}^2 + \sigma_{ADSORPTION}^2 + \sigma_{DET}^2 + \sigma_{ELECTRODISPERSION}^2$$

The subscripts refer to diffusion, injection, temperature gradients, adsorption, detection, and electrodispersion. In certain cases, one of these terms or more can dominate the equation and each of these terms is explained in more detail below.

Joule heating results in temperature gradients, local viscosity changes, and zone broadening (2). The viscosity differences lead to changes in mobility. The temperature difference across the diameter of a capillary depends on the inner radius, thickness of the wall, the thickness of the polyimide coating, and the heat transfer coefficient to the surroundings (2). In CE, the small volumes used minimize the amount of heat generated. Also, the high inner surface area to volume ratio aids in dissipating the heat through the capillary wall. The large outer diameter is beneficial because the insulating properties of the polyimide are less and heat transfer to the surroundings is enhanced. Some possible ways to minimize joule heating are to decrease the electric field, decrease the ionic strength of the running buffer, or to reduce the inner diameter of the capillary. Active temperature control is critical for heat dissipation as well as for sustaining constant

capillary temperature. A fan or a cooling system is frequently employed to remove the generated heat.

The sample plug length should be small because if the length is longer than the dispersion caused by diffusion, resolution and efficiency will be reduced. In practice the sample plug length should be less than the standard deviation due to diffusion $(2Dt)^{1/2}$ (2). A general rule for injection length is that it should be less than 2% of the total length of the capillary. This corresponds to 7 millimeters or 14 nanoliters for a 50 micron internal diameter capillary of a length of 70 centimeters.

Interactions between the wall and solute are not desirable in CE. Peak tailing and complete adsorption of the solute can occur. Possible causes of adsorption are ionic interactions between the solute and the negatively charged SiO^- groups as well as hydrophobic interactions. There are three commonly employed strategies to minimize these interactions. One method is to increase the concentration of the running buffer. This method minimizes solute wall interactions by reducing the effective surface charge. Another method is to work at extremes of pH. Finally, coating the capillary wall is usually effective in minimizing these interactions. For example, small amines such as putrescine have been utilized to prevent wall adsorption by covering the adsorption sites (5).

Electrodispersion refers to peak shape distortions as a result of differences in conductivity and field in each zone. When the solute has a higher mobility than the running buffer, the front edge of the solute zone experiences a higher field upon entering the buffer zone (2). This causes the diffusing solute to accelerate away from the solute zone and zone fronting occurs. Conversely, when the solute has a lower mobility than

the running buffer, the solute experiences a lower field in the opposite direction of migration so tailing occurs. To minimize these occurrences the buffer and solute mobilities should be matched or sample concentration should be lower and solvents buffered by addition of the running buffer to the sample.

A reduction in the inner diameter of the capillary can be beneficial if the σ^2_{TEMP} term dominates in equation 1.12. The temperature gradient caused by the joule heat generated can be minimized by reducing the inner capillary diameter (6).

As the buffer concentration is increased the electrophoretic and electroosmotic mobilities are decreased. This can be explained in that the effective charge at the wall is decreased so the zeta potential is less. It has been shown that as the concentration of the buffer increases the solute migration time increases and the separation factor improves (7). The larger the difference in net mobility of two neighboring solutes the greater is their separation factor.

Buffer concentration and applied voltage exert a significant influence on column efficiency and resolution. From equation 1.10, the number of theoretical plates is increased with increasing voltage. So, the greatest efficiency is produced at the highest applied voltage. The CE instrument cannot sufficiently dissipate the heat generated at very high voltages. The production of temperature gradients becomes a problem at these conditions. Consequently, N approaches a maximum as the applied voltage is increased then drops with further increase of the voltage (7). The applied voltage at which N plateaus depends on the ionic strength, column length, and radius.

At constant buffer concentration resolution finally increases with high voltage but then falls at higher voltages due to joule heat and subsequent zone broadening (7). One

should think about heat production, analysis time, and separation parameters before deciding which parameter should be optimized (7). For example, if the applied voltage is doubled there is a four-fold increase in generated heat but doubling the buffer concentration causes a two-fold increase in generated heat. Therefore, resolution may be better improved by increasing buffer concentration at a moderate applied voltage.

1.2.3 Resolution

Resolution of the components in a mixture is the main goal of chromatography and electrophoresis. Resolution is given by:

$$(1.13) R = (t_2 - t_1)/4\sigma$$

The migration time is t and σ is the standard deviation of the Gaussian band profile.

Frequently, small differences in mobility allow for sufficient resolution. An equation that is paramount for resolution in CE is:

$$(1.14) R = \frac{1}{4} N^{1/2} (\Delta\mu / |\bar{\mu} - \mu_{EOF}|)$$

where $\Delta\mu = \mu_2 - \mu_1$ and $\bar{\mu} = (\mu_2 + \mu_1)/2$

In this equation, N is the number of theoretical plates, $\Delta\mu$ is the mobility difference between the two solutes, and $\bar{\mu}$ is the average mobility of the two solutes.

1.2.4 Selection of the Running Buffer and Capillary Material

The selection of the running buffer is of critical importance in CE (2). The EOF is sensitive to pH so a buffer that maintains constant pH is necessary. Some buffers have more than one useful pK_a (phosphate, citrate) and can be used in more than one pH range. Also, large minimally charged ions to reduce current generation and joule heat production are preferred. A final important quality of a good running buffer is that it should have a close mobility match with the solutes. This is necessary so that peak distortions such as fronting and tailing are minimized.

There are a number of desirable qualities needed when choosing the capillary material. It is preferred that the material be supple and inexpensive. Also, the material should be chemically and electrically inert. Fused silica fulfills most of these requirements so it is utilized most frequently. Once a capillary is chosen, the way in which it is conditioned is important for obtaining good reproducibility. The capillary surface must be reproducible in order to acquire consistent migration times for the solutes. Usually conditioning of the capillary is done with base to remove adsorbates and to produce a fresh surface of deprotonated silanol groups.

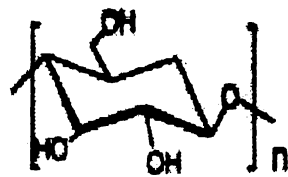
1.3 Background on Select Modes of Capillary Electrophoresis

Other separation modes were developed to help resolve neutral solutes that are not separable by CE. In these separation modes, solutes can differentially partition between the aqueous component of the buffer and an additive that creates a pseudostationary phase. This pseudostationary phase has its own mobility and when a solute is partitioned within the additive its mobility changes as compared to its free mobility. Differences in

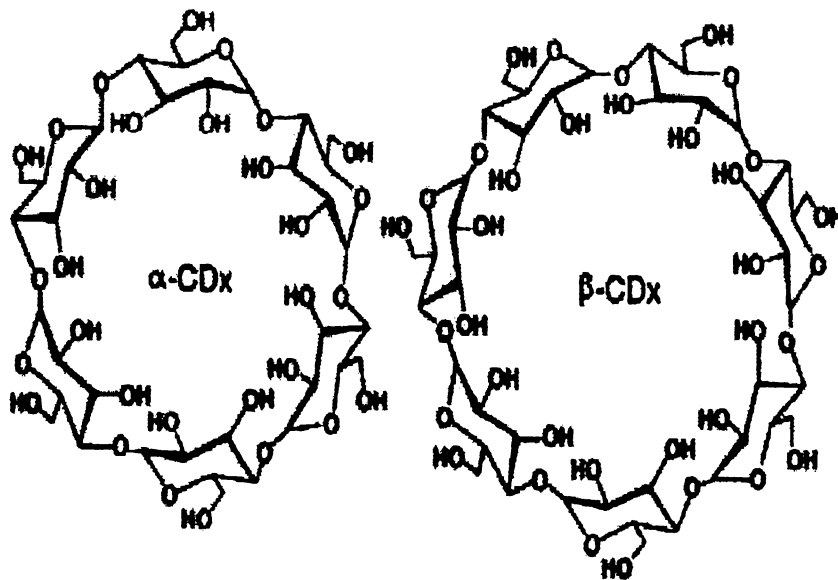
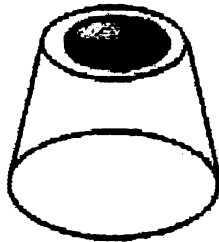
the association constants of the solutes with the additive are important for a separation. These buffer additives not only allow for the separation of neutrals but selectivity towards anionic and cationic species may be affected as well. The most common additives are cyclodextrins (CDs) and surfactants. The use of surfactants forms the basis of micellar electrokinetic chromatography (MECC). The next sections are devoted to the use of such buffer additives as CDs and surfactants.

1.3.1 Cyclodextrin Capillary Electrophoresis

Cyclodextrins are macrocyclic oligosaccharides formed from enzymatic digestion of starch by bacteria. These compounds are formed with 6, 7, or 8 glucopyranose units (attached by α -1,4 linkages) and are called α -, β -, γ -CD respectively. A depiction of these native CDs can be seen in Figure 1.5. The physical properties of the three native CDs are quite different in terms of cavity width, solubility, and molecular mass. The native CDs have different cavity dimensions because of the number of glucopyranose units in their structure. The hydrophobic interior of the cavity allows for the formation of inclusion complexes with solutes. If the solute is too large, a complex won't be formed but if the solute is too small the resolution may be poor due to the weak formation of a solute-CD complex. In the inclusion process the solutes can fit completely or their hydrophobic portion fits into the CD cavity entering through one of the two openings (8). The cavity of β -CD can host a wide number of solutes, particularly of pharmaceutical interest, but its solubility is the lowest of the native CDs. Forces that are important in complex formation are hydrogen bonding, van der Waals, and hydrophobic interactions.



$n = 6, \alpha\text{-CDx}$
 $n = 7, \beta\text{-CDx}$
 $n = 8, \gamma\text{-CDx}$



Cyclodextrin

Figure 1.5 Depiction of alpha- and beta-cyclodextrin molecules.

The CD complex can be stereoselective due to the optically active carbohydrate structure. For this reason, many applications involving CDs are in the field of chiral recognition. The CDs form a heterogeneous phase within the aqueous solution. For the resolution of enantiomers, the effective mobilities of the solutes are selectively modified by the addition of CDs. The native CDs are useful for the separation of charged solutes because when a solute is complexed with the CD, the mobility can be sufficiently modified to cause a separation. For example, solutes with normally identical mobilities such as enantiomers can be separated based on differences in their inclusion constants. One of the benefits of CDs as a buffer additive in CE is the lowering of capillary wall adsorption (8). On the other hand, the efficiency is compromised because partitioning (mass transfer) is involved when CDs are inserted into the running buffer.

The enantioresolution is influenced by parameters such as the type and concentration of CD, applied voltage, pH of the running buffer, and the addition of organic modifiers (8-10). The type of CD is important because the formation of the inclusion complex depends on the solute being able to fit into the cavity of the CD. Thus, the appropriate CD should be selected based on the size of the solutes of interest. In most cases, only one type of CD is added to the running buffer in a separation. However, in some cases multiple CDs have been added into the running buffer to alter the selectivity in the separation. The concentration of CD present in the running buffer is fundamental in order to obtain a successful separation of the solutes. If the CD concentration is too low there may not be enough complexation in order for resolution of the enantiomers. On the other hand, if the concentration is too high the enantiomers can be fully complexed with the CD and, again, no separation will occur. The buffer pH must be

chosen wisely since it affects the EOF and the charge of the solutes. Organic modifiers such as methanol that are added to the running buffer can affect the inclusion constants of the CD-solute complexes, the EOF, and the solubility of the CD and/or the solute. These modifiers can improve resolution of the enantiomers in some cases.

The hydroxyl groups on the rim of CDs can be altered by chemical reactions in order to obtain CD derivatives with different degrees of substitution. Commonly used neutral CD derivatives are methylated, hydroxypropylated, and hydroxyethylated. Some charged CDs that are commonly used are methylamino, carboxymethyl, and sulfated derivatives. The impetus for synthesizing these modified CDs is to alter the properties of the native CDs to improve selectivity in the separation (10). These modified CDs can offer possible increased solubility and potential for the separation of neutral solutes. Charged CDs can be helpful in method optimization in capillary electrophoresis. The modified CD moves with its own electrophoretic mobility, which plays an important role in the separation. To illustrate this, the movement of a charged CD in the opposite direction to that of the solute causes an increase in the mobility difference between the free and complexed solute. A negatively charged CD will cause longer migration times for neutral solutes because the anionic CD is attracted to the anode and hence the neutral solute will move slower when complexed with the CD.

1.3.2 Micellar Electrokinetic Chromatography

A technique utilized commonly for the separation of neutral compounds is called micellar electrokinetic chromatography (MECC). In this technique, a pseudostationary phase is created by the addition of surfactants to the running buffer. Surfactants are

molecules that consist of long hydrophobic tails and polar or charged head groups. At concentrations higher than the critical micelle concentration (CMC) the surfactant molecules form aggregates called micelles. Figure 1.6 provides a cartoon depiction of an anionic micelle associated with a solute in MECC. This process of micelle formation occurs in order to reduce the free energy of the system (8). The aggregate generates a hydrophobic core as a result of the molecules orienting their hydrophobic tails towards each other. The shape and stability of the micelles are determined by van der Waals attraction of the chains and electrostatic repulsion of the polar head groups. At or above the CMC, the properties of the micellar solution such as conductivity, surface tension, and solubilizing power are changed from their previous pure surfactant values (8-9). Equilibrium is established with the surrounding environment upon micelle formation. Surfactant molecules and solutes are free to exchange between the micelle and the external media.

The surfactant that is most commonly used in MECC is sodium dodecyl sulfate (SDS). SDS is highly water-soluble and possesses a high degree of lipid solubilizing power. SDS has a CMC of 8 mM and it is fairly inexpensive. It is anionic and attempts to migrate towards the anode, which reduces the micellar velocity compared to the bulk EOF. At typical pH ranges, EOF is larger than the micellar electrophoretic velocity, which results in a net micellar flow toward the cathode. A solute can partition in and out of the micelle, and, hence, its migration velocity is affected as well. The solute velocity is reduced when it is partitioned into the micelle because the micelle is attracted to the anode. Neutral solutes are swept along with the EOF if they are present in the bulk

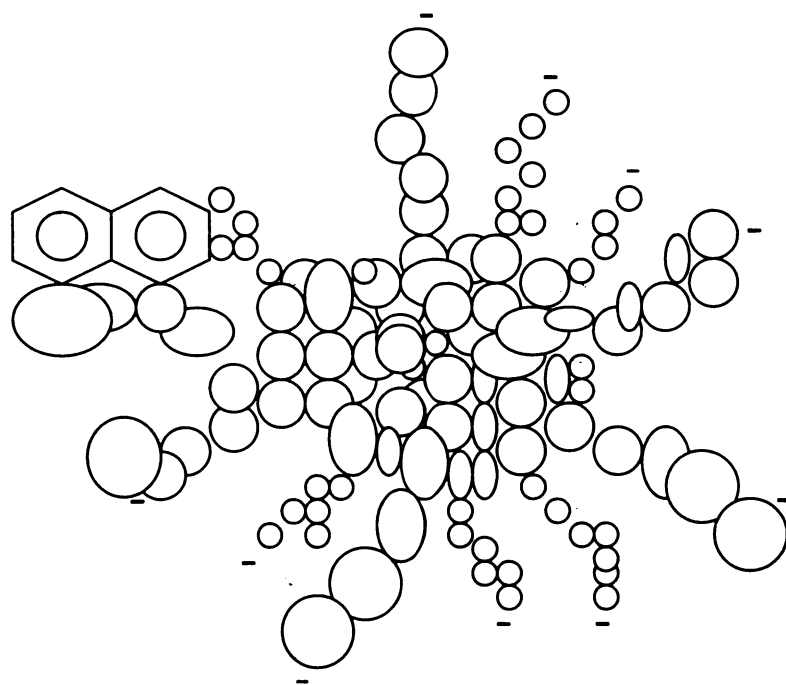


Figure 1.6 Conception of an anionic micelle associated with a solute, naphthalene. The - indicates the anionic head group.

phase. MECC is capable of separating anionic, neutral, and cationic species in a single run. It is difficult to predict the elution order in MECC because hydrophobic solute-micelle and electrostatic interactions have to be considered as well as the solute's electrophoretic properties.

Band broadening is more complex for MECC than for CE due to the presence of the pseudostationary phase (8-9). Important factors in MECC that contribute to band broadening are the rate of the solute moving into and out of the micelle, thermal gradients, and resistance to mass transfer. It has also been found that changes in the partition coefficient of the solute can occur due to joule heating. The constant exchange of monomer (surfactant) between micelle and bulk solution can cause the size of a particular micelle to vary with time. It is advisable to work at surfactant concentrations at least three times greater than the CMC in order to decrease dispersion due to micellar polydispersity. Micelle polydispersity has a significant bearing on the choice of a particular surfactant as a pseudostationary phase in MECC. Systems that contain micelles with a wide range of sizes and shapes can have a range of migration velocities, which leads to broad solute bands.

The proper selection of the pH is determined by the pKs of the solutes and the desired selectivity. The capacity factor (k') decreases for bases with increasing pH because the positive charge is reduced. Bases have longer retention times below the pK_a due to electrostatic interactions with the micelles. Acidic compounds will repel the micelles if the pH is adjusted above the pK_a . Plots of migration time versus pH are beneficial for obtaining the optimal separation conditions.

The flow in MECC along with solute-micelle association is depicted in Figure 1.7 (8-9). The elution range of MECC is defined by t_0 and t_{MC} terms. The t_0 term can be determined by measuring the time it takes for a neutral solute that has no affinity for the micelle to reach the detector. The micellar migration time (t_{MC}) is obtained by the use of a water insoluble dye that binds to micelles. Decreasing the EOF with a treated capillary can increase the elution range in MECC. The equation for resolution in MECC is:

$$(1.15) \quad R = N^{1/2} / 4 \cdot (\alpha - 1) / \alpha \cdot k'_2 / (1 + k'_2) \cdot (1 - t_0 / t_{mc}) / (1 + (t_0 / t_{mc}) k'_1)$$

Here, k'_1 and k'_2 are the capacity factors of the two solutes, α is the selectivity factor defined as k'_2 / k'_1 , and t_{mc} is the effective migration time of a micelle. If the desired effect is to speed up the separation then increasing the concentration of a non-ionic surfactant can decrease the net micellar charge. Brij 35 is a non-ionic surfactant that is used to decrease the micellar migration time (t_{MC}). Finally, organic solvents are used to alter the elution range in MECC. Solutes that are very hydrophobic interact strongly with the micelles and therefore elute near t_{MC} . The addition of an organic solvent can lower k' and change the partition coefficients of these solutes. Some commonly used organic solvents are methanol, acetonitrile, and tetrahydrofuran. The percent organic modifier must be chosen wisely because it can alter the CMC, aggregation number, and rate of exchange of surfactant between the micelle and bulk solution.

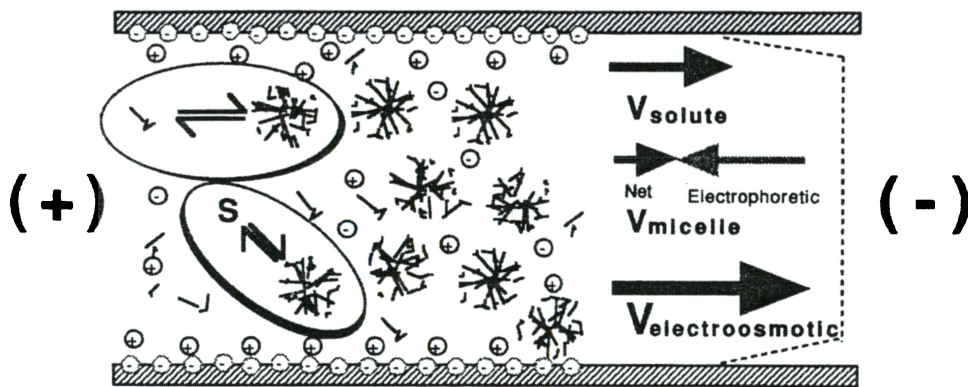


Figure 1.7 Depiction of flow in MECC with arrows for EOF ($V_{\text{electroosmotic}}$), micellar velocity, and solute velocity. Also, solute micelle association is shown to demonstrate that even solutes that totally associate with the micelle are eventually eluted.

1.3.3 Cyclodextrin-Modified Micellar Electrokinetic Chromatography

Cyclodextrins can be mixed with micelles in a separation with capillary electrophoresis (8-11). Micelles and CDs will interact with each other minimally in aqueous solution. Native CDs have a hydrophilic outer surface and therefore have little driving force for micellar interaction. An advantage of this approach is that enantiomeric separations are performed at much lower cost as compared to gas chromatography (GC) or high performance liquid chromatography (HPLC). Another benefit is that for method development it is much easier to change separation conditions in cyclodextrin-modified micellar electrokinetic chromatography (CD-MECC). In CD-MECC, all one needs to do is to change the solution conditions for method development, but GC and HPLC require the changing of columns. Sodium dodecyl sulfate (SDS) is the most commonly used surfactant for the formation of micelles in CD-MECC. The neutral CD is carried by the EOF towards the negative electrode (cathode), and the anionic SDS micelles electrophorese with their own mobility towards the positive electrode (anode). A depiction of the process in CD-MECC is seen in Figure 1.8. Hydrophobic solutes that bind with the micelle can form inclusion complexes with the CDs. Thus, the separation mechanism is based on the differences in a solute's partition coefficient between the CD and the micelle (8-11). The mobility of the solutes will be modified according to their different partition between the micelle and CD. An increase in the neutral CD concentration will decrease the migration times of the solute due to the formation of an inclusion complex that migrates towards the cathode. Improvements in selectivity can be obtained if the proper CD is employed for obtaining a good molecular fit with the solute

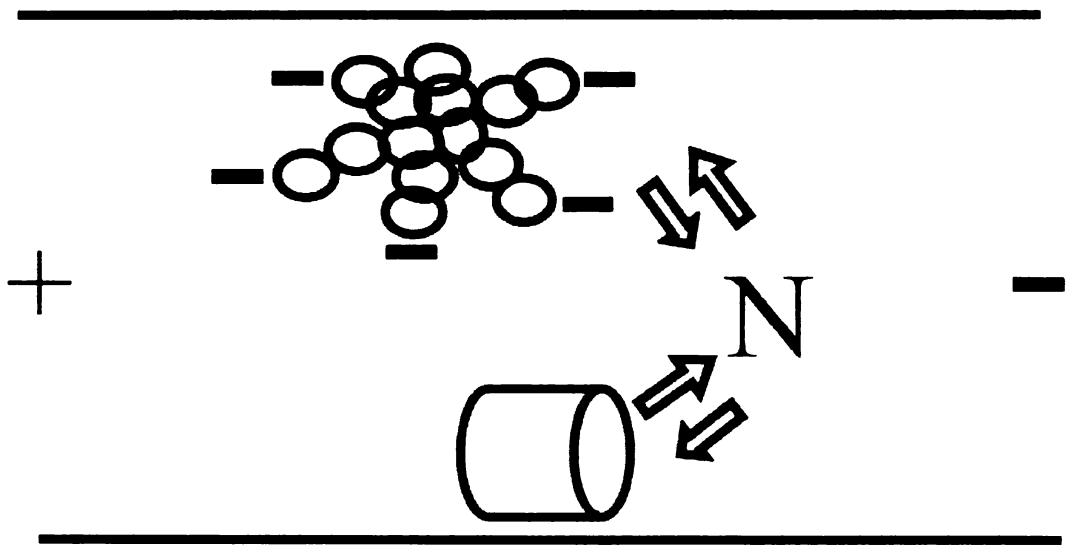


Figure 1.8 Depiction of the process of a neutral molecule partitioning in CD-MECC upon application of voltage.

(10). CD-MECC can be used for the separation of drugs, amino acids, and hydrophobic compounds such as polyaromatic hydrocarbons. Important parameters in CD-MECC are the type and concentration of CD and surfactant, pH, and the presence of organic modifiers.

1.4 Injection in Capillary Electrophoresis

The type of sample introduction chosen in CE has important implications for quantitative methodology (9). Peak area repeatability in CE is partly a function of the precision of the injection technique. The two types of injection encountered in CE are hydrodynamic injection and electrokinetic injection. Hydrodynamic injection is the common method of injection in CE. Hydrodynamic injection involves the introduction of a small plug of sample into the capillary by applying a pressure difference across the capillary while the inlet resides in the sample. In general, hydrodynamic injection is the most precise sampling technique because it is based strictly on volume loading of the sample (9). Vacuum injection offers the greatest reproducibility because it is easier to maintain the physical parameters involved with this approach. Electrokinetic injection is influenced by many parameters such as sample type, solution conductivity, and the chemistry of the capillary surface. Electrokinetic injection involves electrophoretically introducing a small volume into the capillary by applying a voltage. The amount of solute introduced in the capillary is a function of the EOF and the electrophoretic mobility of the solute.

1.4.1 Hydrodynamic Injection

There are different mechanisms for hydrodynamic injection as seen in Figure 1.9. The first method uses the application of pressure at the injection end of the capillary. The second method called gravimetric injection, involves siphoning by placing the injection end at a higher elevation relative to the outlet end. At concentrations within the sensitivity limits of the detector hydrodynamic injection is the preferred approach for free solution and MECC applications. In utilizing hydrodynamic injection the quantity of sample injected is almost independent of the sample matrix. The volume of sample injected depends on many factors. Some of these factors are the capillary dimensions, the viscosity of the buffer, the applied pressure, and time.

1.4.2 Electrokinetic Injection

The other type of injection technique in CE is electrokinetic injection as seen at the bottom of Figure 1.9. In this approach, the capillary and platinum electrode are inserted in the sample vial and high voltage is applied for a certain time interval between the capillary inlet and outlet. The amount of sample introduced is a function of the electric field strength, injection time, mobility of the solute, electroosmotic mobility, and conductivity of the sample. Therefore, parameters that affect the EOF will alter the amount of sample introduced into the capillary. The linearity of electrokinetic injection is affected by sample conductivity (9). To illustrate this, changes in the conductivity of the sample will affect the electroosmotic mobility and can lead to a different sample volume being introduced for different electrokinetic injections. It should be noted that electrokinetic injection is biased towards highly mobile solutes because such solutes are

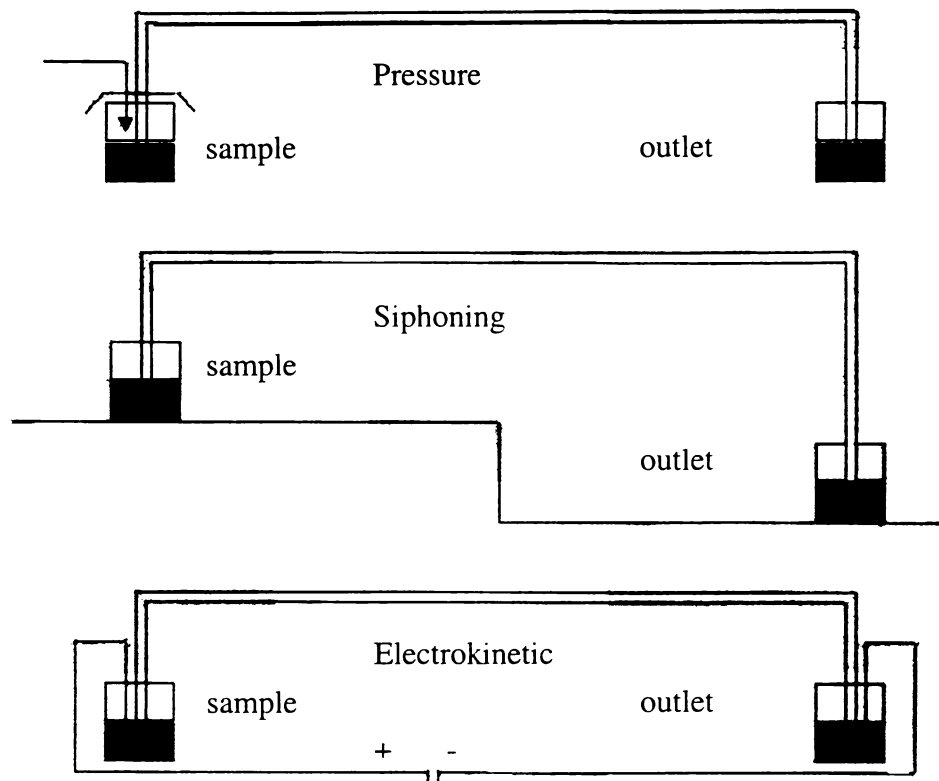


Figure 1.9 Illustration of various injection modes in CE such as pressure injection (top), siphoning (middle), and electrokinetic (bottom).

preferentially introduced into the capillary. This can be a problem if the sample contains low mobility solutes that are near the limit of detection. Cations will be introduced to the greatest extent into the capillary with the use of electrokinetic injection because they are attracted to the cathode more than neutrals or anions (greater electrophoretic mobility). Electrokinetic injection has utility with the use of gel filled capillaries and for sample concentration due to electrophoretic stacking (9). At the expense of sample concentration from stacking, one can reduce the variation in sample loading by matching the conductivity of the sample and running buffer.

Electrophoretic stacking has important consequences when sample concentrations are below the concentration limit of detection. Samples can be concentrated following injection if the conductivity of the sample solution is lower than that of the running buffer solution. In this case, the electric field in the sample medium is much greater than that in the capillary. The solute ions migrate quickly until they come in contact with the running buffer zone of higher conductivity. The sample ions stack until the solute zone conductivity approaches that of the running buffer. This causes the sample zone to be concentrated into a very narrow band, which provides sharp solute peaks.

1.5 Common Detection Techniques in Capillary Electrophoresis

The development of detectors has been a challenge due to the use of small diameter capillaries and the high separation speeds encountered in CE. The high efficiency inherent to CE demands that on-column detection be employed in order to maintain this beneficial attribute. However, maintaining this high efficiency in CE limits the amount of possible detection schemes. The small diameter capillaries are beneficial

for reducing joule heat but they cause reduced sensitivity for path length dependent detection approaches. The fast separation speeds in CE necessitate detection approaches that are amenable to the short residence times of the solutes in the detection zone. The following brief discussion will be limited to the two most common types of optical detection employed in CE, absorbance and fluorescence detection.

1.5.1 Ultraviolet and Visible Absorption

Absorbance detectors are commonly used in CE and many organics can be detected by UV absorbance. Also, most commercial CE instruments are equipped with UV-Vis detectors. High quality fused silica capillaries that are used in CE have a UV cutoff of 170 nm, which allows for the detection of a broad range of compounds. In the small diameter capillaries used with CE the path length dependency of absorbance detection makes solutes with low absorptivities difficult to detect. Beer's Law is important in describing absorbance detection. It has the form of:

$$(1.16) A = \epsilon bc$$

Where A is the absorbance, ϵ is the molar absorptivity, b is the detection cell pathlength, and c is the solute concentration. Absorbance detectors are limited by Beer's Law and the constraints associated with measuring small signal changes in the presence of large backgrounds (12). Hence, absorption techniques have relatively poor concentration detection limits that are typically in the mid to low micromolar range. Attempts have been made to improve absorption detection limits by increasing the detection path length

by changing the capillary shape in the detection zone. An alternative approach to detect molecules with low absorptivities is to employ indirect absorbance methods. In this approach, an additive is added to the buffer system such as phthalic acid that produces a relatively large background signal. The solute band displaces the UV absorbing buffer additive and a decrease in absorbance is observed. The limit of detection in this approach is typically around 1×10^{-6} M in the best cases. Indirect detection requires a large transfer ratio (ratio of the number of signal generating molecules displaced in the detection zone by a single solute molecule), a stable background, and the proper selection of the UV absorbing buffer additive.

1.5.2 Laser Induced Fluorescence

Laser induced fluorescence (LIF) is a highly sensitive approach that in some cases can provide limits of detection below 1×10^{-13} M. Swaile and Sepaniak were the first to demonstrate native fluorescence of a protein with on-column detection using UV excitation (13). In this approach, a beam of a few mW is focused to the dimensions of the capillary bore. However, most molecules are not highly fluorescent in their native state. LIF is less common than absorbance detection and detectors for LIF can be more expensive. Also, it is often necessary to use different lasers for various applications. Biological molecules such as proteins and some peptides can be detected by LIF. The small optical pathlength in CE affects the concentration detection limits for this approach to a lesser extent because the laser power can be increased which increases the fluorescence signal (14).

A common approach for obtaining low detection limits of compounds with low quantum efficiencies is to derivatize them with suitable reagents. The derivatization can include the formation of covalent bonds between the solute and reagent or there can be non-covalent association between them. The covalent interactions occur between functional groups on the solute and the derivatization reagent. The reagent can be a species that is a natural fluorophore or it may fluoresce strongly only when associated with the solute. Some examples of such reagents are dansyl chloride (DNS), fluorescein isothiocyanate (FITC), and o-phthalaldehyde (OPA) (15). The derivatization of solutes prior to separation can be disadvantageous because of the time it takes to perform the reaction. Also, the production of chemical by-products in the sample and the possibility of multiple derivatization products can complicate the sample. On-column labeling of solutes is another approach for LIF but fast kinetic exchange between the solute and reagent is required in order to maintain the high efficiency inherent to CE. Off-column labeling has been performed with the use of a sheath flow cell (16-18). The effluent from the capillary is mixed with the reagent by diffusion but band dispersion can be more of a concern with off-column labeling approaches.

Indirect fluorescence can be used for solutes that exhibit weak native fluorescence because the detected solutes do not have to exhibit the measured optical property. In this approach, the buffer additive that is inserted into the running buffer produces a relatively large fluorescence background. The solute band displaces the additive and a negative response peak is generated as the band passes the detection zone. The disadvantages of this approach are the noisy background signal of the buffer additive and the possible distortion of peaks (fronting or tailing) as a result of field inhomogeneity in the solute

band (12). Peak distortion is intensified if there is a large mobility difference between the solute and the buffer additive. The limits of detection for this technique are typically around 1×10^{-5} to 1×10^{-6} M which is comparable to indirect UV-Vis detection but not as good as on-column LIF mainly due to background fluctuations because of laser intensity instability.

1.6 Reproducibility in Capillary Electrophoresis

Capillary electrophoresis has become a powerful separation technique due to its short analysis times and high separation efficiency. However, in quality control applications its implementation is somewhat limited because of the diminished precision in CE as compared to other separation techniques (19). There are several important factors that limit precision in CE such as injection variability, irreproducible flow rate (EOF), and peak integration errors. In the last few years, there have been some efforts made to try to increase the precision of CE and chapter two herein addresses the issue of precision in CE.

1.6.1 Injection and Precision in Capillary Electrophoresis

Injection is considered to be a significant factor that limits precision in CE. The volume injected in CE is very small (nanoliters) and it is difficult to inject such small volumes in a reproducible manner. The lack of a fixed loop injector in CE as compared to high performance liquid chromatography (HPLC) causes the amount of sample injected to vary each time. A change in the temperature can generate precision problems for electrokinetic injection. This mode of injection depends on the mobility of the solute

and the EOF. The change in temperature will affect the EOF, which then causes a different amount of sample to be injected with the use of electrokinetic injection. It is for this reason, that proper temperature control is important in CE applications. The most commonly employed manner of controlling such injection errors with CE is the use of internal standards.

1.6.2 Electroosmotic Flow Variation

Another important factor affecting the precision in CE is the variation in the EOF. The surface properties (zeta potential) are responsible for the generation of the EOF and its velocity. Therefore, migration time precision depends on the pretreatment of the inner capillary surface before and during analysis (19). The usual rinsing procedure in most CE applications is flushing the capillary for several minutes with base, water, and running buffer before each separation. The selection of these rinse steps have a significant impact on the consistency of the migration times. To correctly identify peaks by their migration times it is essential to employ systems that provide precise migration times. The choice of the rinsing procedure is an important and additional optimization parameter in CE method development. More complex rinse procedures were found to stabilize and improve the reproducibility of migration times of solutes as the surface is reconditioned and adsorbed solutes are removed (20). These adsorbed molecules can influence the surface properties of the capillary and therefore affect the EOF.

Proper temperature control has an impact on the migration time repeatability since it depends on the viscosity of the running buffer. A change in buffer viscosity will affect the EOF and produce variations in the migration time of the solutes (19). Problems with

temperature control can be encountered if a method is transferred from one instrument to another due to different cooling capacities of the instruments. Finally, changes in pH due to electrolysis of the running buffer can limit migration time reproducibility because pH changes will affect the EOF. It is generally recommended that after every six injections the buffer vials should be changed to eliminate electrolysis effects caused by changes in the pH of the running buffer. On column detection in CE makes peak area a function of flow rate because the solutes can migrate at different velocities as they pass the detection zone. To compensate for this in CE, the total peak area can be divided by the migration time (corrected area) because the solute can pass the detector cell at different velocities if fluctuations in the EOF are present. The corrected area can help to compensate for these fluctuations that will lead to changes in the raw area.

1.6.3 Peak Integration and Precision

A final factor that has received less attention in CE precision studies is the accuracy of peak integration (19). This problem arises from the asymmetric and triangular shaped peaks commonly observed in CE. Significant differences were found for software from different manufacturers or of different age of production. Some of the older software was originally designed for control and data acquisition of HPLC systems whereas new software has been designed for the use with CE systems. Peak identification algorithms and integration have been designed for use with CE systems. An integration algorithm that uses a weighted integration allows for the obtainment of lower relative standard deviation (RSD) values. For example, an integration algorithm called CEPLOT has been produced that divides every signal point by its corresponding

migration time and then calculates the sum over all fractions. In general, it was found that with the old software the reproducibility was not as good as that found with the new software (19). Strongly tailing peaks at low signal to noise ratios seemed to cause the most variability for integration with the old software. Only the new software can correctly identify the start and end of peaks that are close to the detection limit. Therefore, the older software is not determining the total actual peak area or baseline noise is being added to the total area. These problems can lead to a decrease in precision at low signal to noise ratios. However, at higher signal to noise ratios it was found that the mistakes with peak start and end detection could be neglected.

Chapter 2. Parameters Affecting Reproducibility in Capillary Electrophoresis

2.1 Introduction

Capillary electrophoresis (CE) applications have increased in recent years due to its high efficiency, speed of analysis, and minimal sample volume requirements. Much research has been done in CE in terms of increasing resolution and efficiency. CE has been criticized for its lack of reproducibility and poor quantitative ability (21-24). In some cases poor reproducibility is linked to an on-column mode of detection. It is important for an analytical method to be reproducible in order for it to gain acceptance for routine analysis in pharmaceutical, environmental, and other applications. There are many factors (e.g. sample matrix composition and the injected sample volume) that affect reproducibility in CE (25-29). Samples with high salt content can cause localized heating of the sample zone and poor peak shape (28). It was found that washing the capillary with NaOH after each injection or use of a high ionic strength buffer minimizes the effects of proteins in serum samples on migration time reproducibility. Jorgenson and co-workers found that as the sample volume in the injection vial is reduced, the amount of sample introduced into the capillary is decreased. Buffer concentration and electrolysis effects have been investigated as well (25-26, 30-32). Buffer electrolysis due to the prolonged application of voltage leads to poor quantitation due to the pH gradient that is generated across the capillary. Kelly et al. found that these problems could be reduced by using high capacity buffers or zwitterionic buffers (30). An alternative way of reducing buffer depletion is the use of short-end injections, which reduce the analysis time (28). Another important factor influencing reproducibility is the consistency of electroosmotic flow (EOF). The integrity of the capillary surface, age of the capillary,

and rinsing procedures are significant factors in controlling EOF (19, 25-26, 33-45). It has been determined that the best migration time reproducibility is obtained when the capillary is rinsed after each run. Schwartz and co-workers obtained improved reproducibility by use of a replenishment system, which allowed for fresh buffer solutions to be used before each analysis (46). In one study it was found desirable to replace the buffer solutions in the reservoir every four to six injections (44). Also, it was found in that study that inconsistent migration times are related to non-equilibrium conditions between the buffer and the capillary wall, which cause variations in the total current. Fallor and co-workers demonstrated that the choice of the flushing buffer solutions could play an important role in migration time reproducibility (19).

Temperature variations and corresponding changes in viscosity have been determined to be detrimental to obtaining reproducible results (22, 30, 40, 47-48). With an increase in temperature the viscosity decreases, the rate of EOF increases, and buffer depletion occurs more rapidly. More directly, changes in viscosity alter the amount injected for both electrokinetic and pressure injection (49). Temperature variations will cause a change in analyte mobility, which leads to poor migration time reproducibility. Proper control of temperature can minimize these temperature related difficulties (46, 50-53).

A significant parameter that has received little attention is the precision of various CE injection methods (27). In CE, there is not a fixed loop injector as in HPLC that allows for the same quantity of sample to be introduced with each injection (53).

Therefore, in CE it is difficult to reproducibly introduce the same small (nL) volume (19, 46, 48, 54-56). The reproducibility of the injection process can be the limiting factor in obtaining precise results (46, 54, 57-58). It is important to investigate whether

hydrodynamic or electrokinetic injection methods produce more reproducible results.

Electrokinetic injection is biased towards highly mobile solutes because solutes with the highest electrophoretic mobilities are preferentially introduced.

In this chapter I present parameters that affect precision that have not been previously studied. Some of these parameters include the use of multiple sample vials, the presence of air bubbles, and the effect of slope sensitivity on reproducibility. Finally, much work was done comparing electrokinetic injection to pressure injection with the goal of determining what injection condition allows for the most reproducible results. These studies were performed using a commonly employed commercial CE instrument that employs on-column spectrophotometric detection.

2.2 Experimental

2.2.1 Materials

β -Cyclodextrin was obtained from Sigma Chemical Company (St. Louis, MO, USA). Mono and dibasic sodium phosphate was also purchased from Sigma. The dansylated amino acids Dns-Lysine (Dns-Lys), Dns-Leucine (Dns-Leu), Dns-Asparagine (Dns-Asn), Dns-Proline (Dns-Pro), Dns-Cysteic Acid (Dns-Cys), and Dns-Glutamic Acid (Dns-Glu) were purchased from Sigma. Canada Dry club soda was purchased from a local grocery store. The running buffer used for all separations was 10 mM β -cyclodextrin in 50 mM phosphate buffer. Stock solutions of the various amino acids were made up in deionized water. All solutions were filtered through a 0.22 μ m pore size filter from Micron Separations Inc. (Westboro, MA, USA).

2.2.2 Apparatus and Methods

All CE experiments were performed using a Hewlett Packard (HP) automated Capillary Electrophoresis system (HP^{3D}CE) interfaced to a HP Pentium I personal computer. The applied voltage was 16 kV for all the separations and temperature control (24°C) was used in all experiments. Detection was accomplished on-column by monitoring UV absorbance at 214 nm. The migration order was established by injecting the amino acids individually. Fused silica capillaries (50 μm i.d. X 360 μm o.d.) were obtained from Polymicro Technologies Inc. (Phoenix, AZ). The capillaries were cut to a total length of 50 cm and a 1 cm section of the capillary coating was removed at 41 cm for on-column detection. New capillaries were conditioned for 30 minutes with 0.1 N NaOH and for 30 minutes with deionized water. At the beginning of each day, the capillary was rinsed for 5 minutes with deionized water, 5 minutes with 0.1 N NaOH, 5 minutes with deionized water, and 5 minutes with running buffer. The flush procedure between runs was for 2 minutes with 0.1 N NaOH, 4 minutes with deionized water, 3 minutes with running buffer, and a 90 second application of 15 kV between the inlet and outlet.

2.3 Results and Discussion

2.3.1 Pressure Injection Studies

An experiment was performed to compare high pressure (15 mbar, 3 sec.) to low pressure (3 mbar, 15 sec.) injection conditions. In this experiment a mixture of 6 amino acids in two different sample vials were used with eight injections for each set of injection conditions (48 data points). A typical electropherogram for these conditions can

be seen in Figure 2.1. It was expected that the relative importance of uncertainty in injection time and pressure would be highlighted in this study. It has been advised to use longer injection times because the ability of a CE instrument to self-regulate injection is reduced with short injection times (58). It has been found that typically the range of average RSD's for peak area in CE are 1-2% (43, 59-62). The results seen in Table 2.1 show that high pressure injection conditions are better than low pressure injection conditions. In the first experiment, the average RSD for corrected peak area for high pressure was 1.59% and the average RSD for corrected peak area for low pressure was 2.38%. Peak area RSD's were in the range of 0.54% to 2.56% for high pressure and 0.86% to 3.55% for low pressure. The second time this experiment was performed it showed the same trend; the high pressure average RSD was 1.42% and the low pressure average RSD was 2.02%. In this data set the peak area RSD's ranged from 0.63% to 2.34% for high pressure and 1.09% to 3.47% for low pressure. In this study uncertainty in injection time is shown not to be particularly important in determining overall reproducibility as the shorter injection time, which is expected to exhibit a larger relative uncertainty in time, yielded better results.

Raw and corrected areas are both presented in Table 2.1. The corrected areas were obtained by dividing raw area by the migration time to compensate for the effects of long-term changes in mobility on peak area. It has been shown that peak area precision is improved by normalization (63-64). The raw area RSD values are low and very similar to the corrected area RSD values in the first data set. The corrected area exhibited a more significant impact on area reproducibility in the second data set because the migration time reproducibility was not as good. It is worth noting that the second data set was

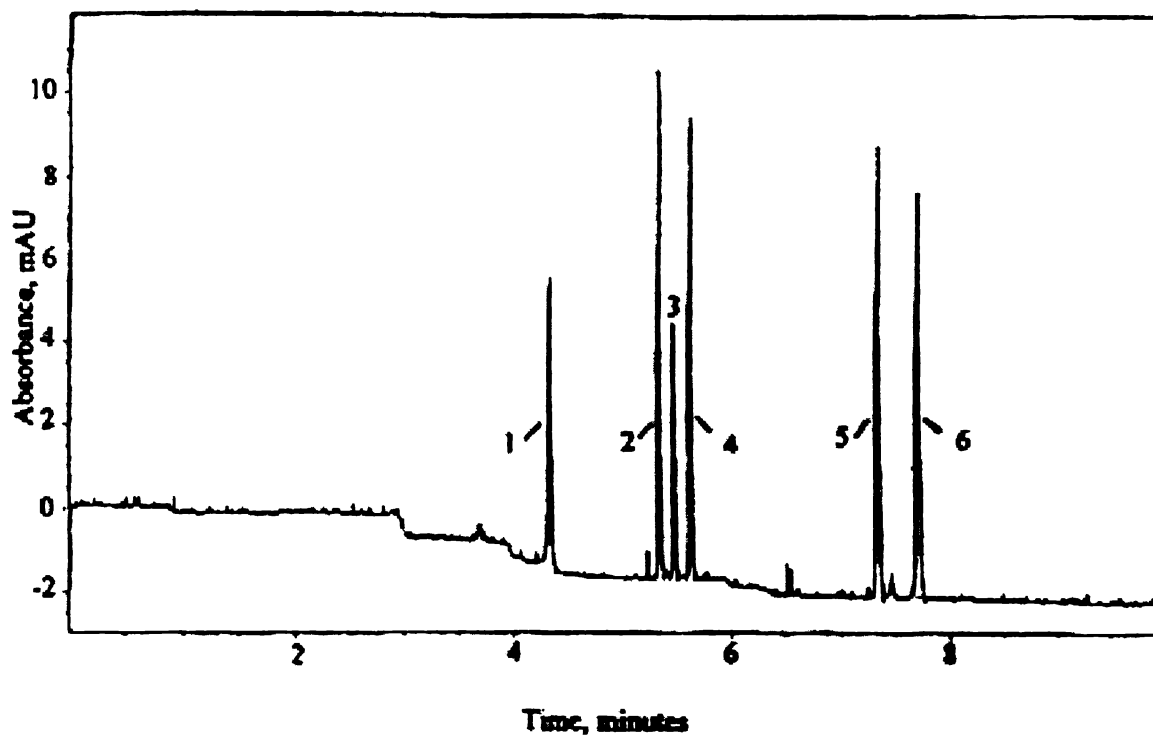


Figure 2.1 Separation of six dansylated amino acids. Separation conditions: 50 cm capillary, 16 kV, 10 mM β -CD in 50 mM phosphate running buffer, injection for 15s at 3 mbar. Peak identity: 1. Lys; 2. Leu; 3. Asn; 4. Pro; 5. Cys; 6. Glu.

Table 2.1 A Comparison of High Pressure Injection Conditions to Low Pressure Injection Conditions (RSD Values)

Experiment 1						
<u>High Pressure</u>				<u>Low Pressure</u>		
Analyte	Migration Time	Raw Area	Corr. Area	Migration Time	Raw Area	Corr. Area
Dns-Lys	4.62E-2%	0.56%	0.54%	5.88E-2%	2.06%	2.04%
Dns-Leu	4.41E-2%	2.14%	2.16%	5.35E-2%	0.83%	0.86%
Dns-Asn	4.58E-2%	2.60%	2.56%	5.22E-2%	3.56%	3.55%
Dns-Pro	4.06E-2%	1.26%	1.25%	5.66E-2%	1.55%	1.55%
Dns-Cys	4.77E-2%	2.11%	2.08%	6.00E-2%	3.29%	3.29%
Dns-Glu	4.70E-2%	0.97%	0.93%	6.22E-2%	2.99%	3.00%
	4.52E-2%	1.61%	1.59%	5.70E-2%	2.38%	2.38%

Experiment 2						
<u>High Pressure</u>				<u>Low Pressure</u>		
Analyte	Migration Time	Raw Area	Corr. Area	Migration Time	Raw Area	Corr. Area
Dns-Lys	0.38%	2.32%	1.51%	0.50%	3.89%	3.47%
Dns-Leu	0.46%	3.24%	2.34%	0.54%	2.85%	1.70%
Dns-Asn	0.47%	2.01%	1.35%	0.55%	1.26%	1.18%
Dns-Pro	0.48%	0.47%	0.63%	0.44%	1.30%	1.09%
Dns-Cys	0.61%	1.27%	1.90%	0.57%	2.77%	2.41%
Dns-Glu	0.64%	0.75%	0.79%	0.60%	2.56%	2.29%
	0.51%	1.68%	1.42%	0.53%	2.44%	2.02%

obtained a week after the first and the capillary had been used for a few weeks. This indicates the potential importance of capillary history in determining reproducibility. If an analyte migrates at a different rate past the detection window from injection to injection, dividing by the migration time may compensate for this problem.

Hardware and software are provided with the HP^{3D}CE instrument to minimize variations in injection conditions (65). First, the system calculates the expected area under a pressure vs time profile curve. An ambient valve isolates the sample vial from atmospheric pressure; concurrently a rise valve applies airflow through an internal restriction into an internal chamber. The volume of this chamber is twenty times larger than that of an empty sample vial. The rise valve deactivates when the upslope of the profile has reached its maximum pressure and pressure is drawn from the vial as the fall valve activates. Plateaus in the profile are generated by the action of the rise and fall valves while the area in the profile is calculated. Thus, the system can compensate to a degree for changes in pressure “tightness” from run to run. However, the pressure is measured in the chamber not at the sample vial; i.e. not directly at the point of injection. The error in pressure compensation by the system appears to be smaller for higher injection pressures.

2.3.2 Use of Multiple Sample Vials

Another experiment of interest was to study the effect of using multiple sample vials on reproducibility. In this experiment four sample vials were used with two injections from each vial containing six amino acids at low pressure conditions (3 mbar, 15 seconds). The average RSD value for the corrected peak area was 2.6%; higher than

what is normally obtained for pressure injection conditions. Each vial may be crimped differently and this is a source of variability.

It should be noted that several studies were performed in which 15 injections of a six component mixture were done from the same sample vial. Since a septum is pierced on each injection, it was felt that at some point the seal would begin to fail. In each of these studies, the precision did not degrade from injecting more than a dozen times from the same vial. These studies indicate that the instrument can reproducibly inject from the same vial but it can not, presumably, compensate completely for differences in pressure that may occur when sample vials are changed.

2.3.3 Migration Time Reproducibility

Migration time reproducibility in CE has been studied previously (22-25, 30, 33, 47, 53-54, 66-68). In an inter-company cross validation exercise Altria and co-workers were able to obtain precise results for migration time and peak area using instruments from three different suppliers (63). Migration time reproducibility can be affected by siphoning effects in which the solution heights in the buffer vials are unequal (69). This problem can be avoided by using different vials for rinsing and for separation. Poor migration time reproducibility due to high current can be corrected by using a lower voltage or a more dilute buffer (24). Hage and co-workers obtained RSD values of 2.1 to 4.6% for migration time in amino acid separations (22). They improved the migration time reproducibility by use of mobility and migration time ratios. The use of migration indices has also aided in obtaining more reproducible migration times (47). Kenndler found that it is best to store capillaries dry to prevent a porous gel layer from forming on

the capillary surface, which hinders migration time precision (70). A common way to improve migration reproducibility is to add markers to the sample or use internal standards to account for changes in EOF (53, 71-77). Sepaniak and Holland were able to improve migration time reproducibility to less than 1.0% with micellar electrokinetic chromatography by normalizing the analytes to adjacent eluting solutes (78). They found that the normalization procedure improved precision depending on the appropriateness of the solute used as the normalization standard. In the studies reported herein, the RSD values for migration time are always less than 1.0%. Migration time reproducibility directly impacts qualitative reproducibility. However, it may also impact quantitation, as seen above, if peaks are corrected for changes in retention time due to long-term changes in flow rate. In this regard, long-term changes are those that occur on a time frame longer than the separation time.

2.3.4 Use of an Internal Standard

A common method of compensating for fluctuations in electrophoretic conditions is the use of an internal standard. To investigate this idea, the data from Table 2.1 was used and the third peak (Dns-Asn) from the separation was chosen as the internal standard.

The formula used for calculating the normalized area (A_{norm}) was:

$$(2.1) A_{\text{norm}} = \frac{A_{\text{ISave}}}{A_{\text{IS}}} \times A_{\text{sam}}$$

where A_{ISave} is the average corrected area of the internal standard for all runs, A_{IS} and A_{sam} are the corrected areas of the internal standard and sample component for the run investigated. It can be seen from the data in Table 2.2 that the internal standard improved the precision of the low pressure injections. In the first study, the average corrected area RSD was 2.38% and the internal standard improved the precision to 1.88%. In this data set the peak area RSD's ranged from 1.35% to 2.71%. In the second data set the average corrected area improved from 2.02% to 1.80% with the use of an internal standard. The peak area RSD's ranged from 0.54% to 3.58% in this second low pressure data set.

The use of an internal standard did not improve the reproducibility for the high pressure injections. In the first study, the average corrected area RSD was 1.59% and the use of the internal standard produced a value of 1.70%. In this data set the peak area ranged from 1.36% to 2.24%. The trend was the same in the second data set as the RSD values for the average corrected area went from 1.42% to 1.66%. In this second high pressure data set the peak area range was from 0.80% to 2.70%. In principle, pressure injection, while possibly variable from run to run, should not show any bias between analytes for a given injection. Nevertheless, in comparing the first two injections in the high pressure Experiment 1 case, the internal standard corrected area increased by 0.89% from $2.3717E-2$ to $2.3927E-2$. In these same two runs, Dns-Lys decreased by 2.4% from $4.5656E-2$ to $4.4543E-2$. In another example of this, the internal standard decreased by 1.66% from $2.3717E-2$ to $2.3323E-2$ in injections one and five. In these same two runs Dns-Leu increased by 1.57% from $4.6735E-2$ to $4.7469E-2$. In general, the late eluting peaks showed a decrease in corrected area when the internal standard corrected area increased. The internal standard method does not correct for these fluctuations in peak

Table 2.2 Use of Peak #3 (Dns-Asn) as an Internal Standard for the Data in Table 2.1 (RSD Values)

Experiment 1

<u>High Pressure</u>			<u>Low Pressure</u>	
<u>Analyte</u>	<u>Norm. Area</u>	<u>Corr. Area</u>	<u>Norm. Area</u>	<u>Corr. Area</u>
Dns-Lys	1.36%	0.54%	1.98%	2.04%
Dns-Leu	1.71%	2.16%	2.71%	0.86%
Dns-Pro	2.24%	1.25%	1.71%	1.55%
Dns-Cys	1.66%	2.08%	1.35%	3.29%
Dns-Glu	1.54%	0.93%	1.63%	3.00%
	1.70%	1.39%	1.88%	2.15%

Experiment 2

<u>High Pressure</u>			<u>Low Pressure</u>	
<u>Analyte</u>	<u>Norm. Area</u>	<u>Corr. Area</u>	<u>Norm. Area</u>	<u>Corr. Area</u>
Dns-Lys	1.46%	1.51%	3.58%	3.47%
Dns-Leu	2.70%	2.34%	1.66%	1.70%
Dns-Pro	0.80%	0.63%	0.54%	1.09%
Dns-Cys	2.29%	1.90%	1.27%	2.41%
Dns-Glu	1.03%	0.79%	1.93%	2.29%
	1.66%	1.43%	1.80%	2.19%

area from run to run. Perhaps the problem is related to short-term changes in flow rate. The improvement for the low pressure injection may be a simple matter of the poorer reproducibility for that data relative to the high pressure injection case (i.e. there was greater room for improvement).

2.3.5 Electrokinetic Injection Studies

The reproducibility of the electrokinetic injection process is influenced by many parameters. The amount of sample introduced into the capillary depends on the EOF and the electrophoretic mobility of the solute. Therefore, factors that alter the EOF will affect the precision of the sample volume introduced into the capillary. For example, changes in ionic strength and buffer composition will affect the electroosmotic mobility and can lead to a different amount of sample introduced for different electrokinetic injections. It is for this reason that electrokinetic injection is usually not as reproducible as pressure injection (79). Pressure injection conditions are generally only affected by this problem if the viscosity of the buffer is drastically changed. Yeung and co-workers have improved the precision of electrokinetic injection by correction with the integrated current during the period from injection to detection (21).

Previously, Cohen and co-workers studied the effect of a jagged edge capillary on separation efficiency for electrokinetic injection (80). They found that plate count decreased and the migration time reproducibility decreased for capillaries with a jagged edge at the inlet side relative to smooth cut capillaries. Their explanation is that the jagged edge causes a current density difference between the inlet and outlet that can affect electroosmotic and electrophoretic mobilities. Also, they point out that because a

wall does not bind part of the jagged inlet the electroosmotic flow profile can become distorted and this can have adverse effects on peak shape and efficiency. Altria et al. determined that careful cutting of the capillary end is important in obtaining uniform sample injection and good peak shape (41, 69). They also noted that a jagged capillary tip will lead to poor precision but no RSD's were given. To investigate this, eight injections were performed at 7 kV for 20 seconds with a jagged edge capillary. Three amino acids, the -1 charged Dns-Pro, Dns-Leu, and Dns-Asn, were used in this study (24 data points). After these eight injections, the inlet end was cut smoothly and eight more injections were performed at 7 kV for 20 seconds. The average RSD values for corrected area were not much different for the jagged edge (9.8%) compared to the smooth cut (8.9%). This indicates that electrokinetic injection does not work well for anions; however, the shape of the inlet does not appear to be important. Our results agree with Cohen and co-workers in that we also noticed that the smooth cut gave better RSD values for migration time relative to the jagged edge case.

The significance of injection conditions for electrokinetic injection was studied as well. High voltage for a short time (20 kV, 7 sec.) was compared to low voltage for a long time (7 kV, 20 sec.). The data for this experiment in Table 2.3 in which 8 injections were performed with the same three component mixture shows that low voltage for a long time is better for electrokinetic injection. It was expected that low voltage injection conditions might produce better results due to electrolysis effects with high voltage injection conditions. Other problems associated with such high voltage injection conditions in CE instruments include the production of electrochemical reaction products as current flows through the sample (27). These by products formed can contaminate the

Table 2.3 Electrokinetic Injection Study of High Voltage for a Short Time Versus Low Voltage for a Long Time

<u>High Voltage Injection RSD Values</u>		<u>Low Voltage Injection RSD Values</u>	
Migration Time	Corrected Area	Migration Time	Corrected Area
9.68E-2%	16.1%	0.14%	5.61%
0.102%	17.0%	0.15%	5.63%
8.62E-2%	16.6%	0.14%	4.16%
0.095%	16.6%	0.14%	5.13%

sample and changed the injected amount due to slight changes in EOF (46). Clearly, quantitative reproducibility for electrokinetic injection was far inferior to pressure injection in these studies. Our results agree with Jorgenson and co-workers in a study in which they found that pressure injection produced an average RSD of 2.9% for peak area whereas 4.1% was obtained for electrokinetic injection (27). Schwartz et al. obtained better precision for peak areas with electrokinetic injection for a mixture of dansylated amino acids (46). Their explanation is that the frequency of the on/off duty cycle of the modulator valve is not rapid enough at short injection times to make vacuum level differences average out. It is expected that the use of an internal standard would exhibit a more dramatic improvement in precision for electrokinetic injection, despite the fact that all analytes are not injected equally, because the unnormalized RSD values were so poor.

2.3.6 Effect of Slope Sensitivity on Reproducibility

The precision of peak integration can be important in determining CE reproducibility. In a recent study, Faller compared commercially available software's with different sets of identical raw data files (19). It was found that the "old" software's originally developed for HPLC data acquisition produced higher RSD's for corrected peak area than the new software's especially designed for CE. New software contains integration and peak identification algorithms designed for CE. Weinberger has studied the onset of peak splitting and the presence of spikes in an electropherogram (81). In our studies, slope sensitivity was varied to determine the effect it had on reproducibility. The corrected peak area was used to account for analyte mobility differences and RSD values were calculated from a study in which six amino acids were separated following injection by

pressure. In this study slope sensitivity was changed using the HP system software by increments of 10-20 mAu/min for three amino acids; a slightly tailing peak (Dns-Lys), a non-tailing peak (Dns-Pro), and a non-tailing peak with an air peak nearby (Dns-Leu). Tailing peaks were investigated because they can generate poor precision due to variable integration (58). These peaks exhibited heights in the range of 6.1-12.5 mAu and widths of 0.018-0.032 minutes in this experiment. The RSD values for corrected peak areas were calculated for each slope sensitivity value and plots were generated (see Figure 2.2). It was observed that the area decreases as the slope sensitivity increases. Above a slope sensitivity of 50 mAu/min the peak area does not change much, which agrees with Hewlett Packard data at various slope sensitivities (Pritchett, B., personal communication). In looking at Figure 2.2, it is noticeable that the RSD values remain roughly constant at slope sensitivity values ≥ 40 mAu/min.

The HP integration software (82) produces an initial baseline level by taking the first data point as a prospective baseline point. In order for a data point to be considered as a baseline point it must fall within the defined baseline envelope. Also, the curvature of the baseline at the data point has to be below a certain value determined by the slope sensitivity setting. A baseline envelope is produced from the slope of the baseline using a baseline-tracking algorithm in which the slope is determined by the first derivative and the curvature is determined by the second derivative. After the integrator has sampled a certain number of data points, it alters the baseline from the initial baseline point to the current baseline point. The start of a peak occurs when the baseline points generate a baseline curvature greater than the value determined by the slope sensitivity. If the slope remains above the limit a peak is identified and a cardinal point is defined.

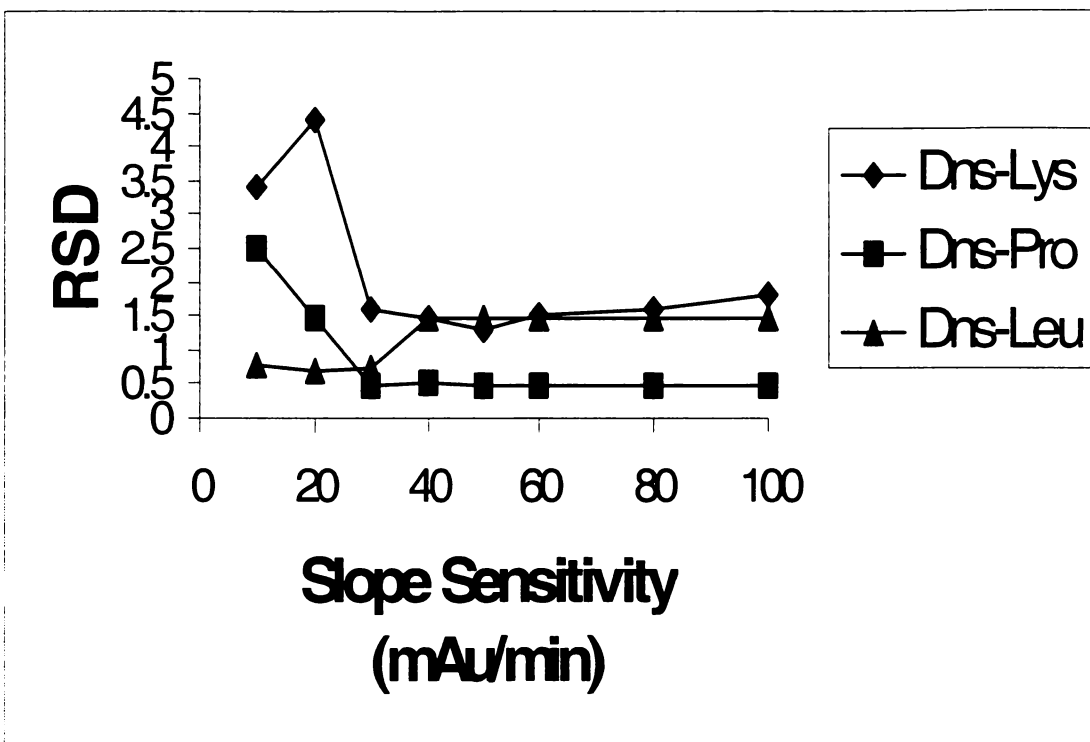


Figure 2.2 Plot of RSD versus slope sensitivity for a non-tailing peak (Dns-Pro), a non-tailing peak with an air peak nearby (Dns-Leu), and a slightly tailing peak (Dns-Lys).

As the curvature becomes negative a front inflection point is produced and another cardinal point is defined, as the slope becomes negative. When the curvature becomes positive, a rear inflection point is produced. The integrator picks these cardinal points to define and quantify a peak. The designated cardinal points are baseline points, valley points, peak apex, and points of inflection. Each cardinal point contains a horizontal coordinate elapsed time, a vertical coordinate of height from the baseline, and other parameters that are utilized by the integrator to calculate the peak areas.

The RSD values were not as good at low slope sensitivity for Dns-Pro and Dns-Lys because the point the program picks to start integration is too far from the start of the peak. Therefore, in this case baseline noise and any nearby peaks are integrated. The HP standard integrator algorithm identifies a start and end time for each peak and marks these points with vertical tick marks. The integrator calculates the area above the baseline between the tick marks for baseline-to-baseline peaks. In this study, if higher values of slope sensitivity are used only the peak of interest is integrated. For Dns-Leu, there were a few injections with air bubbles near the analyte. This example is a special case in which there was an injection with a particularly low area. At low slope sensitivity the presence of air bubble peaks inflated the area and the injection that had the low area was rejected by the Q-test. This explains why the RSD values were slightly better at low slope sensitivity. At higher slope sensitivities the air bubbles were not integrated as part of the analyte area and this made the area smaller. Thus, the injection with the particularly low area was not rejected and the RSD values were not as good.

There is a built in program in the HP software that prevents the trailing edge from being cut off in a tailing peak. Thus, the RSD values did not change at high slope sensitivity for the slightly tailing peak (Dns-Lys). In the case of a tailing peak, the time the peak exceeds upslope and downslope criteria is noted and one quarter of that time is added at the end of the peak before the end of the peak is confirmed. The data in Figure 2.2 shows that slope sensitivity is not a significant parameter in obtaining good RSD values. Our results agree with the findings of the instrument manufacturer in that good precision can be obtained for a wide range of slope sensitivity values.

2.3.7 Effect of Air Bubbles on Precision

Despite efforts to degas running buffers prior to use, the presence of gas bubbles in CE capillaries during runs is very common and this can degrade the appearance of electropherograms for all CE instruments. In fact, the high efficiency inherent to CE analyte bands can sometimes make it difficult to distinguish between real and “bubble” peaks. It is also possible that gas bubbles or pockets in the capillary can lead to short-term changes in flow rate. A capillary containing several bubbles can be modeled as a series of low resistance zones composed of running buffer and high resistance bubble zones. If one assumes a thin (<1 μm) layer of conducting running buffer along the capillary surface in a bubble zone, the resistance in that zone can be two or more orders of magnitude greater than in a non-bubble zone. This will diminish the field in the non-bubble zone. As bubbles are generated and expelled an analyte would be expected to experience short-term changes in flow rate. Obviously this will influence peak area in an

unpredictable manner. Changes in observed capillary current may be attributed to this occurrence (although there are other possible causes).

To test this hypothesis a study was performed in which a zone of bubbles (a pocket) was purposely produced in the capillary by injecting club soda into the capillary at 6 kV for 60 seconds. In the first of the two cases studied, Dns-Leu was injected in conjunction with the bubble zone with timing such that the zone was in the capillary during detection. The timing was altered for the second case such that the bubble zone exited the capillary prior to detection of the Dns-Leu. A representative electropherogram for the first case is shown in Figure 2.3 along with the observed capillary current. It is clear that we have exaggerated the effect by injecting a substantial zone of bubbles to illustrate the influence of short-term changes in flow rate on reproducibility.

Table 2.4 shows the effect of the presence of a bubble zone on RSD values for twelve injections (6 case 1, 6 case 2). For the injections where the bubble zone is in the capillary when the analyte passes the detector the RSD for peak area was 3.24%. As can be seen in Figure 2.3 the current fluctuated right before the bubble zone exits the capillary, which leads to imprecise results for peak area. More importantly, the size of the bubble zone was not the same for each injection, as seen by different average currents from run to run. This situation effectively produces long-term changes in flow rate, which can be corrected to a degree, by using corrected areas (see Table 2.4).

The other case of interest is when the bubble zone has exited the capillary when the analyte passes the detector. The current and flow rate increases after the bubble zone exits the capillary, but then both are expected to remain steady. In this instance a

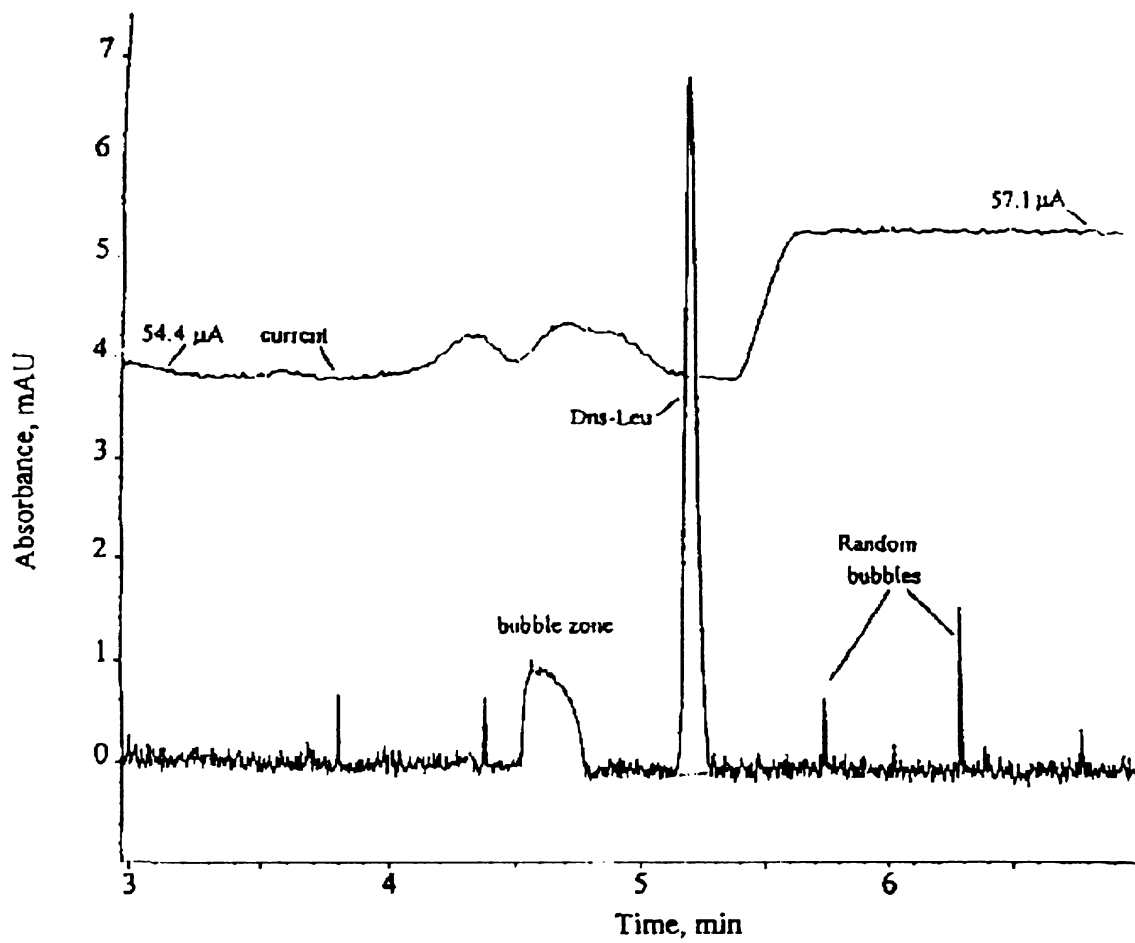


Figure 2.3 Electropherogram depicting the bubble zone within the capillary as the analyte passes the detector.

Table 2.4 Effect of the Zone of Bubbles on Precision (RSD)

Bubble zone out of capillary prior to detection		Bubble zone in the capillary during detection	
Area	Corrected Area	Area	Corrected Area
1.85%	5.25%	3.24%	2.80%

All twelve areas mixed together 3.92%

All twelve corrected areas mixed together 6.85%

relatively good RSD value was obtained for the analyte (1.85%). The use of corrected areas made the RSD values for peak area worse (see Table 2.4). Correcting based on the total migration time can not compensate for the sudden increase in current and the corresponding change in mobility that occurs after the bubble zone exits the capillary.

In everyday practical use of any CE instrument, there will be separations in which the bubble is either in or out of the capillary when the analyte passes the detector. To simulate realistic conditions all twelve injections were mixed together and the RSD values were calculated for the analyte (12 data points). When this was done the average RSD for peak area was 3.92%. This demonstrates that in day to day use in CE the presence of a bubble may adversely affect precision because of the change in current and flow rate. The use of corrected area was once again not able to compensate for the current increase and it generated a very poor average RSD of 6.85%. These results are exaggerated due to the largeness of the bubble zone but, nevertheless, illustrate an important consideration in obtaining precise results in CE.

A method to compensate for this intermittent bubble problem is to divide by the average current during the period the analyte passes the detector. This process was done for the six injections in which the bubble zone was in the capillary when the analyte passed the detector. The average RSD values improved from 3.24% to 2.21% when the raw area was normalized for electrophoretic current. This same correction process was performed for the 6 injections in which the bubble zone was out of the capillary when the analyte passed the detector. There was only a slight improvement in RSD from 1.85% to 1.77% for the electrophoretic normalization process. The current increased, but then

became very steady after the bubble zone was out of the capillary. Therefore, it is not surprising that dividing by the average current only slightly improved the precision.

2.4 Future Plans

It would be of interest to use higher buffer concentrations and operating voltages to study the effect of higher column temperatures. An increased column temperature can affect solute stability, buffer viscosity, and EOF. It would also be of interest to see how these parameters affect the RSDs of migration time and peak area. For example, the injection volume could be variable due to the change in viscosity of the buffer. This could be studied by using moderate buffer concentrations for separations and comparing the results to those obtained with separations at high buffer concentrations. At high buffer concentrations there will be more joule heat generated and this leads to an increase in column temperature. In all of our studies, the autosampler tray was kept at constant temperature in order to maximize precision. Thermostating of the tray is important in minimizing evaporation effects and in improving solute thermal stability. Fluctuations in temperature can occur due to heat generation by the instrument or from temperature fluctuations in the room. The thermostating function of the instrument could be turned off to demonstrate evaporation effects. This could be especially important for electrokinetic injection because the concentration of the sample components would increase as the solvent evaporates. Changes in the sample solution will affect the ionic strength and alter the conductivity of the solution. Hence, different quantities of the solute would be injected due to variations in sample concentration and ionic strength. However, internal standards could be used to help compensate for evaporation losses. It

would be desirable to have data without the capillary thermostated but with internal standards present in order to demonstrate that internal standards can compensate for this error.

2.5 Concluding Remarks

This chapter presents an overview of prior work and the results of current investigations of parameters that affect reproducibility in CE such as type of sample injection conditions, presence of air bubbles, and the use of multiple sample vials. It was found that high pressure injection conditions can routinely produce RSD values of less than 2.0% for corrected peak area. In many but not all instances corrected peak areas exhibited RSD values that were superior to values for raw area. These studies should provide researchers with useful information when attempting to maximize precision. Still, the best precision that we and others have obtained in CE is not as good as generally observed in HPLC with fixed loop injection and off-column detection.

Chapter 3. Optimization Strategies and Modeling of Separations of Dansyl-Amino Acids by Cyclodextrin-Modified Capillary Electrophoresis

3.1 Introduction

The enantiomeric separation of amino acids is significant for peptide chemistry, amino acid biochemistry, and the dating of fossils. Also, the different biological activities of stereoisomers make their separation important. A number of chiral selectors have been used for the separation of enantiomers in capillary electrophoresis (83-84). Wistuba et al. used bovine serum albumin (BSA), α_1 -acid glycoprotein, ovomucoid, and casein as chiral selectors but found it necessary to use extensive rinse procedures every ten runs to remove the wall adsorbed proteins (85). A dextran polymer network containing a chiral additive has been used to separate amino acids and drugs (86). Another approach used by Kuhn et al. is the use of the chiral crown ether, 18-crown-6-tetracarboxylic acid, for enantiomeric separations (87-88). The macrocyclic antibiotic vancomycin has been employed as a chiral buffer additive in CE due to advantages that it provides such as high solubility and the ability to provide excellent separation selectivity and efficiency (89-90). Coated columns are necessary to minimize the wall adsorption of vancomycin that leads to poor separation efficiency and problems with migration time reproducibility. In our laboratory, we have obtained migration time reproducibility of less than 1% for the separation of amino acids with cyclodextrins (91). Micellar electrokinetic chromatography (MECC) with CDs as selectors has been employed for the separation of many analytes but the analysis times can be somewhat lengthy (92-97). The use of derivatized CDs with MECC has been demonstrated to be an excellent alternative to beta cyclodextrin (β -CD) for the separation of NDA derivatized amino

acids because an optimum concentration can be obtained without solubility problems (93).

An advantage of the use of nonaqueous media is that it can allow for higher concentrations of chiral selectors that are poorly soluble in water (98-99). Nevertheless, the most common approach for separating amino acids is the use of CDs in aqueous media (100). Vigh and co-workers synthesized a single isomer sulfated γ -CD that was capable of resolving many individual amino acid enantiomer pairs at low pH with high resolution (101). High resolution was possible because the amino acids are positively charged at low pH and will migrate in the opposite direction of the sulfated CD, which enlarges the enantiomeric separation window. Hydroxypropyl substituted CDs (102-104), methylated CDs (104-107), an L-Ala-crown-L-Ala capped β -CD (108), and cationic CDs (109-111) have all been employed for the separation of amino acids. Native CDs, used individually, have been employed for amino acid separations (112-116). Finally, buffers with dual CDs (anionic and neutral) have been prepared for enantioseparations (117-120). The CE multiple-CD work described herein differs in the use of simplex methods and molecular modeling to better optimize and understand these enantioseparations.

The identification of the optimal separation conditions for a complicated mixture of enantiomeric pairs can be time consuming and difficult due to the combination of chiral and achiral separation elements. Separation of the enantiomers is desired but excess resolution is a problem due to the possibility of the co-migration of enantiomers of different compounds in the mixture. In this report, the simplex method has been utilized for the rapid determination of the optimum separation conditions prior to engaging in lab

work for the separation of mixtures of five amino acid enantiomeric pairs with dual-CD systems. The five amino acids were chosen because they represent different classes of amino acids such as nonpolar (Leu, Val), polar (Ser), and an acidic R group (Glu, Asp). This set can present a complicated separation because up to ten peaks can be obtained and three classes of amino acids are represented. Single isomer substituted CDs have been synthesized and were evaluated for Dns-amino acid separations. Molecular mechanics modeling of amino acid-CD interactions has been performed to assist in the understanding of experimental results.

3.2 Experimental

3.2.1 Materials

Dns- leucine (Leu), -valine (Val), -serine (Ser), -glutamic acid (Glu), and -aspartic acid (Asp) were purchased from Sigma Chemical Company (St. Louis, Mo USA). β -CD, sodium phosphate, and sodium borate were also purchased from Sigma Chemical Company. γ -CD was purchased from Cyclodextrin Technologies Development, Inc. (Gainesville, FL USA). Carboxymethyl β -CD degree of substitution 1 (1-CM- β -CD) was purchased from Advanced Separation Technologies Inc. (Whippany, NJ USA). Heptakis-(2,3-dimethyl-6-carboxymethyl)- β -CD (HDMCM- β -CD) and octakis-(2,3-dimethyl-6-hydroxy)- β -CD (16-me- γ -CD) were synthesized in house (121). The running buffer (pH 8.1) used for all separations was 0.01 M sodium phosphate and 0.006 M sodium borate with the appropriate amount and type of CD in the buffer.

3.2.2 Apparatus and Methods

CE experiments were performed using a Hewlett Packard automated capillary electrophoresis system (HP^{3D}CE) interfaced to an HP Pentium 1 personal computer. An applied voltage of 16 kV and temperature control (24°C) was used in all experiments. Detection was accomplished on-column by monitoring UV absorbance at 214 nm. The migration order was established by injecting the amino acids individually. Fused silica capillaries 50 µm ID x 360 µm OD were obtained from Polymicro Technologies (Phoenix, AZ). The capillaries were cut to a total length of 60 cm and a 1 cm section of the capillary coating was removed at 51 cm for on-column detection. New capillaries were conditioned for 30 minutes with 0.1 N sodium hydroxide and for 30 minutes with deionized water. At the beginning of each day, the capillary was rinsed for 5 minutes with deionized water, 5 minutes with 0.1 N sodium hydroxide, 5 minutes with deionized water, and 5 minutes with running buffer. The flush procedure between runs was for 2 minutes with 0.1 N sodium hydroxide, 4 minutes with deionized water, 3 minutes with running buffer, and a 90 second application of 15 kV between the inlet and outlet. Column void time (t_0) was marked by a baseline solvent disturbance resulting from the inclusion of mesityl oxide in most sample solutions. Mobilities of the anionic Dns-amino acids were calculated from migration times after adjusting for electroosmotic flow, EOF. The mobility is expressed in $\text{m}^2 \cdot \text{min}^{-1} \cdot \text{V}^{-1}$ units and for the sake of simplicity they are given as absolute values.

3.2.3 Molecular Modeling

The modeling experiments were performed using Sybyl 6.6 molecular modeling software (122) and run on a Silicon Graphics Octane workstation with dual 270 MHz MIPS processors and 768 MB RAM. The Dns-amino acids were constructed with the SKETCH feature in Sybyl. The CD molecules were built by using SKETCH to modify β -CD and γ -CD structures obtained from the Cambridge Crystallographic Data Center's structural database. The molecules were then structurally minimized in a water environment using the Sybyl MAXIMIN2 function with the Tripos force field and the Geistiger-Huckel charge calculation method. A program called MOLCAD that provides a measure of a molecule's hydrophobicity was used to generate the depiction in Figure 3.6. Sepaniak group member, Shannon Fox, assisted modeling studies in this chapter.

A macro program was written in Sybyl Programming Language to achieve grid search docking for each amino acid with the different CDs. This program systematically translates and rotates the amino acid into the cavity of the CD as described in previous work (123). Each CD was minimized 1000 times in a water environment. The centers of mass were used to aid in the alignment of the amino acid and CD prior to docking. Each Dns-amino acid was translated from -10.0 \AA out of the CD cavity to 0 \AA in increments of -0.1 \AA . At each of these translational positions, the solute was rotated 360 degrees, in increments of 5 degrees. The solute-CD complex configuration was energy minimized using 250 iterations at each step with the dielectric constant set to 20. Further details on these approaches to molecular modeling can be found in reference 123.

3.2.4 Computational Methods

Plots of mobility versus CD concentration that appear in this paper were generated using the TableCurve 3.0 plotting program developed by Jandel Scientific (San Rafael, CA USA). TableCurve fits the data to many equations in its database and ranks the equations by goodness of fit and the selected values for each of its constants are based on the best fit for the curve of observed mobility versus CD concentration. The MultiSimplex Lite program used for the simplex procedure was purchased from MultiSimplex AB (Karlskrona, Sweden). This software uses an optimization algorithm patterned after that developed by Betteridge (124). Mobility, resolution, and a chromatographic response function (CRF) are calculated using Microsoft Excel programs.

CRF values are calculated after each optimization step and serve as a measure of the success of the separation. The CRF is defined by Equation 3.1:

$$(3.1) \text{ CRF} = a \sum \ln R_{so}/R_s + b \sum \ln R_s/R_{so}$$

wherein a and b are operator selectable numbers. R_{so} is optimal resolution (1.5 used in this work) and R_s is the resolution between any two neighboring peaks. The operator selectable numbers (a and b) can play an important role in the separation by placing more weight on a certain term in the CRF equation. CRF values as computed via Equation 3.1 are always negative and approach zero when each pair of adjacent peaks is optimally resolved. The excess resolution factor (a term) weights those peaks with $R_s > R_{so}$ (1.5) and determines the penalty for excess resolution. The bounds of the a parameter are set

on the low end by long analysis times and at the high end by the complexity of the sample. A value of 5 worked well in this application. The overlap degradation factor b is the selectable number that determines the CRF penalty for inadequately resolved peaks, which in most cases will involve enantiomer resolution. We have found that higher numbers for the overlap degradation factor (50 used herein) are better because insufficient resolution can dramatically affect a separation but the a and b terms in Equation 3.1 can be adjusted to suit the needs of the operator. Simplex methods can be employed for optimizing separation conditions (125). The simplex program supplies three sets of CD concentrations as possible conditions for the separation. Excel programs generate mobility and resolution for the amino acid enantiomers and a CRF value is generated from Equation 3.1 for each of the first three sets of CD concentrations. Typical plate counts per meter were 350,000 and this value was used when calculating resolution. The program generates the next set of conditions for β and γ -CD concentrations using simplex optimization. If the conditions are within experimental boundaries a new set of calculations from these conditions are generated along with a new CRF value. This process continues on until an optimum is obtained.

3.3 Results and Discussion

3.3.1 Mobility and K_c Data

The observed mobility of an analyte (μ_{obs}) depends on its distribution between the free and complexed forms as seen in Equation 3.2 (126).

$$(3.2) \quad \mu_{\text{obs.}} = \frac{\mu_f + \mu_c K_{\text{CD}} [\text{CD}]}{1 + K_{\text{CD}} [\text{CD}]} \quad \text{with} \quad K_{\text{CD}} = \frac{[\text{CD-analyte}]}{[\text{CD}] [\text{analyte}]}$$

In this expression the μ_f term is the apparent free mobility of the analyte, the μ_c term is the apparent mobility of the analyte-CD complex, and K_{CD} is the inclusion constant. It is expected that μ_f and μ_c will be equal for pairs of enantiomers since these analytes are mirror images. However, results obtained in our laboratory indicate that μ_c is not always the same for the D and L enantiomers of certain amino acids (the diastereomer complexes can have slightly different mobilities). Nevertheless, $\Delta\mu_{\text{obs}}$ (difference in mobility for enantiomer pairs) is primarily influenced by differences in K_{CD} values.

Separation performance was evaluated over a range of β -CD and γ -CD concentrations. At high CD concentrations many enantiomers co-migrate which is most likely due to the enantiomers becoming fully complexed at such high CD concentrations and, therefore, their mobilities ($\mu_{c,L}$ and $\mu_{c,D}$) are equal or nearly equal. In some cases the enantiomers of two different amino acids will co-migrate (116, 127). An example of the difficulty of enantiomeric separation of all the amino acid pairs with only γ -CD can be seen in Figure 3.1 in which the L-enantiomer of Dns-Leu co-elutes with the D-enantiomer of Dns-Val. The one amino acid that is problematic is Dns-Ser; no enantiomeric resolution is possible when γ -CD is used, very little when both γ -CD and β -CD are used, and only partial resolution is observed with β -CD alone.

Figure 3.2 and Table 3.1 contain data from studies on the effect of β -CD and γ -CD concentration on the mobility of the Dns-amino acids. The figure illustrates μ_{obs} for the Dns-Glu enantiomers over the range of 0 to 15 mM β -CD. The value of μ_{obs}

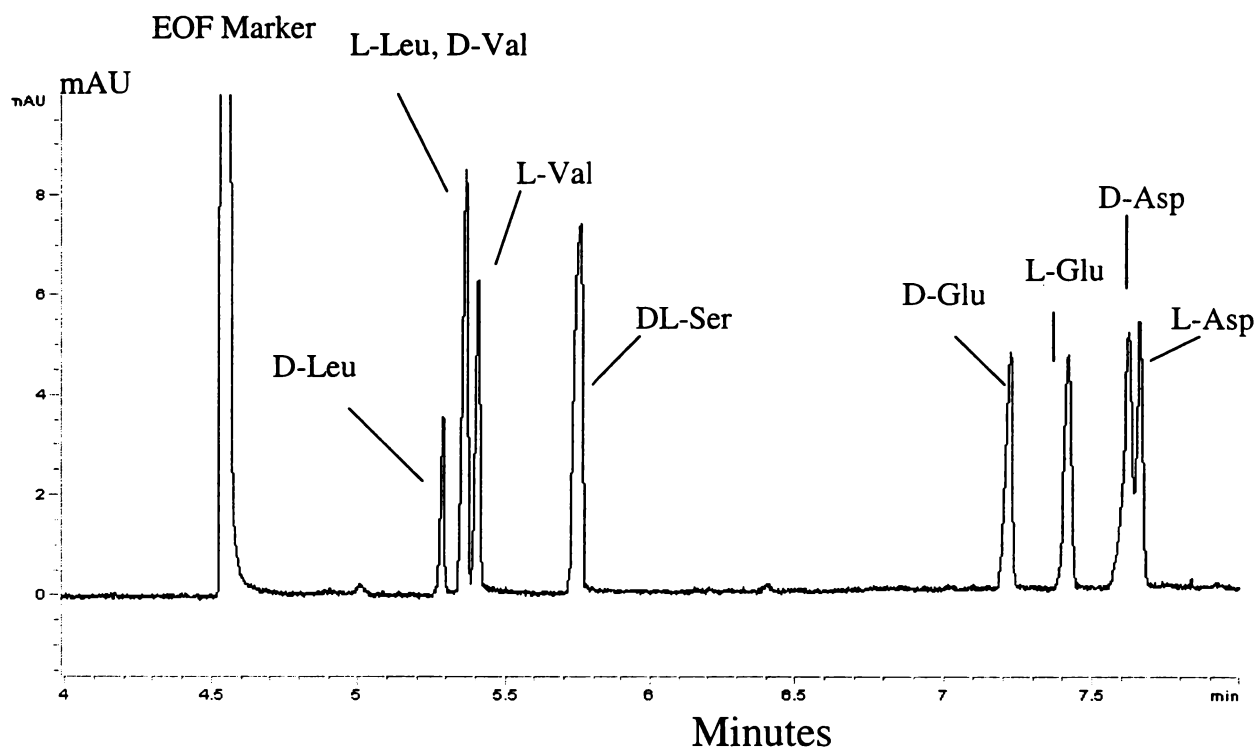


Figure 3.1 Separation of five dansylated amino acid enantiomers. Separation conditions: 60 cm capillary, 16 kV, 8.5 mM γ -CD in phosphate/borate buffer, injection for 4s at 15 mbar.

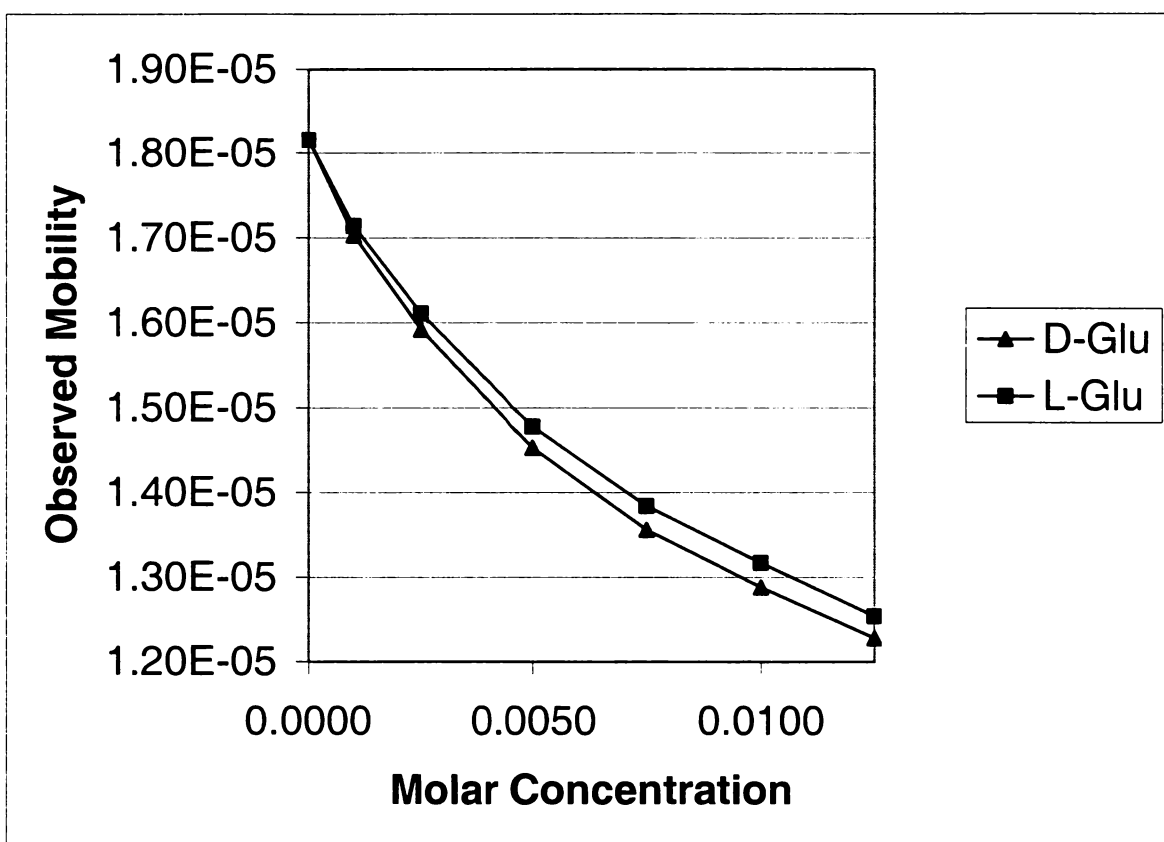


Figure 3.2 Plot of the observed mobility of Glutamic acid enantiomers vs molar concentration of β -CD. Experimental conditions same as in Figure 3.1. Curves plotted based on equation 3.2 yielding correlation coefficients of 0.9995.

Table 3.1 Mobility and K_c Data for Amino Acids with Beta and Gamma Cyclodextrin

β-CD data for dansyl amino acids					
	μ_f	K_c	K_{cD}/K_{cL}	μ_c	μ_{cD}/μ_{cL}
D-Leu	9.70E-7	167	1.12	3.65E-7	0.978
L-Leu	9.67E-7	150		3.74E-7	
D-Val	9.83E-7	202	1.28	4.54E-7	1.05
L-Val	9.87E-7	158		4.34E-7	
D-Ser	1.05E-6	146	1.15	4.50E-7	1.04
L-Ser	1.05E-6	127		4.35E-7	
D-Glu	1.81E-6	120	1.15	8.49E-7	1.02
L-Glu	1.81E-6	104		8.35E-7	
D-Asp	1.88E-6	124	1.17	8.57E-7	0.997
L-Asp	1.88E-6	105		8.59E-7	
γ-CD data for dansyl amino acids					
	μ_f	K_c	K_{cD}/K_{cL}	μ_c	μ_{cD}/μ_{cL}
D-Leu	7.33E-7	51.0	0.995	2.38E-7	1.07
L-Leu	8.02E-7	51.3		2.24E-7	
D-Val	8.06E-7	56.6	1.01	2.52E-7	1.03
L-Val	8.39E-7	56.2		2.45E-7	
D-Ser	1.01E-6	36.1	1.00	1.99E-7	1.00
L-Ser	1.01E-6	36.1		1.99E-7	
D-Glu	1.74E-6	31.4	1.22	3.59E-7	1.17
L-Glu	1.77E-6	25.7		3.06E-7	
D-Asp	1.83E-6	24.4	1.05	2.81E-7	1.04
L-Asp	1.83E-6	23.4		2.71E-7	

decreases as the degree of complexation with the large molecular weight neutral CD increases and the mobility difference between the enantiomers increased in the range that we employed for β -CD. The table shows mobility and K_c data over the range of 0 to 15 mM for β -CD and 0 to 100 mM for γ -CD. A good fit was obtained by the plotting program that employed an expression of the form: $y = (a + cx)/(1 + bx)$ (see Equation 3.2). The values of μ_f , μ_c , and K_c were generated from the constants supplied by the TableCurve fitting program from mobility data covering the full range of β -CD and γ -CD concentrations. Values of μ_f obtained with runs without CD present agreed with curve fit values within 1% for β -CD but had a discrepancy of 10% for γ -CD. The last two columns in the table illustrate the analyte-CD complex mobility and complexed mobility ratios for the enantiomers. It is obvious in the β -CD data that the K_c values for the D enantiomers are larger than for the L enantiomers and that the complexation constant ratio plays a more important role than the complexed mobility ratio for enantiomeric separation. However, in the case of the γ -CD data it seems that there is not much difference in K_c values for each enantiomeric pair except for Dns-Glu. It is also important to note that the K_c values for the γ -CD complexes are much smaller than the K_c values for the β -CD complexes. This suggests that the amino acid fits more sloppily into the larger cavity provided by the γ -CD. Hence, the intermolecular interactions are weaker and this may also contribute to poorer selectivity as reflected in complexation constant ratios near 1.0.

3.3.2 Use of the Simplex Method and CRF Values

Trial and error approaches of finding the appropriate running buffer concentration for enantiomeric separations can be very time consuming. Furthermore, the challenge is increased in proportion to the number of enantiomeric pairs present in the sample.

Simplex methods can locate the true optimum of a response with fewer trials than non-systematic approaches or one variable at a time methods (128). The simplex method has been used for previous applications such as the separation of DNA fragments (129), the achiral separation of amino acids by multidimensional thin layer chromatography (130), and the achiral separation of phenylthiohydantoin (PTH) amino acids by MECC (131). The use of the simplex method with amino acids as a test case is appropriate for quickly determining the optimum concentrations of CDs needed for complex mixture enantiomeric separation. These separations can be complex due to the need for chiral resolution between individual enantiomers and achiral separations of the different compounds in the mixture.

An equation was generated for the calculation of analyte mobility when two CDs are present in the running buffer. In the case of a β - and γ -CD system the observed mobility of an analyte [A] is given by Equation 3.3.

$$(3.3) \mu_{\text{obs}} = f_{\text{rb}}\mu_f + f_{\beta\text{-CD}}\mu_{\text{c}\beta\text{-CD}} + f_{\gamma\text{-CD}}\mu_{\text{c}\gamma\text{-CD}}$$

The f_s are the fractional amounts of the analyte associated with the phases involved (running buffer or CDs) and the μ_s are the apparent mobilities of the analyte when fully

associated with those phases. The final expression for analyte mobility with our two CD system is given by Equation 3.4.

$$(3.4) \mu_{\text{obs}} = \frac{\mu_f + K_{\beta\text{-CD}}[\beta\text{-CD}]\mu_{c\beta\text{-CD}} + K_{\gamma\text{-CD}}[\gamma\text{-CD}]\mu_{c\gamma\text{-CD}}}{1 + K_{\beta\text{-CD}}[\beta\text{-CD}] + K_{\gamma\text{-CD}}[\gamma\text{-CD}]}$$

To apply this equation to other CDs, it is only necessary to determine the appropriate complexation constants and complex mobilities. Furthermore, an expression could be developed for three or more CDs in the running buffer. When using multiple CDs it is assumed that the effects of the CDs on mobilities are additive and the CDs do not interact with each other. The ranges employed in the simplex were 0 to 15 mM for β -CD due to its limited solubility and 0-30 mM for γ -CD due to poor CRF values at high concentrations of γ -CD.

Some example data from the simplex method can be seen in Table 3.2 with the corresponding CRF values. Three conditions from the simplex table, poor, moderate, and good CRF values, were evaluated experimentally. It can be seen from Figure 3.3 that the experimental results concur with the predictions from the simplex. The first separation in Figure 3.3 (Table 3.2, trial 4) shows that the Dns-Val enantiomers are very poorly resolved and the Dns-Leu enantiomers co-migrate. A poor CRF was the result for this condition due to the large penalty for insufficient resolution. In the second separation in Figure 3.3 (Table 3.2, trial 9) it can be seen that now Dns-Leu is somewhat resolved and Dns-Val is resolved better than it was in the first separation in the figure. The CRF was

Table 3.2 Selected Data Points from the Simplex Method With CD Concentrations in mM

Trial number	[β-CD]	[γ-CD]	CRF
1.	0	0	undefined
2.	9.7	7.8	-253.7
3.	2.6	29.0	-491.1
4.	12.3	36.8	-509.6
5.	9.2	27.6	-545.4
8.	11.1	17.4	-444.7
9.	7.45	18.9	-425.5
10.	13.3	9.5	-300.8
13.	7.7	11.3	-279.8
15.	3.5	2.7	-236.0
23.	6.7	2.5	-205.2
26.	8.1	4.4	-220.7
28.	4.6	2.1	-208.0
30.	5.7	1.4	-200.6
33.	5.8	1.8	-201.3
34.	6.0	0.7	-200.3
39.	5.8	0.8	-200.2
*45.	5.8	0.9	-200.2
46.	5.7	0.9	-200.3
*48.	5.8	0.9	-200.2

* Denotes optimum separation conditions according to the Simplex

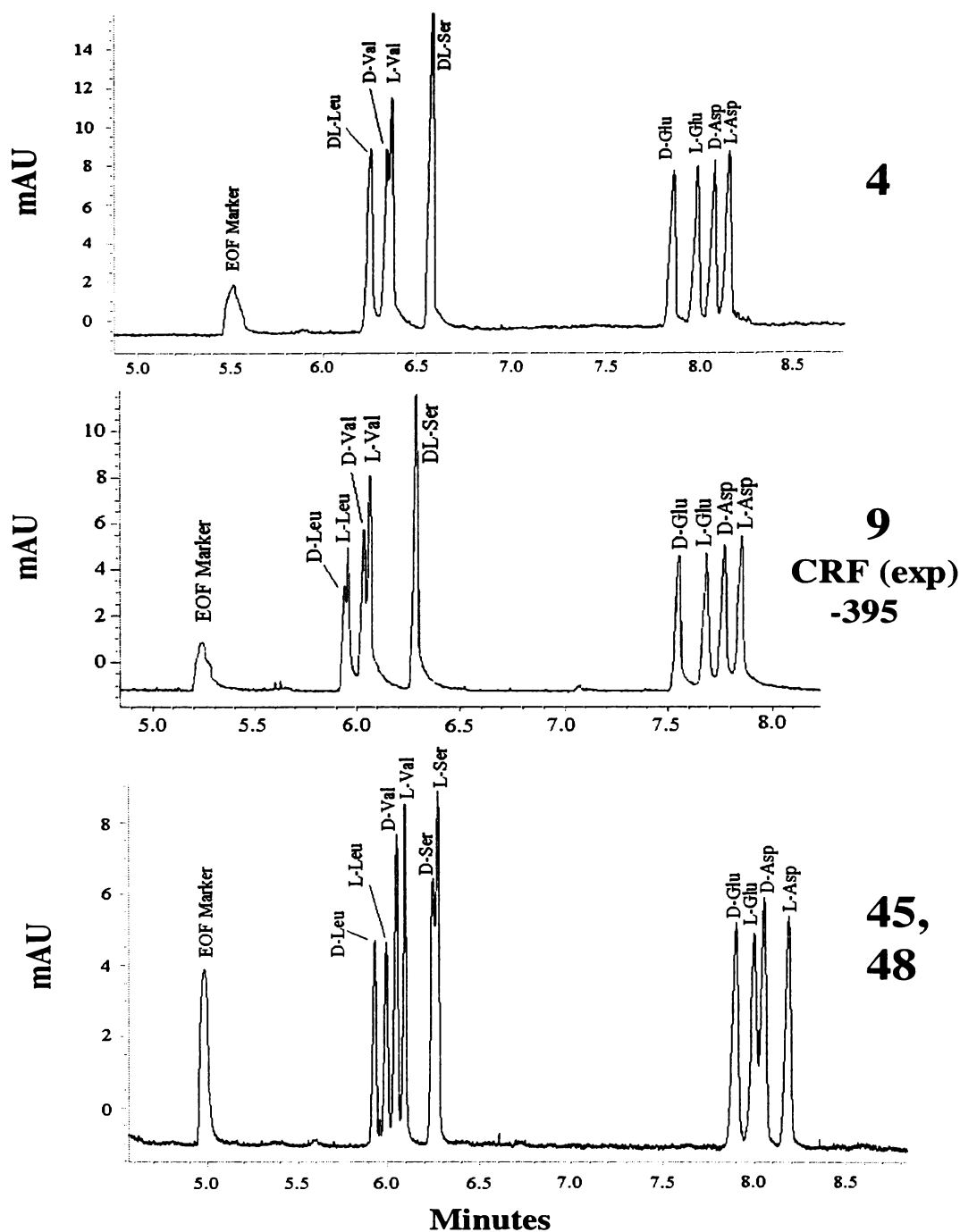


Figure 3.3 Examination of the simplex predictions from Table 3.2 with the separation of amino acids at various CD concentrations. Experimental conditions same as in Figure 3.1. Figure 3.3 top: 9.2 mM β -CD and 27.6 mM γ -CD. Figure 3.3 middle: 7.45 mM β -CD and 18.9 mM γ -CD. Figure 3.3 bottom: 5.8 mM β -CD and 0.9 mM γ -CD. An experimental CRF value is shown for the middle separation.

calculated (Table 3.2, trial 9) using experimentally observed resolution. The experimental (-395) and Equation 3.1 (-425) CRF values agree reasonably well considering the inaccuracy in graphically computing resolution from electropherograms such as these. It should also be noted that the correlation coefficients are not as good for the Dns-Leu and Dns-Val data with γ -CD in Table 3.1 and this could explain why there is a slight difference between the CRF values mentioned above. The bottom separation in Figure 3.3 illustrates that the best conditions predicted by the simplex (Table 3.2 trials 45, 48) provides a superior separation of the amino acids because the enantiomers of Dns-Leu and Dns-Val are resolved and the enantiomers of Dns-Ser show slight resolution. The conditions at the bottom of Figure 3.3 demonstrate that a low concentration of γ -CD is beneficial for the separation of the early eluting enantiomers. This is consistent with the data in Table 3.1 because the K_c values are similar for the enantiomers of Dns-Leu and Dns-Val with γ -CD and therefore high concentrations of γ -CD lead to bunching up of the early eluting enantiomers. Finally, we observed that the use of two CDs in the running buffer does provide a better separation than when only one CD is used.

3.3.3 Studies With Modified Single Isomer Cyclodextrins

Several CDs were used in preliminary studies to determine if they could provide resolution of Dns-amino acid enantiomers. The important factors in determining resolution of enantiomers in these studies are efficiency (uniformly high in this work), selectivity, the ability to manipulate the CD-enantiomer equilibrium to produce a suitable balance between free and complexed forms (poor inclusion into the CD or low CD solubility can be limiting factors), and an appreciable difference in free and complexed

mobilities (an elution window consideration). It is thought that inclusion complex formation between CDs and CD derivatives and Dns-amino acids occurs by inclusion of the dansyl moiety into the cavity. Differences in inclusion constants are attributed to different interactions between the carboxylate and amino acid side chains especially with the secondary hydroxyl groups at the C2- and C3- positions of the CD (107). This situation is depicted in Figure 3.4 and it aids in the visualization for the molecular modeling of amino acids with the cyclodextrin.

Figure 3.5A shows a separation without any CD present in the running buffer. β -CD used alone is able to provide some enantiomeric resolution of all the amino acids (although not as good as certain β - and γ -CD combinations) and good inclusion is seen based on the analyte mobility change upon addition of this CD (Figure 3.5B). The derivatized CDs employed in our studies were all single-isomer because their use facilitates reproducible separations and molecular modeling. It should be noted that most commercial CD derivatives consist of mixtures having different degrees of substitution. One exception is commercially available, single-substituted 1-CM- β -CD, which has been successfully employed for the separation of neutral solutes and seemed to be a reasonable candidate for testing in this work. This CD exhibits fair inclusion with the amino acids as well but it does not provide enantiomeric resolution as seen in Figure 3.5C. This could be due to the narrow elution window that is found with this -1 charged CD. That is to say $\mu_c - \mu_f$ for β -CD and 1-CM- β -CD are both positive but larger for β -CD. It is unlikely that pH adjustment would improve the situation. HDMCM- β -CD (-7 charge) as

DNS-aspartic acid

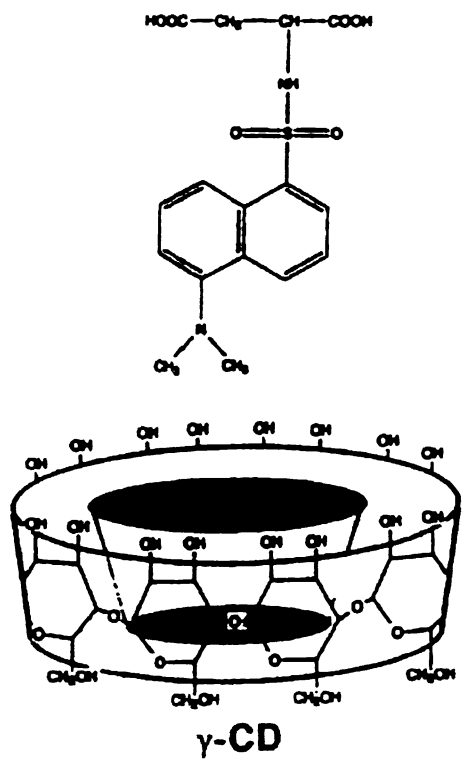


Figure 3.4 Depiction of Dns-Asp with the Dns group poised to insert into the cavity of γ -CD. Secondary hydroxyl groups (two per sugar) are shown on the truncated bottom of the CD.

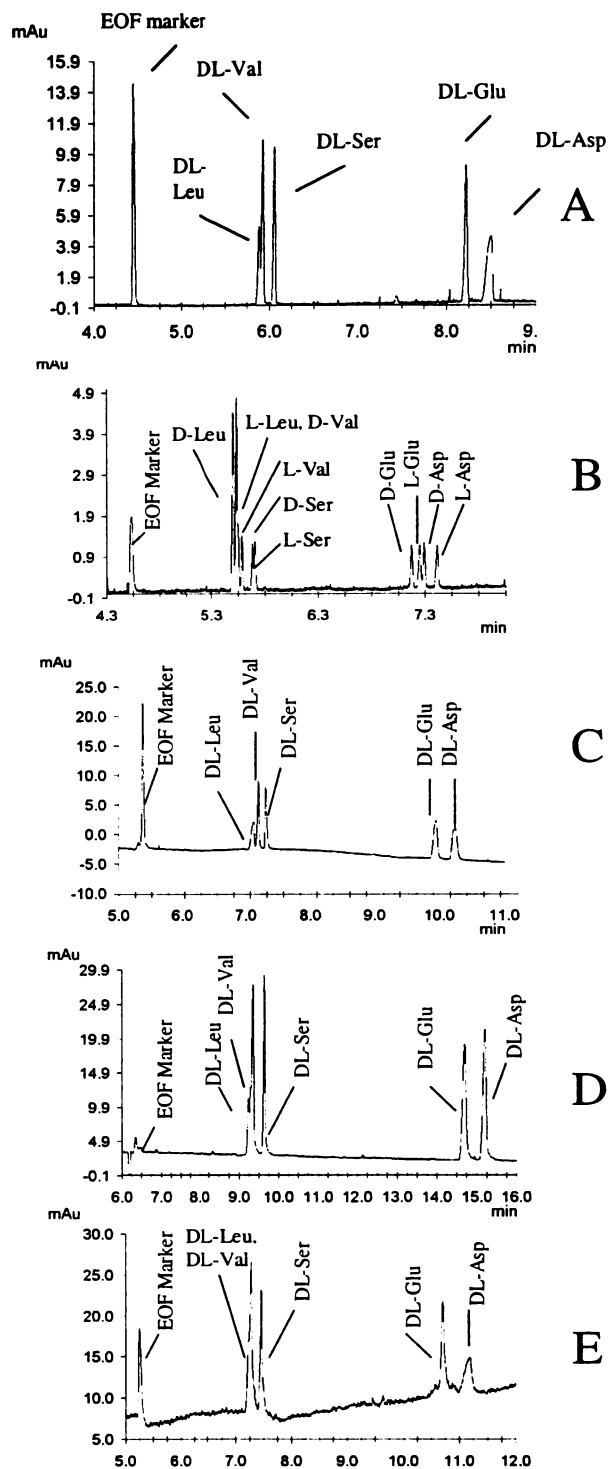


Figure 3.5 Separations of amino acids with various cyclodextrins with the experimental conditions the same as in Figure 3.1. Figure 3.5A: No CD present. Figure 3.5B: 5 mM β -CD. Figure 3.5C: 5 mM 1-CM- β -CD. Figure 3.5D: 5 mM HDMCM- β -CD. Figure 3.5E: 5 mM 16-me- γ -CD.

synthesized in our laboratory by Sepaniak group member, Mustafa Culha, has been used for the separation of naphthalene compounds (121). It was tested because of the presence of the naphthalene ring in the dansyl group of the amino acids. This CD should provide a large separation window ($\mu_c - \mu_f$ is negative and large) due to its high negative charge. However, HDMCM- β -CD (Figure 3.5D) did not provide enantiomeric resolution probably due to electrostatic repulsion that occurs between the negatively charged Dns-amino acids and the highly negative charged HDMCM- β -CD. When adjustments are made for EOF variability the effect of HDMCM- β -CD on the observed mobilities of the amino acids is much smaller than for β -CD. Without a good level of inclusion there can be no enantiomeric resolution.

16-me- γ -CD (also synthesized in our laboratory) did not provide enantiomeric resolution and, surprisingly, also did not provide very good inclusion of the amino acids (Figure 3.5E). A methylated CD seemed to be a plausible buffer additive because it was thought that the naphthalene ring of the amino acid would favorably include into the nonpolar environment of the methylated CD. Regarding enantio-selectivity, it has been found that methylation affects the steric and/or hydrogen bonding interactions between the CD and the analyte. Yoshinaga et al. found that there is major participation of the secondary hydroxyl groups in the chiral recognition process (107). They found that methylation of the C2 hydroxyl groups in β -CD resulted in the absence of enantiomeric resolution except for Dns-DL- α -amino butyric acid. We anticipated that a similar absence in enantiomeric resolution might be observed for our fully methylated γ -CD product, especially since native γ -CD was somewhat less effective than the smaller β -CD.

However, the issue of enantio-selectivity never came into play as we found that the mobilities with 16-me- γ -CD present in the running buffer were similar to the mobilities in the absence of CD, implying only small inclusion with the amino acids and 16-me- γ -CD (see further discussion in Section 3.3.4). Moreover, inclusion cannot be forced by employing high CD concentration because of solubility limitations.

3.3.4 Molecular Modeling of Various Cyclodextrins

An amino acid (valine) was docked into five different single isomer CDs as described in the experimental section. The interaction energies (kcal/mol, average of D & L forms) of the amino acid with the five CDs were as follows: -36.3 (β -CD), -35.0 (γ -CD), -29.3 (1-CM- β -CD), -17.3 (HDMCM- β -CD), and -28.4 (16-me- γ -CD). It should be stated that with quick grid search docking using only 250 minimizations at each grid position the listed relative interaction energies are very approximate (123). Molecular modeling was not performed to study enantio-selectivity in this work because the subtle differences in interactions between CDs and enantiomer pairs would require extremely long, comprehensive modeling approaches (123). It can be seen that native β - and γ -CD have the best interactions with the amino acid possibly due in part to hydrogen bonding between the amino acids and the secondary hydroxyls. In agreement with the experimental data in Table 3.1 the inclusion with β -CD is stronger. 1-CM- β -CD produced an interaction energy that is lower than β -CD, again consistent with experimental findings. Despite the expected substitution of the carboxymethyl group at the C6 primary hydroxyl site (confirmed by NMR), electrostatic repulsion between the similarly charged CD and Dns-amino acid may contribute to the less favorable

interaction energy. The weaker interaction and possible changes in selectivity (relative to native β -CD) are probably less of an issue in terms of enantiomeric resolution with 1-CM- β -CD than the limited elution window (see above). The poorest interaction energy of all was with HDMCM- β -CD (-7 charge) and this partially explains the lack of enantiomeric separation observed experimentally with this CD; although enantioselectivity could also be compromised with the extensive functionalization of this CD.

A comparison of the molecular modeling and experimental findings for 16-me- γ -CD reveals both the value and potential pitfalls of elucidating modes of molecular recognition using modeling approaches. The interaction energy listed above for Dns-Val with this CD is more favorable than with 1-CM- β -CD, yet it exhibited negligible effect on the mobility of the amino acid. This contradiction was resolved by searching for less inclusion-friendly conformations of the 16-me- γ -CD. The minimized open structure shown in Figure 3.6A was used in initial work. By manipulation of the methyl groups inward, another conformer was achieved as shown in Figure 3.6B. The minimized energy of this structure was approximately 1.6 kcal/mol more favorable than the initial Figure 3.6A structure and showed significant van der Waals stabilization, presumably due to intramolecular interactions between the various methyl groups located at the C2 and C3 positions. The local energy minimum structure in Figure 3.6A may have converted to the lower energy conformer in Figure 3.6B with more minimization steps (123). Simulated annealing may be used also to locate the lower energy conformer. The closed cavity of the conformation in Figure 3.6B does not appear to be conducive to inclusion. Moreover, we have noted under certain conditions inter-CD interactions that inhibit inclusion (121). One can envision in an aqueous environment, inter-CD van der

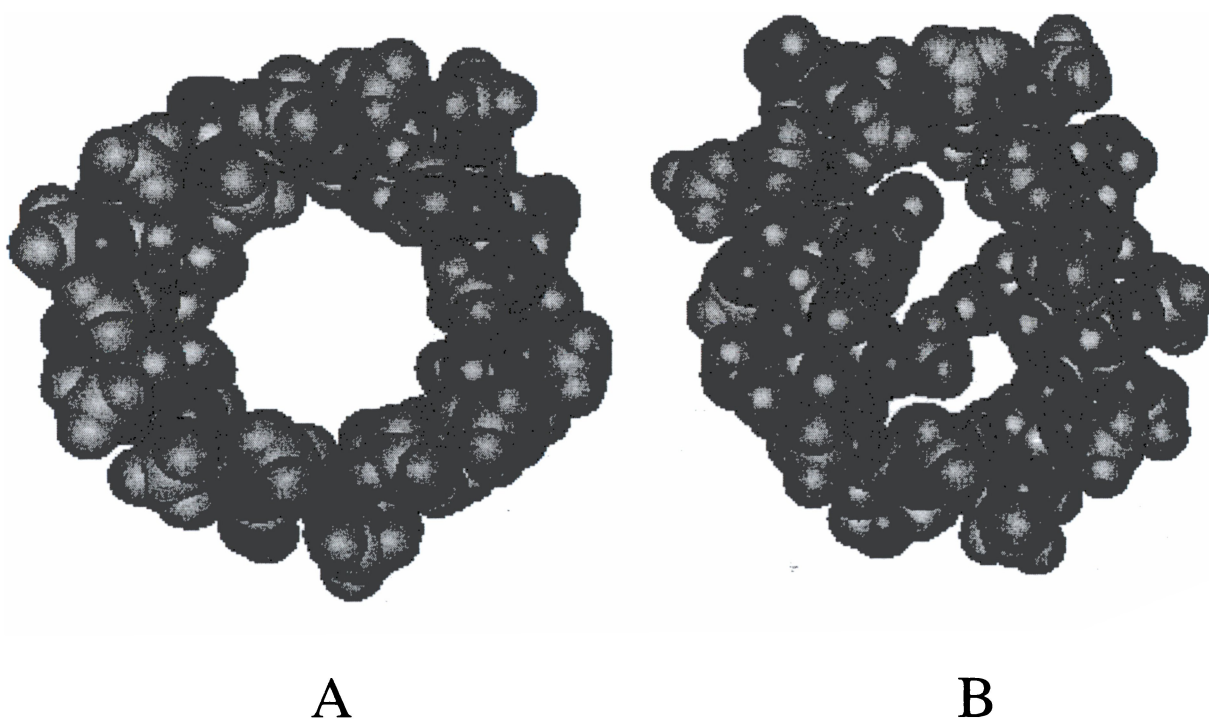


Figure 3.6 Space filled model depictions of the open (A) and closed (B) cavity 16-me- γ -CD conformations used in modeling studies. View is from the top (methylated at C2 and C3 positions) of the CD.

Waals interactions between the lipophilic C2 and C3 methylated portions of two (or more) 16-me- γ -CDs, thereby limiting analyte access to CD cavities. Although none of the derivatized CDs studied herein (Figure 3.5) showed potential for Dns-amino acid enantiomeric separations, the correlation with modeling work illustrates its value.

3.4 Future Work

In our work there were two cyclodextrins present in the running buffer. An interesting idea to try would be to put three cyclodextrins in the running buffer. An equation for mobility with this case could be generated as was done for our two-cyclodextrin system. The equation for the three CD system would be:

$$(3.5) \quad \mu_{\text{obs}} = \frac{\mu_f + K_{\text{CD1}}[\text{CD1}]\mu_{\text{cCD1}} + K_{\text{CD2}}[\text{CD2}]\mu_{\text{cCD2}} + K_{\text{CD3}}[\text{CD3}]\mu_{\text{cCD3}}}{1 + K_{\text{CD1}}[\text{CD1}] + K_{\text{CD2}}[\text{CD2}] + K_{\text{CD3}}[\text{CD3}]}$$

Chromatographic response function (CRF) values could be generated as before and the optimum separation conditions could be located by the Simplex in a short period of time. In this case, the Simplex would require four sets of CD concentrations. Various CRF values generated by the Simplex could be tested with the CE instrument to check the accuracy of the predictions of the Simplex. More solutes could be added to the mixture to determine if the Simplex still functions properly with a more complicated mixture. There were five enantiomeric pairs in our mixture but it would be more interesting to see if even more pairs could be separated successfully. A final idea would be to use a real sample such as a physiological one that contains amino acids and employ the Simplex

method to locate the optimum separation conditions. In all of our work, the amino acids were dansylated and therefore the amino acids in the real sample would need to be dansylated as well in order to use the inclusion constant and mobility data that was previously mentioned in this work.

The molecular modeling in this work was somewhat limited due to the excessively long time that it takes for the docking of these solutes into a cyclodextrin. There were five amino acid enantiomeric pairs that were docked in these studies and each pair took a couple of days for completion. Comprehensive docking of each enantiomeric pair would provide a more accurate result for the molecular modeling of these amino acid enantiomers. It would take a couple of months to do this comprehensive docking because the computing time is fairly significant. The comprehensive docking procedure may help to elucidate further the results for the methylated cyclodextrin. Also, in our studies we did not consider the solvent since this would have greatly increased the computational time as well. The limitation of not considering the solvent is that the random interactions of the solvent with the CD are not considered in our studies. In the quick grid search docking that we did the conformer was open and falsely lead us to believe that the methylated CD would be a good candidate for the separation of dansylated amino acids. If we had performed comprehensive docking then the closed methylated CD conformer of lower energy would have been found instead of the open conformer.

One disadvantage of minimization algorithms is their inability to distinguish between absolute and local minima, which is probably what occurred with the methylated CD. Hence, the conformation that is generated by the minimization

procedure may not necessarily represent the most probable conformation of the molecule. The simulated annealing algorithm was used to locate the closed methylated CD conformer and this algorithm applies a high temperature to surmount the torsional barriers of the system. The applied energy is removed by reducing the temperature in order to obtain a reasonable structure. The annealed molecules are re-minimized to ensure that the true low energy state is found. This annealing approach accelerates the sampling of the conformational space that aids in overcoming the problem of multiple minima. Comprehensive docking would also allow for more subtle information in terms of the enantiomeric interaction between the amino acids and the CDs. This could allow for further information on why a certain amino acid had a larger inclusion constant or why the two enantiomers of dansyl serine have the same inclusion constant with gamma CD. Sulfated CDs have been used in the literature for separations and these could be used in our molecular modeling studies as well (132-146). The sulfated CDs would then be used for separations of these amino acids to see if they could provide enantiomeric resolution. The molecular modeling results would then assist in the explanation of the quality of the separation provided by the sulfated CDs by looking at their interaction energies.

3.5. Concluding Remarks

This chapter presents the separation of mixtures of Dns-amino acid enantiomers with native CDs and the subsequent determination of mobility and K_c data. An equation was developed to predict the analyte mobility for a two CD system in the running buffer. The best separation conditions were quickly located with the use of a

Simplex optimization method. Various conditions from the simplex data were tested to see if a CRF used in this work was an accurate measure of the quality of the separation. It was found that the predictions from the simplex agreed with the experimental results obtained with the CE instrument. These studies should provide researchers with useful information when attempting to optimize separation conditions for complicated mixtures in a short period of time. A few additional commercial or synthesized single isomer CDs were evaluated as to their potential for Dns-amino acid separations with disappointing results. Poor separations of enantiomers can be attributed to factors such as elution window reduction, poor inclusion, and/or loss of enantio-selectivity. Molecular modeling studies were informative with regard to poor inclusion and could provide insights into enantio-selectivity in future studies.

Chapter 4. Raman Theory and Surface Enhanced Raman Spectroscopy with Capillary Electrophoresis

4.1 Raman Theory

If light impinges on any molecular system a small amount of it is scattered at the same frequency as the incident light (Rayleigh scattering) and an even smaller portion is scattered at frequencies different from the incident frequency (147-149). The fraction of light scattered at optical frequencies different from the frequency of the incident photons is less than one in 1×10^7 photons. The ground state vibrational energy levels of the molecule in question correspond to the frequency shifts in the latter case. This additional type of scattering is due to molecules vibrating at frequencies corresponding to various normal modes of motion. These characteristic vibrational frequencies can interact with the incident light to generate scattered radiation at different frequencies. C. V. Raman first discovered this in 1928 and this effect has utility in the determination of vibrational properties of molecules, which leads to structural information. The difference in energy between the incident photon and the Raman scattered photon is equal to the energy of a vibration of the scattering molecule and can be used as a complement to infrared spectroscopy.

Raman has been used frequently for the study of biological molecules since the early 1970's (150-156). This technique has been used for generating specific bonding arrangements and conformational properties of biomolecules. Raman scattering can be used to discover, explain, or confirm functional mechanisms of biomolecules when structural information is already available. Finally, the physics of scattering processes in

large molecular systems may be studied by the use of Raman for complex biomolecules such as proteins and nucleic acids.

A small amount of light is scattered at a shifted frequency when it impinges on a molecular system. This frequency shift of the scattered light is determined by the energy of one of the normal vibrational modes (147). The equation is shown in 4.1.

$$(4.1) \quad h\nu_i - h\nu_s = E_{q_i}$$

In this equation, ν_i and ν_s are the frequencies of the incident and scattered light, and E is the vibrational energy of a normal mode q_i . The process can be seen for a single vibrational mode in Figure 4.1. In this figure, the ground state vibrational level is designated by g_v and the excited vibrational level by g_v' . The frequency difference between those two states is $\Delta\nu$ and is equal to the frequency difference between the incident and scattered light frequencies. The vibrational energy is dissipated as heat but due to the low intensity of Raman scattering, the heat dissipation does not generate a noticeable temperature rise in a material. The Raman scattering intensity I_s is governed by the proportionality shown in equation 4.2.

$$(4.2) \quad I_s \propto \nu_s^4 I_0 \Delta P^2$$

In this equation, ν_s is the frequency of the Raman scattered photon, I_0 the intensity of the incident photon field, and ΔP is the change in polarizability induced by the vibrational

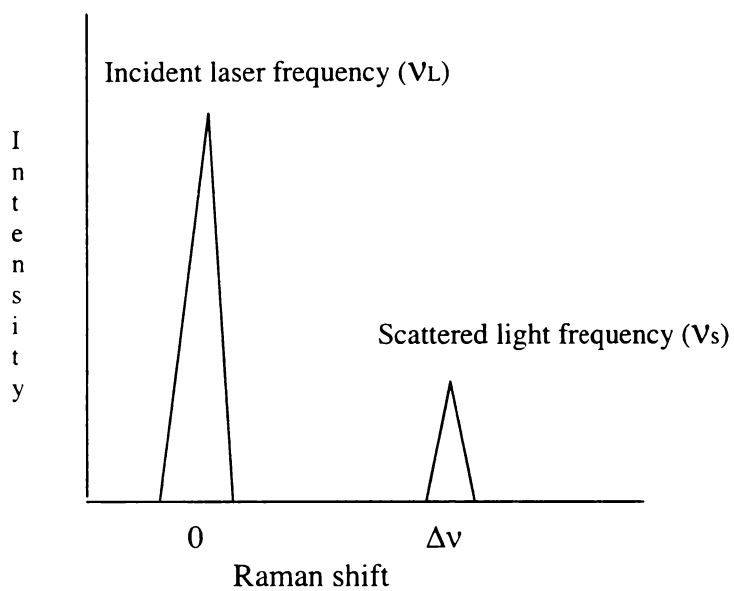
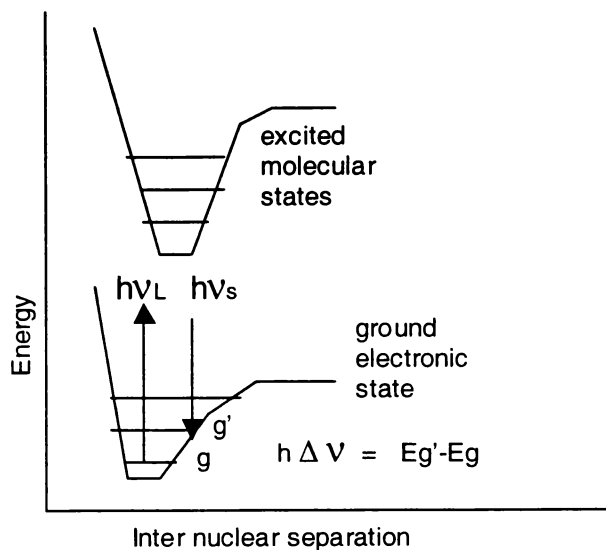


Figure 4.1. Schematic of Raman scattering in which incident laser light beam of frequency ν_L interacts with a molecular system resulting in Raman scattering at frequency ν_s . The difference between the incident and scattered frequencies is $\Delta\nu$, the frequency of a vibrational normal mode of the molecule.

transition (147).

At room temperature, the thermal population of vibrational excited states is low. Hence, the initial state in the scattering process is the ground state. Consequently, the scattered Raman photon will have lower energy (longer wavelength) than the exciting photon. The scattered light that is shifted to frequencies lower than the incident frequency is referred to as Stokes scattered light and anti-Stokes scattering refers to scatter at higher frequencies. An energy level diagram depicting Stokes scattering and anti-Stokes scattering can be seen in Figure 4.2. The Stokes shifted scatter is usually observed in Raman spectroscopy applications. A small fraction of the molecules are in vibrationally excited states and Raman scattering from these molecules can leave the molecule in the ground state. The scattered photon is at higher energy and this anti-Stokes shifted Raman spectrum is usually much weaker than the Stokes shifted spectrum. The ratio of anti-Stokes to Stokes intensity at any vibrational frequency is a measure of temperature, since the intensity of the anti-Stokes scattering is dependent on the thermal population of the vibrational mode g' . The normal mode frequencies that are allowed by symmetry can be detected in the spectrum. A vibration of a given symmetry will be Raman active if it belongs to the same symmetry species as one of the six components of the polarizability tensor. These components transform as the product of two rectangular coordinate axes (x^2 , y^2 , z^2 , xy , xz , and yz). The selection rule for Raman dictates that there must be a change in polarizability during the vibration. An unfortunate limitation of normal Raman scattering is that even transitions that are allowed by selection rules are still very weak. For example, cross sections for fluorescence are typically $\sim 1 \times 10^{-19} \text{ cm}^2$ whereas Raman cross sections are typically $\sim 1 \times 10^{-29} \text{ cm}^2$.

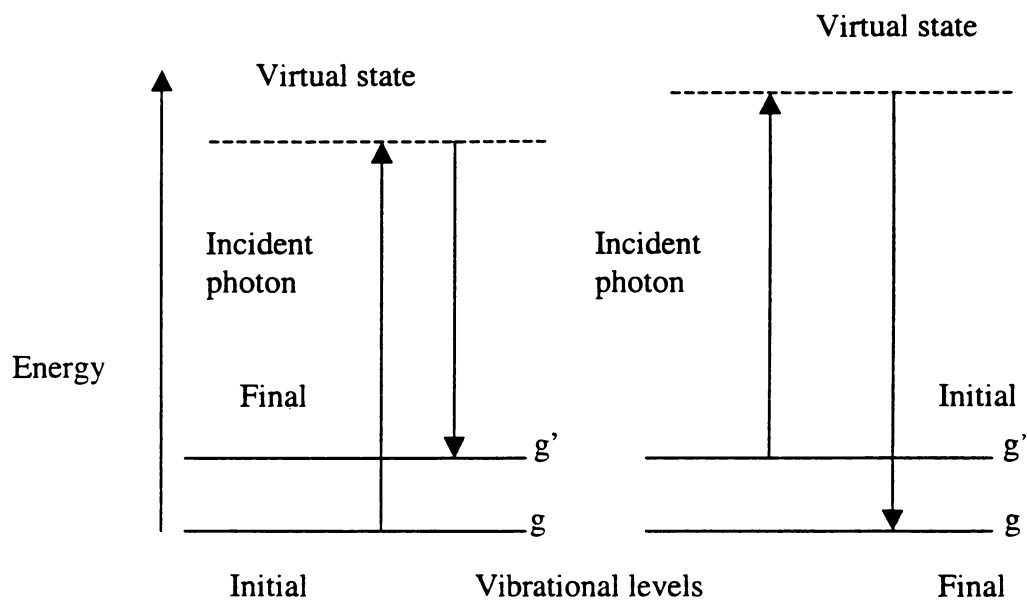


Figure 4.2 Energy level diagram for Raman scattering with Stokes Raman on the left and anti-Stokes Raman scattering on the right.

4.2 Surface Enhanced Raman Spectroscopy

4.2.1 Background and Theory

In the 1970's Fleischmann et al. observed large Raman signals from pyridine adsorbed onto roughened silver electrodes (157). Further studies by Jeannaire and Van Duyne demonstrated the Raman scattering cross section per molecule was enhanced by four to six orders of magnitude compared to pyridine without metal present (158). To this day, the mechanisms for surface enhancement are not completely understood. However, inspection of Equation 4.2 reveals that the intensity of the incident field, or the magnitude of the electricmagnetic field, and the polarizability of the analyte due to the vibration in question are important. It follows that the two most common models of surface enhanced Raman scattering (SERS) focus on these important factors.

The electromagnetic model states that molecules at certain metal surfaces can experience an electromagnetic field that is far greater than that provided by the incident radiation (148-149). The amount of field enhancement depends on factors such as the dielectric properties of the metal, distance from the metal surface, energy of the incident radiation, surface morphology, and size of the surface roughness. Roughened surfaces or isolated nanoscale metal particles are significant because they can enhance Raman scattering by many orders of magnitude. When radiation impinges on the nanoscale metallic particles, conduction electrons move in response to the field causing an oscillating dipole. If the metallic features are largely isolated there is a characteristic resonance frequency for the incident radiation. The resonance frequency depends on the dielectric properties of the particle as well as its size and shape. The oscillating dipole produces a surface plasmon field (basically an electromagnetic field at the characteristic

incident field frequency) that can be extremely intense at the particle surface but decays very rapidly with distance from the surface. It is also possible to observe concerted plasmon related fields between closely spaced nanoparticles. Figure 4.3 depicts such a condition showing extremely intense fields between two spherical nanoparticles. It is this large electromagnetic field near the metal surface in this model that overpowers the low probability of Raman scattering and causes large signal enhancements.

The chemical enhancement model proposes that charge transfer between the metal and solute generates an increase in the value of the transition polarizability (148-149). An interaction between the molecule and the metal results in the molecule being chemisorbed. This process is facilitated by the presence of lone pair electrons in the molecule such as a nitrogen heterocycle. Polyatomic molecules generally have sets of discrete energy levels that are grouped by electronic state and within each state is a series of more closely spaced vibrational levels. Metals have several bands of energy levels and the valence electrons form the conduction band. Frequently, this band is not completely filled with electrons and in silver the conduction bands are derived from the 4s and 4p atomic orbitals. Creighton found that if the energy levels of the pyridine molecule are comparable with those of the metal it can be seen that one electron charge transfer reactions from lower levels of the metal to the adsorbate's empty π^* orbital correspond to visible range photons (159). Charge transfer reactions such as these are expected to produce a large increase in the polarizability of the molecules at the surface if they are exposed to optical fields with frequencies inside the charge transfer band. Other chemically based mechanisms for enhancement have also been proposed (148-149).

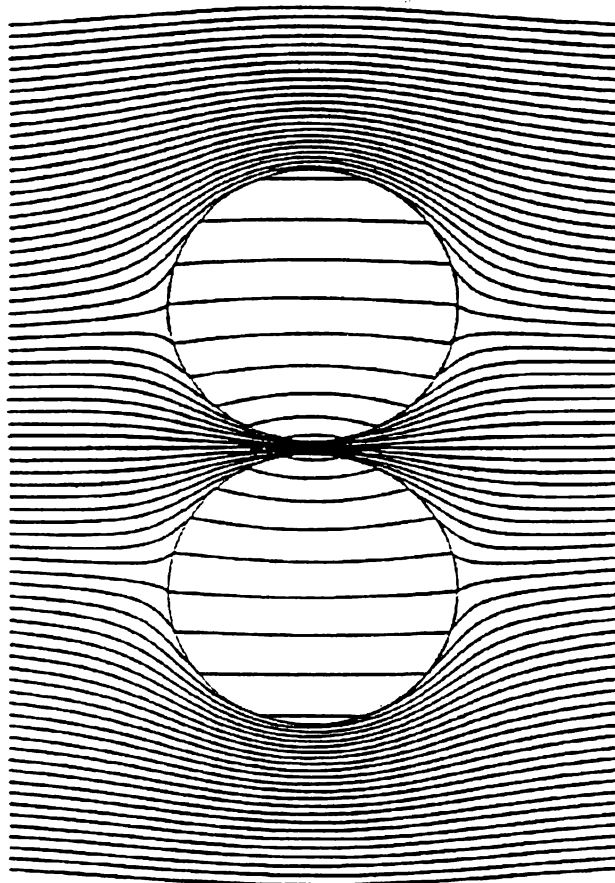


Figure 4.3 Closely spaced metal nanospheres or other shapes can produce large enhancements of incident fields due to concerted plasmon field effects.

Common strong Raman scatterers are molecules with distributed electron clouds such as those present in conjugated systems. The pi-electron cloud of a double bond is easily distorted in an external electric field. Molecules with lone pair electrons also can have strong SERS signals. Aromatic nitrogen or oxygen containing compounds such as phenols or aromatic amines are strongly SERS active. Electron rich functional groups such as carboxylic acids also can be strongly SERS active. A bend or stretch of the bond changes the distribution of electron density and causes a large modification in polarizability. Of the metals commonly used in SERS, scattering is strongest on silver but it is observable on gold and copper. At practical excitation wavelengths, enhancement with other metals is not that significant. The incident wavelength should match the plasmon wavelength of the metal for SERS. The plasmon wavelength is to the red of 650 nanometers for copper and gold.

The basic elements of a SERS experimental configuration are similar to those used in a normal Raman instrument as seen in Figure 4.4. In a typical Raman spectrometer there is a monochromatic radiation source, a sample cell, a monochromator or other wavelength selector, a detector, and amplifier/signal processing components. The monochromatic radiation source is usually a continuous wave laser. The use of a laser source is needed to provide the required power to generate a detectable Raman signal. A filter is placed in the optical path before the focusing lens to eliminate undesirable laser plasma lines. The scattered light is comprised of the intense Rayleigh band at the excitation frequency of the laser and the weaker frequency shifted bands. A holographic notch filter is often employed to remove the incident light of the laser from

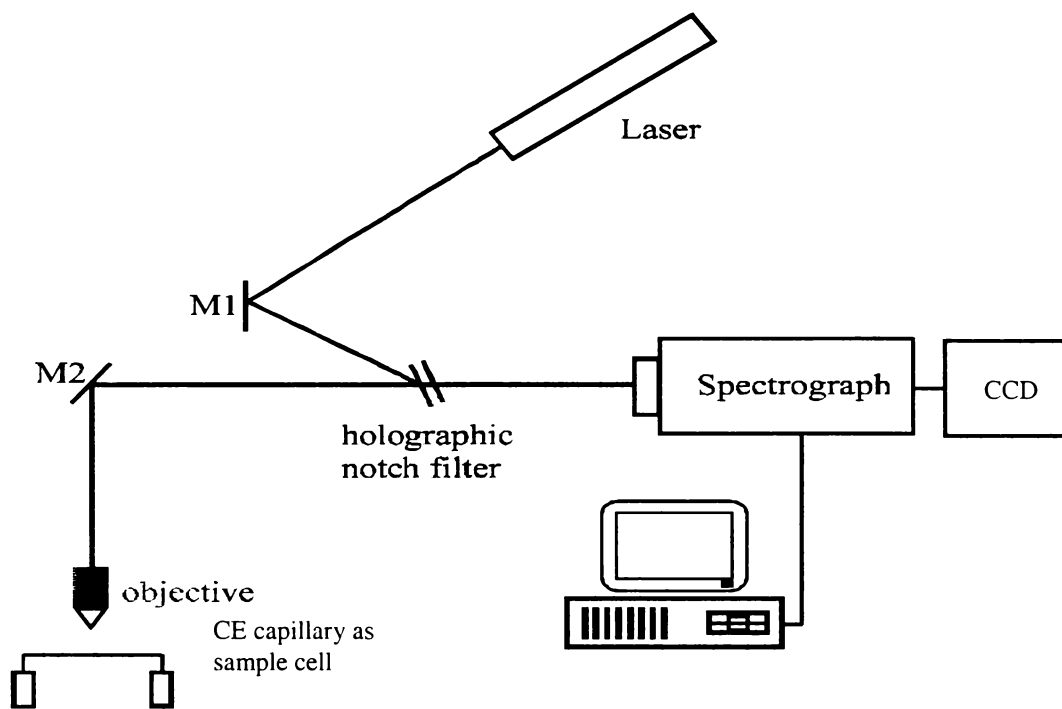
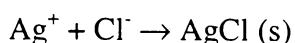


Figure 4.4 A typical arrangement for Raman spectroscopy.

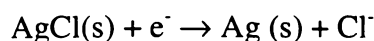
reaching the detector. The monochromator must also reject the Rayleigh scatter while providing adequate spectral resolution and throughput to obtain authentic Raman spectra. Traditionally, double or triple monochromator spectrometers were used to provide the required Rayleigh rejection. The throughputs of multiple monochromator spectrometers can be low and this compromises detectability. More recently, very efficient holographic notch filters that reflect the laser light (and Rayleigh scatter) and transmit the frequency shifted light are used in conjunction with simple single monochromator Raman systems. The confocal system shown in Figure 4.4 employs a notch filter as both a beam splitter to direct the laser to a microscope objective and as a Rayleigh rejection filter. Typically, cooled charge couple device (CCD) detectors are employed. The area detector is placed at the exit focal plane of the spectrograph and spectra are obtained without scanning or with only one or two discrete jumps in wavelength.

4.2.2 SERS Substrates

To generate SERS spectra from adsorbates, special techniques are needed to produce substrates with surface roughness or small clusters isolated in solution (148-149). Electrodes have been used for the production of SERS signals from molecules absorbed onto them. Surface roughness is produced by running electrochemical oxidation-reduction cycles. A metal salt is formed at the electrode surface during the oxidation half cycle:



As the silver is reduced it does not redeposit uniformly on the electrode surface. The silver forms clusters at the surface:



The size of these small clusters are on the scale of one to 500 nanometers. An advantage of the use of electrodes is that the surface potential of the SERS substrate can be controlled and SERS then becomes a structurally sensitive tool for in situ studies of potential dependent effects on surfaces.

A commonly used substrate for SERS is the metal sol. Metal colloids are generated by reducing a metal salt in aqueous or non-aqueous solvents such as ethanol or acetonitrile (148-149). For example, silver nitrate solution can be reduced with sodium borohydride, sodium citrate, or hydrazine dihydrochloride. This process produces sols that are comprised of spherical silver particles 10-200 nanometers in diameter. These sols are stable for three months without the addition of any stabilizing agents.

Interference from borate has been observed in SERS spectra of amines obtained with sodium borohydride reduced silver colloid (160). Borate bands have been observed in the spectra of other basic analytes and also when certain variations are made in the silver colloid preparation. It has been found that the relative intensities of the analyte and borate depends on the pH of the colloid, the extent of oxidation of the colloidal surface, and the adsorptivities of the analyte and borate. Typically, the colloidal solution is filtered and then sonicated for several minutes before use. The most intense SERS signals are from aggregated metal sols, which can be produced by the addition of sodium

chloride. The metal colloids are fairly easy to prepare and the solutes of interest are added to the sol at low concentration. An alternative approach for the preparation of colloidal silver is a cryochemical synthesis with acrylic polymers added as a stabilizing agent (161). The silver nanoparticles are stabilized by the addition of 2-dimethylaminoethyl methacrylate. Colloids prepared with cryochemically synthesized silver nanoparticles in various solvents such as acetone, water, and toluene were found to be sterically stabilized by poly-2-dimethylaminoethyl methacrylate layers formed at the surface of the silver nanoparticles.

The final commonly employed substrates for SERS are vacuum deposited island films (148-149, 162). These island films are more stable than colloids but they can be difficult to prepare. If the substrate in the vacuum is not cooled, the temperature increases metal atom mobility, which causes nuclei to grow into islands. These island films are small clusters that are nanometers in diameter. A cold substrate (below 120K) on which metal vapor is deposited forms a rough film due to the reduced mobility of the metal atoms on the cold substrate. The magnitude of the SERS effect depends on the size, shape, and spacing of the metal nanostructures for electric field enhancement. Vapor-deposited metal island films are among the most widely used substrates due to their fair SERS activity and the ease of controlling the experimental parameters. It has been found that higher evaporation rates (higher temperatures) of silver lead to smoother surfaces with a less well-defined island structure (162). On the other hand, substrates that are metallized at very low deposition rates had more separated silver islands on average. The residual pressure in the deposition chamber can affect the energy of the metal vapor. For example, at lower chamber pressures the collision-induced cooling of the silver in the

gas phase should be less and hotter silver particles can be deposited. The introduction of an inert gas (argon) leads to the cooling of the gaseous metal particles and allows for easier control of the island growth. It was found that at an elevated Ar pressure during deposition (1×10^{-3} millibar), a more distinct island formation was observed. Deposition geometry and postdeposition annealing are other important parameters in vacuum deposition (162).

4.3 Introduction to Surface Enhanced Raman Spectroscopy/Capillary

Electrophoresis

The implementation of CE in chemical analysis has been thwarted by concerns of EOF variability and the limitations in detection (163). This chapter focuses on developing a SERS approach as a reliable, selective, and information rich detection technique for CE. An approach for SERS/CE with the goal of obtaining distinctive Raman spectra of moderately polarizable, non-resonant enhanced biological compounds is presented. The ability to obtain distinctive spectra in SERS/CE for such solutes will expand detection capabilities and allow for the unambiguous identification of solute bands, which reduces the previously mentioned EOF reproducibility limitation. Therefore, the development of SERS/CE can address the two main limitations of CE and provide a low cost alternative to CE-mass spectrometry (CE-MS) approaches.

Detection in CE has not been developed as thoroughly as with other separation techniques in terms of providing spectroscopic information for high selectivity or for solute identification purposes. Unambiguous solute identification by the combination of observed migration times and spectral information is needed because the parameters

affecting the CE migration times are not easily controlled with real samples that contain unknown interferences (163). An advantage of the combination of CE and SERS is that Raman spectroscopy has the ability to generate spectral information of solutes in the aqueous media that is frequently used in CE. The narrow band in Raman spectroscopy provides enhanced spectral selectivity compared to luminescence based spectroscopy. Raman has good potential for multi-component analysis and it is a non-destructive analytical approach (164). Hence, the identification of baseline interferences and co-migrating bands in CE could be possible with Raman detection.

There are few reports of Raman spectroscopy interfaced with capillary electrophoresis. Morris and co-workers performed isotachopheric separations of herbicides on a microchip with normal Raman spectroscopy (165). Also, this group detected inorganic anions via field-amplified injection with normal Raman spectroscopy (166). Ruddick developed a Raman detector that incorporated a hyperhemispherical element that produced millimolar range detection limits for carbohydrates and inorganic ions (167). Finally, resonance Raman was employed with CE for the detection of methyl red and methyl orange (168). Resonance Raman occurs when the photon energy of the exciting laser beam is equal to the energy of an electric dipole allowed transition. In this case, the exciting light coincides with an electronic absorption and the Raman spectra is more intense.

The combination of SERS with CE is desirable because many current CE detection techniques lack sensitivity and Raman signals can be greatly enhanced by SERS. Also, laser based techniques such as Raman are compatible with the small capillaries employed in CE and Raman spectrometers can be constructed from relatively

low cost components. Nirode and Sepaniak first reported the coupling of traditional CE with SERS by employing an on-column silver colloidal running buffer approach (169). This on-column approach is easy to implement and does not suffer from transfer related band dispersion that can be problematic with off-column approaches. However, a disadvantage of this approach is that aggregation and activation of the SERS media can be strongly influenced by the separation conditions. Large enhancements in SERS require the close approach or adsorption of the solute to the SERS active surface. If the kinetics of this process are slow on a chromatographic time scale then band dispersion can occur. Therefore, it is reasonable to isolate the separation and detection processes in SERS/CE to allow for their independent optimization. Therefore, an off-column SERS/CE approach was developed that employs the deposition of the column effluent onto a moving planar SERS substrate (170). The attractive features of off-column approaches include long time constants or signal averaging to improve detectability and the prospect of using separation and detection conditions that are incompatible. These reports illustrate the feasibility of SERS/CE but expanding the applicability of this hybrid technique is necessary for its further development and to aid in the understanding of the important parameters. In this chapter, a novel SERS/CE approach is described in which the CE separation capillary is inserted into a large diameter capillary that delivers colloidal silver to the detection zone. It was postulated that this end of capillary approach may possess some of the attributes of both of the previously mentioned approaches.

4.4 Experimental

4.4.1 Materials

Sodium phosphate (monobasic) and sodium phosphate (dibasic) were purchased from Sigma (St. Louis, MO) and were used to prepare running buffers. Cytosine, adenosine, guanine, Rhodamine 6G, and hypoxanthine were purchased from Sigma (St. Louis, MO) and used as obtained to prepare 1×10^{-3} M stock solutions and diluted as needed. Nile Blue and sodium fluorescein were purchased from Sigma Chemical for the fluorescence studies. Silver nitrate (ACS) grade and sodium citrate were purchased from Sigma (St. Louis, MO) for silver sol preparation. Fused silica capillaries were purchased from Polymicro Technologies (Phoenix, AZ).

4.4.2 Silver Colloidal Solution Preparation

Ninety milligrams of silver nitrate was dissolved in 500 milliliters of water. The silver nitrate solution was heated to a boil and, while stirring, a one percent citrate solution (10 mL) was added dropwise over a ten minute period (169). The solution changed from colorless to a greenish color five minutes after the citrate was added and the solution was then heated for one hour. The solution was cooled and diluted to the 500 mL mark with water. When prepared in this manner the resulting silver colloidal solution is comprised of silver particles 10-200 nm in diameter and exhibits an absorption maximum at 430 nm. At the start of all experiments, the colloid is sonicated for five minutes and then filtered with a 0.45 μ m filter.

4.4.3 Capillary Preparation and Utilization

Fused-silica capillaries were purchased from Polymicro Technologies (Phoenix, AZ) and were cut to a total length of 45-50 cm using a capillary cutter. An on-column detection window was made by removing a section of the polyimide coating at 5 cm from the inlet end of the large diameter capillary. The separation capillary had an internal diameter of 50 microns and an outer diameter of 365 microns. The capillary used to provide a counter flow of silver colloid at the separation capillary outlet had an internal diameter of 525 microns and had an outer diameter of 705 microns. The end of the separation capillary was tapered to promote a smooth flow profile by the use of a cutting stone to produce a cone shape. The end of the capillary was viewed under a microscope to determine if it was tapered properly. New capillaries were conditioned by flushing with 0.1 N sodium hydroxide for thirty minutes and water for thirty minutes. At the start of each day, the separation capillary was flushed for five minutes each with 0.1 N sodium hydroxide, water, and finally with 3 mM phosphate buffer. Samples were injected by the application of +5 kV for 20 seconds unless otherwise noted. Following injection, the capillary inlet was inserted into the running buffer vial. The separation conditions were 3 mM phosphate buffer (pH 6) with an application of 15 kV to the separation capillary. A high voltage power supply (Spellman, Brewster, NY) was utilized for the application of voltage to the capillary.

4.4.4 SERS/CE Apparatus

The Raman instrument used was an Acton Spectrapro 275 (Acton, MA) with a Helium-Neon laser (Meredith Industries) at a wavelength of 633 nanometers. The

SERS/CE instrument design is a typical configuration with the presence of an objective for focusing, filters, and CCD for detection (see Figure 4.4). The microscope objective (20x) was used to focus the laser radiation and to collect the 180° Raman scattering. Stages were employed that allowed for x, y, and z translation for focusing the laser beam through the capillary. Static spectra were obtained by mixing 50 μL of colloidal silver, 20 μL of sodium chloride, and 10 μL of the solute in a microtiter plate. A drop of this solution was then placed on a glass slide in order to obtain the static spectra. Capillaries were filled with the test analyte via electrokinetic pumping by a high voltage power supply for dynamic studies. Under CE conditions, the separation occurs in the small diameter capillary that is inserted into a large capillary via ferrules and a tee. A syringe pump pushes the colloidal silver solution at a specified flow rate through the large diameter capillary towards the end of the separation capillary. The laser is focused through the objective at the exit of the separation capillary and solutes are detected in the large (550 μm i.d.) fused silica capillaries. Figure 4.5 illustrates the migration of a solute band toward the end of the separation capillary and the detection zone in the flowing colloidal silver in the large diameter capillary. The large arrows demonstrate the flow pattern of the colloidal silver solution.

4.5 Results and Discussion

The end of capillary approach was designed in order to combine some of the attributes of the previous SERS/CE techniques. The current approach is easy to implement as is the case with the on-capillary design mentioned previously and results

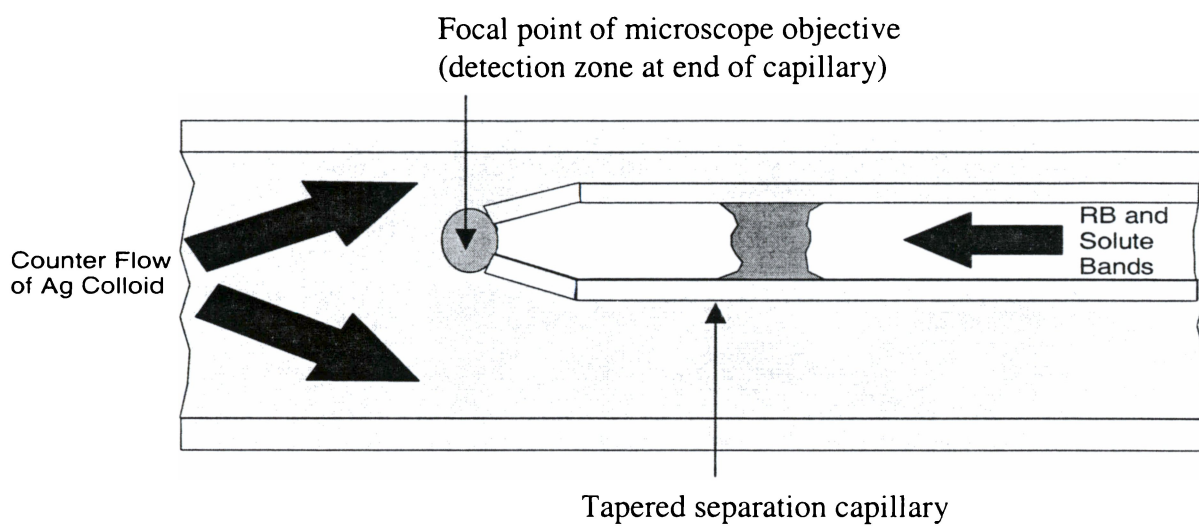


Figure 4.5 Schematic of the flow of colloidal silver towards the separation capillary.

can be obtained quickly as the solute elutes from the separation capillary. The off-column electrofilament deposition approach allows for the separation and detection conditions to be optimized independently as is the case with the SERS/CE approach presented in this chapter. Also, the absence of colloidal silver in the running buffer in the end of capillary approach is advantageous in that the colloidal silver can decrease the separation efficiency. However, some potential problems with the end of capillary approach described in this chapter are the loss of efficiency due to the counter flow of colloidal silver (band dispersion due to detection) and dilution of the solute band as it encounters the flowing colloidal silver (detectability). Although the colloidal solution is flowing, the issue of contamination at the end of the separation capillary was also a concern.

4.5.1 Effect of Sodium Chloride on SERS Intensity

The static spectra of the solutes of interest in these studies can be seen in Figure 4.6. A fairly low laser power (5.4 milliwatts at the sample) was employed for these spectra. It is known that sodium chloride can enhance the signal in SERS presumably due to aggregation of the silver particles. To illustrate this, a 1.25×10^{-4} M solution of hypoxanthine was used with different concentrations of sodium chloride (Figure 4.7). It can be seen that at low concentrations of sodium chloride the SERS signal is weak. At a moderate concentration of sodium chloride the signal increased as seen in Figure 4.7B. The signal increased even further at a higher concentration of sodium chloride as seen in Figure 4.7C. It is thought that the addition of sodium chloride causes the silver to aggregate and Raman hot spots (high field location) form that allow for a greater

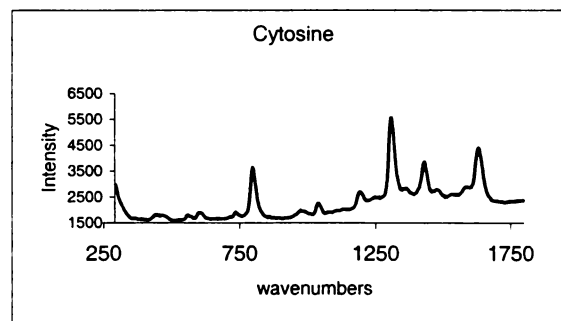
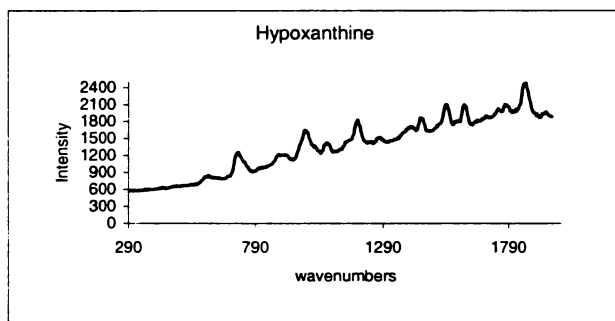
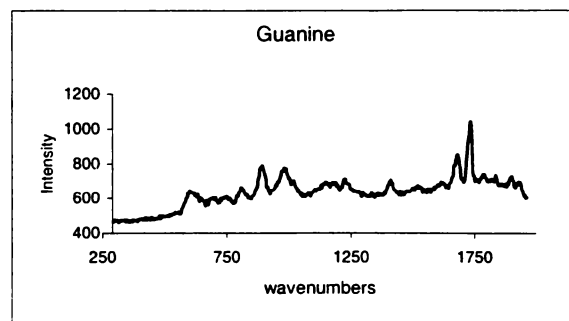
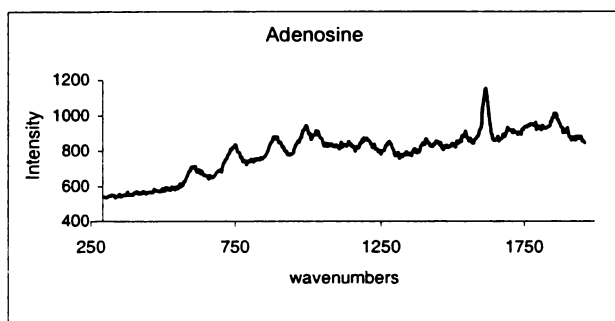
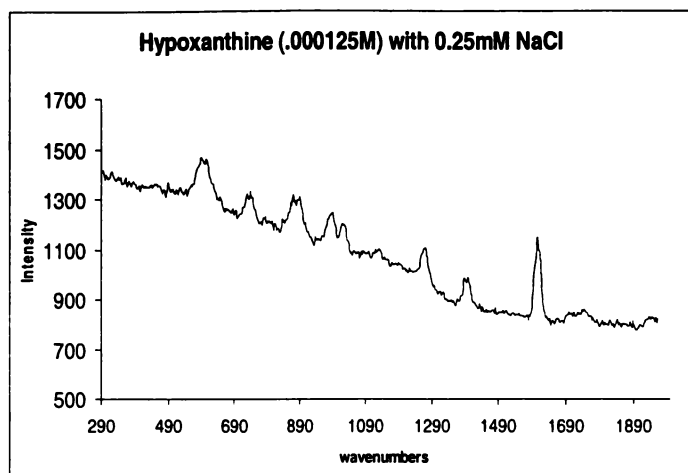
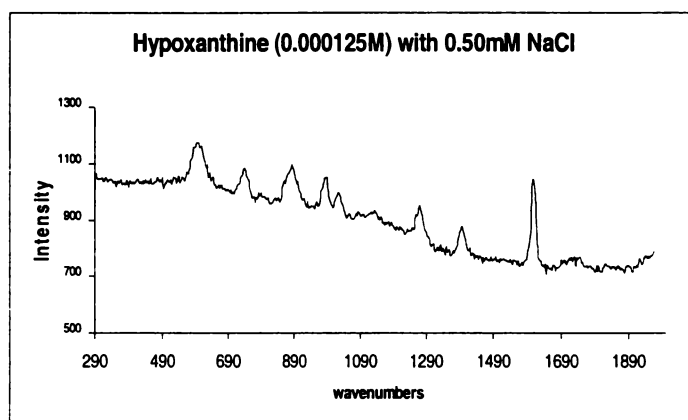


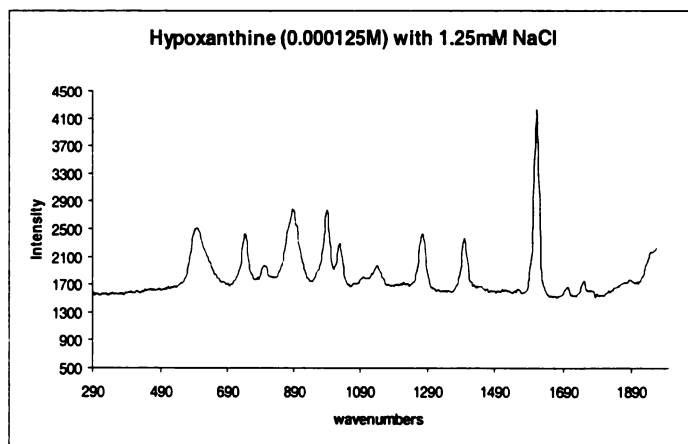
Figure 4.6 Static SERS spectra of the solutes of interest at 1.7×10^{-4} M.



A



B



C

Figure 4.7 The effect of sodium chloride on static SERS intensity.

enhancement. No solute signal was observed at concentrations of sodium chloride employed that were higher than those used in Figure 4.7C. If there are too many large aggregates this will dilute the effect of the hot particles and the SERS intensity will decrease. The significance of the sodium chloride concentration is that it demonstrates that the running buffer conditions are critical in SERS/CE. The concentration of sodium chloride must be optimized in order to improve the detectability in SERS/CE.

4.5.2 Initial Optimization of Flow Rates

It was of interest to locate a reasonable flow rate for the colloidal silver in the large diameter capillary that flows towards the detection zone. An acceptable flow rate for the colloidal silver would be one in which a SERS signal is obtained as the solute elutes from the separation capillary and shortly thereafter the solute is washed away by the flow of the colloidal silver. If the colloidal flow rate is too fast then the solute might be overly diluted or the available detection zone too constricted. Conversely if the flow is too slow, a large duration of signal from the solute and the possible signal overlap of solutes may occur. To achieve an acceptable flow rate of colloidal silver the design of Figure 4.5 was used along with a CCD camera and an ultraviolet lamp. A plug of 1×10^{-3} M fluorescein was injected into the separation capillary at 6 kV for 20 seconds and various flow rates of the colloidal solution were obtained by the use of a syringe pump. The CCD camera was focused at the outlet of the separation capillary and a UV lamp was there as well in order to visualize the fluorescein on the monitor as it eluted from the separation capillary.

The flow rates with the syringe pump that produced a reasonable flow profile were in the range of 2.0 - 3.0 mL/hr. A reasonable flow profile is one in which it appears that the efficiency is maintained. Figure 4.8 displays the images of the separation capillary at 2.0 and 2.5 mL/hr. flow rates of colloidal silver from the syringe pump. At a colloidal flow rate of 2.0 mL/hr. the fluorescein profile appeared to be acceptable. It can be seen that the solute stayed fairly close to the exit of the separation capillary and didn't spread down the large diameter capillary. At flow rates of 2.5 and 3.0 mL/hr. the fluorescein profile remained even closer to the exit of the small capillary as expected. Figure 4.8 was important for observing the flow profile of the solutes as they elute from the separation capillary and for the determination of a colloidal flow rate. It was determined that a colloidal solution flow rate of 2.0 mL/hr the penetration of the separation capillary effluent, as indicated by the fluorescein emission, was approximately equal to the estimated beam spot diameter of the focused laser beam (about 30 μm) in subsequent SERS experiments. Furthermore, the effective flow cell volume can be estimated by the overlap of the laser beam with the fluorescein zone. This was estimated to be 0.1 nL which, when compared to typical solute band volumes of 10 nL, indicates that band dispersion due to detection may be negligible under these conditions.

The flow profile of this SERS/CE system was further studied using LIF detection. Nile Blue at a concentration of 1×10^{-3} M was continuously injected into the separation capillary and the fluorescence intensity was measured at known distances from the exit of the separation capillary using a HeNe laser (633 nm) for excitation. Translational stages allowed for the measurement and control of the distance from the exit of the separation

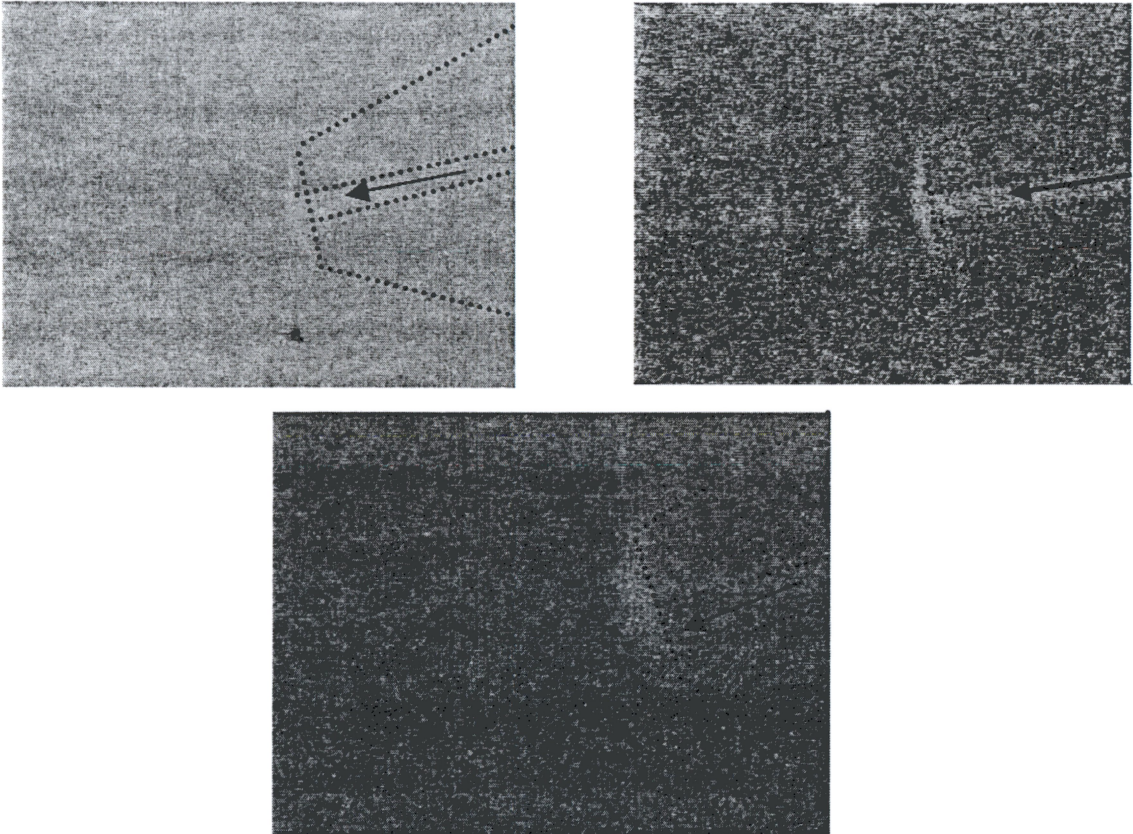
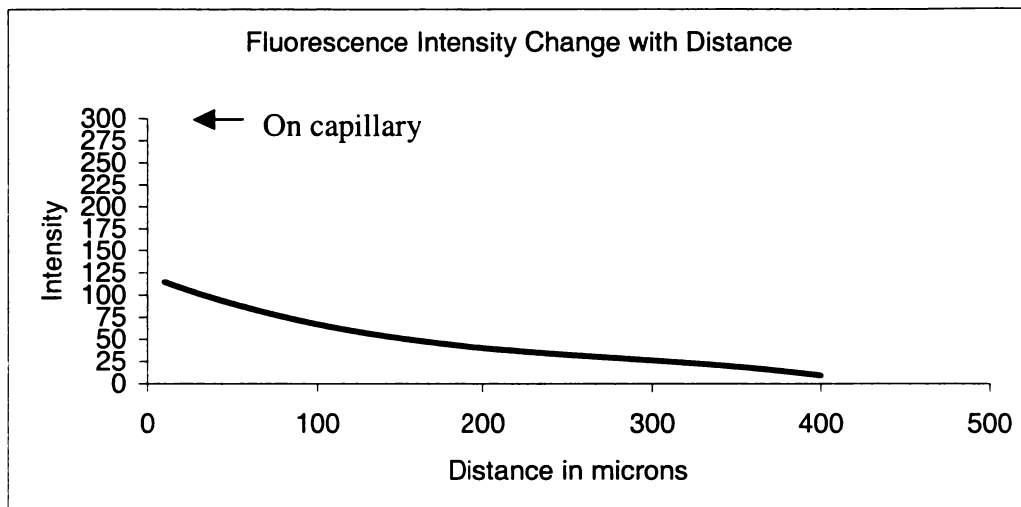


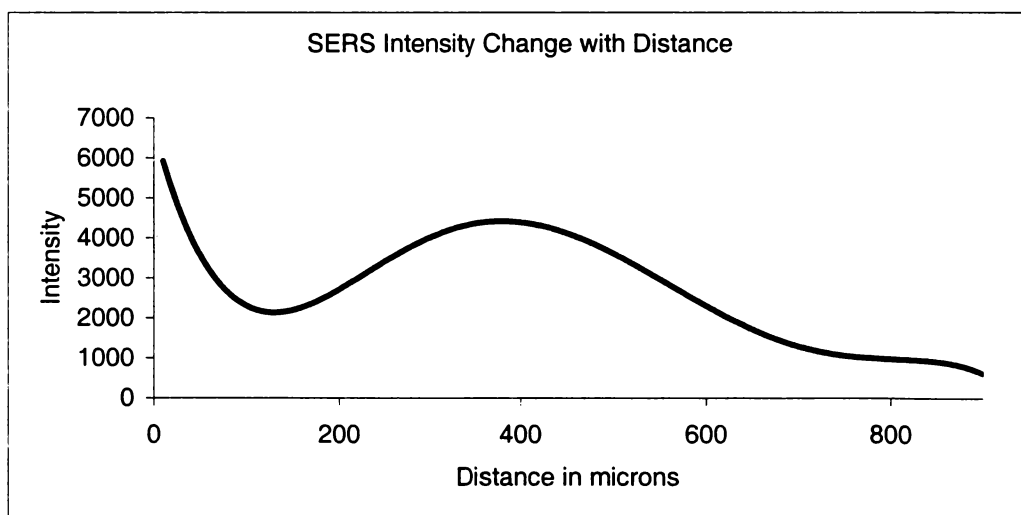
Figure 4.8 Flow profiles of the separation capillary with varying the syringe pump flow rate in the large capillary. The syringe pump was at a flow rate of 2.5 mL/hr. in the top two figures but at a flow rate of 2.0 mL/hr. in the bottom figure.

capillary throughout these studies. Phosphate buffer at a concentration of 3 mM was continuously pumped to the detection zone through the large capillary via a syringe pump at a flow rate of 2.0 mL/hr. It can be seen in Figure 4.9 that the fluorescence signal was most intense close to the exit of the separation capillary and then the intensity dropped off rapidly as the laser was moved further away from the separation capillary. This observation is consistent with the fluorescein profiles shown in Figure 4.8.

Conversely, a different intensity profile was seen with SERS detection. A 1×10^{-3} M solution of hypoxanthine was continuously injected into the SERS/CE design and the intensity was measured at known distances as described before. In this experiment, colloidal silver was continuously pumped at a flow rate of 2.0 mL/hr. by a syringe pump through the large diameter capillary. The hypoxanthine band at 1620 cm^{-1} was used for the measurement of the intensity at each distance away from the separation capillary. Figure 4.9B shows that the intensity decreased as the laser was focused further away from the separation capillary but later increased again. The large signal very close to the capillary may indicate contamination represented by stagnant or adhesive silver colloidal particles with adsorbed hypoxanthine on their surfaces. The increase in signal and the appearance of a maximum at about $400 \text{ }\mu\text{m}$ indicates the dynamic mixing and subsequent dilution of hypoxanthine and colloid. It was not surprising that the flow profile of fluorescence was different than that of SERS. The fluorescence signal does not depend on the solute mixing with another species to generate a signal, as is the case with SERS. In SERS, the colloidal silver must first come in contact with the eluting solute in order to generate the enhancement.



A



B

Figure 4.9 Fluorescence with Nile Blue and excitation by He-Ne laser (a) SERS/CE with hypoxanthine and colloidal silver (b).

Many attempts were made to inject solutes and detect them with our SERS/CE arrangement. The final goal was to determine the separation (CE) efficiency of this system and compare it to the efficiency of the automated CE system in the lab. It was thought that our SERS/CE arrangement could have problems with band broadening due to the counter flow of the solute and the silver colloidal solution. Figure 4.9B provides evidence of this potential problem. The majority of the time that samples were injected at 5 kV for 20 sec. with a 3 sec. acquisition time there was no signal seen at all. Therefore, the efficiency of our system was never calculated because of the detection problem. The reason for the detection problems must be due to the colloidal silver flowing in the large diameter capillary which dilutes the solute. To illustrate this dilution effect, it was seen in the fluorescence experiment mentioned earlier (Figure 4.9A) that the signal intensity was decreased in the large diameter capillary as compared to the signal obtained on the separation capillary. The final attempt was to inject a solute that is known to work very well for Raman applications (Rhodamine 6G). A 1×10^{-4} M solution of Rhodamine 6G was injected into the separation capillary and a signal was obtained but it persisted for one minute. This indicates that it is sticking to the walls of the capillary and the flow of colloidal silver was unsuccessful at sweeping the solute away in a timely fashion.

4.5.3 Alternative Approaches for SERS/CE

A vacuum deposition approach was employed in our studies with SERS/CE. This approach seemed attractive due to the many attributes that it shared in common with SERS/CE designs mentioned previously. First, detection is accomplished on capillary which preserves the efficiency in CE (no band dispersion due to detection as in off-

column approaches). Also, detection on-column permits data to be obtained on the fly. In addition, this vacuum deposition approach also would not have the detectability problem that the end of capillary approach had due to the colloidal flow of silver (dilution) into the detection zone. Finally, the use of deposited silver could lead to large enhancements with surface plasmon resonance. It has been established for SERS that enhancement in the Raman scattered radiation can be achieved when the frequency of the incident radiation and scattered radiation overlap the surface plasmon resonance frequency of the substrate. Weimer has developed a method for producing SERS active silver film substrates with tunable surface plasmon resonance wavelengths (171). This development is important to vacuum deposition approaches because the plasmon resonance of the substrate could be matched to the fixed frequencies of readily available laser sources.

In this on-capillary approach, CE capillaries were placed into a vacuum deposition apparatus and silver was deposited inside of the end of the CE capillary. The laser was focused on the end of the capillary where the deposited silver was located and the SERS signal would be measured as the solutes migrate out of the capillary. The problem with this approach is that the deposited silver is only stable for a few days. The contamination problem was expected to be large due to adsorbed solutes on the stagnant silver surface. This approach was abandoned because some of the deposited silver would wash off when flushing the capillary or during actual separations. Under a microscope it could be seen that there were streaks or portions of the capillary where silver was not present where it had originally been deposited at the end of the CE capillary.

4.6 Concluding Remarks

The main advantage of Raman spectroscopy over on-line laser induced fluorescence and ultraviolet/visible absorption detection in CE is the ability to generate spectra that reveal detailed information about the vibrations of the analyte molecules. The vibrations are specific for a particular functional group, which are useful for identification purposes but can also aid in the elucidation of the structures of unknown compounds. The data presented in this report illustrate that SERS/CE is a feasible approach but this particular arrangement is not the best design. The only advantage that the current arrangement provides over the previous on-capillary SERS/CE design by Nirode is that the colloidal silver does not affect the separation since it is left out of the CE running buffer. It was shown that the concentration of sodium chloride is important in SERS and that the change in intensity with distance for fluorescence and SERS detection are different in our current arrangement. Finally, the images of fluorescein aided in visualizing the flow profile of the arrangement and where the laser should be positioned for detection. Unfortunately, this SERS/CE approach suffers from detectability problems due to serious dilution effects that preclude detection of most solutes.

List of References

- [1] Jorgenson, J. W., Lukacs, K. D., *Anal. Chem.* 1981, 53, 1298-1302.
- [2] Heiger, D. N., *High Resolution Capillary Electrophoresis*, Hewlett-Packard, Waldbronn, Germany 1992, pp. 13-21, 24, 26-28, 32, 37, 44, 79.
- [3] Jandik, P., Bonn, G. *Capillary Electrophoresis of Small Molecules and Ions*, VCH Publishers Inc., New York, 1993, pp. 23, 25, 134-135.
- [4] Camilleri, P., *Capillary Electrophoresis Theory and Practice*, CRC Press, Boca Raton, Florida, 1993, pp. 43, 80-81.
- [5] Lauer, H. H., McManigill, D. *Anal. Chem.* 1986, 587, 160-170.
- [6] Lukacs, K. D., Jorgenson, J. W. *J. High Res. Chromatogr.* 1985, 8, 407-411.
- [7] Issaq, H., Atamna, I. Z., Muschik, G. M., Janini, G. M. *Chromatographia* 1991, 32, 155-160.
- [8] Weinberger, R., *Practical Capillary Electrophoresis*, Academic Press, New York, 1993, pp. 148-157, 160-163, 171-175, 177-179.
- [9] Grossman, P. D., Colburn, J. C., *Capillary Electrophoresis Theory and Practice*, Academic Press Inc., San Diego, CA 1992, pp. 159-163, 314-316, 319.
- [10] Fanali, S. *J. Chrom. A*, 2000, 875, 89-122.
- [11] Otsuka, K., Terabe, S. *J. Chrom. A*, 2000, 875, 163-178.
- [12] Swinney, K., Bornhop, D. J. *Electrophoresis* 2000, 21, 1239-1250.
- [13] Swaile, D. F., Sepaniak, M. J. *J. Liq. Chromatogr.* 1991, 14, 869-889.
- [14] Mathies, R. A., Peck, K., Stryer, L. *Anal. Chem.* 1990, 62, 1786-1791.
- [15] Prata, C., Bonnafous, P., Fraysse, N., Treilhou, M., Poinso, V., Couderc, F., *Electrophoresis* 2001, 22, 4129-4138.
- [16] Chen, D. Y., Swerdlow, H. P., Harke, H. R., Zang, J. Z., Dovichi, N. J. *J. Chromatogr.* 1991, 559, 237-246.
- [17] Swerdlow, H. P., Wu, S., Harke, H. R., Dovichi, N. J. *J. Chromatogr.* 1990, 516, 61-67.
- [18] Wu, S., Dovichi, N. J. *J. Chromatogr.* 1989, 480, 141-155.

- [19] Faller, T., Engelhardt, H. *J. Chromatogr. A* 1999, 853, 83-94.
- [20] Ehmann, T., Bachmann, K., Fabry, L., Rufer, H., Serwe, M., Ross, G., Pahlke, S., Kotz, L., *J. Chromatogr. A* 1998, 816, 261-275.
- [21] Lee, T. T., Yeung, E. S., *Anal. Chem.* 1992, 64, 1226-1231.
- [22] Yang, J., Bose, S., Hage, D. S., *J. Chromatogr. A* 1996, 735, 209-220.
- [23] Altria, K. D., Bryant, S. M., *LC.GC* 1997, 15, 448-454.
- [24] Altria, K. D., *LC.GC* 1999, 17, 28-35.
- [25] Shihabi, Z. K., Hinsdale, M. E., *Electrophoresis* 1995, 16, 2159-2163.
- [26] Garcia, L. L., Shihabi, Z. K., *J. Chromatogr. A* 1993, 652, 465-469.
- [27] Rose, D. J., Jorgenson, J. W., *Anal. Chem.* 1988, 60, 642-648.
- [28] Altria, K. D., Kelly, M. A., Clark, B. J., *Chromatographia* 1996, 43, 153-158.
- [29] Song, L., Quingyu, O., Weile, Y., Guifang, X., *J. Chromatogr. A* 1995, 696, 307-319.
- [30] Kelly, M. A., Altria, K. D., Clark, B. J., *J. Chromatogr. A* 1997, 768, 73-80.
- [31] Shafaati, A., Clark, B. J., *Anal. Proc.* 1993, 30, 481-483.
- [32] Sun, Y. L., Zhang, C. X., Ling, D. K., Sun, Z. P., *JHRCC* 1994, 17, 563-564.
- [33] Smith, S. C., Strasters, J. K., Khaledi, M. G., *J. Chromatogr.* 1991, 559, 57-68.
- [34] Lauer, H. H., McManigill, D., *Anal. Chem.* 1986, 58, 166-170.
- [35] Terabe, S., Otsuka, K., *J. Microcol. Sep.* 1989, 1, 150-154.
- [36] Liu, J., Cobb, K. A., Novotny, M., *J. Chromatogr.* 1988, 468, 55-65.
- [37] VanOrman, B. B., Liversidge, G. G., McIntire, G. L., Olefirowicz, T. M., Ewing, A. G., *J. Microcol. Sep.* 1990, 2, 176-180.
- [38] Zhu, M., Rodriguez, R., Hansen, D., Wehr, T., *J. Chromatogr.* 1990, 516, 123-131.
- [39] Towns, J. K., Regnier, F. E., *Anal. Chem.* 1992, 64, 2473-2476.

- [40] Chang, H. T., Yeung, E. S., *Electrophoresis* 1995, 16, 2069-2073.
- [41] Altria, K. D., Bryant, S. M., Clark, B. J., Kelly, M. A., *LC.GC* 1997, 15, 34-38.
- [42] Altria, K. D., Hindocha, D., *LC.GC* 1998, 16, 835-841.
- [43] Watzig, H., Dette, C., *J. Chromatogr.* 1993, 636, 31-38.
- [44] Thomas, B. R., Fang, X. G., Chen, X., Tyrell, R. J., Ghodbane, S., *J. Chromatogr. B* 1994, 657, 383-394.
- [45] Coufal, P., Stulik, K., Claessens, H. A., Cramers, C. A., *JHRCC* 1994, 17, 325-334.
- [46] Schwartz, H. E., Melera, M., Brownlee, R. G., *J. Chromatogr.* 1989, 480, 129-139.
- [47] Lee, T. T., Yeung, E. S., *Anal. Chem.* 1991, 63, 2842-2848.
- [48] Altria, K. D., Fabre, H., *Chromatographia* 1995, 40, 313-320.
- [49] Rush, R. S., Karger, B. L. *Beckman Technical Bulletin TIBC* 1990, 104, 1-2.
- [50] Goodall, D. M., Williams, S. J., Lloyd, D. K., *TrAC* 1991, 103, 272-279.
- [51] Altria, K. D., Kelly, T., Clark, B., *LC.GC* 1996, 14, 398-404.
- [52] Karger, B. L., Cohen, A. S., Paulus, A., *Chromatographia* 1987, 24, 15-24.
- [53] Wynia, G. S., Windhorst, G., Post, P. C., Maris, F. A., *J. Chromatogr. A* 1997, 773, 339-350.
- [54] Altria, K. D., Goodall, D. M., Rogan, M. M., *Electrophoresis* 1994, 15, 824-827.
- [55] Honda, S., Iwase, S., Fujiwara, S., *J. Chromatogr.* 1987, 404, 313-320.
- [56] Kunkel, A., Degenhardt, M., Schirm, B., Watzig, H., *J. Chromatogr. A* 1997, 768, 17-27.
- [57] Terabe, S., Cheng, N., Otsuka, K., *Adv. Electrophoresis* 1994, 7, 87-153.
- [58] Altria, K. D., *Capillary Electrophoresis Guidebook. Principles, Operation, and Applications*, Humana Press, Totowa, NJ 1996, pp. 61, 63-64.
- [59] Ackermans, M. T., Beckers, J. L., Everaerts, F. M., Seelen, I. G. J. A., *J. Chromatogr.* 1992, 590, 341-353.

- [60] Tsai, E. W., Singh, M. M., Lu, H. H., Ip, D. P., Brooks, M. A., *J. Chromatogr.* 1992, 626, 245-250.
- [61] McLaughlin, G. M., Nolan, J. A., Lindahl, J. L., Morrison, J. A., Bronzert, T. J., *J. Liq. Chromatogr.* 1992, 15, 961-1021.
- [62] Moring, S.E., Colburn, J. C., Grossman, P. D., Lauer, H. H., *LC.GC*, 1990, 3, 46-54.
- [63] Altria, K. D., Harden, R. C., Hart, M., Hevizi, J., Hailey, P. A., Makwana, J. V., Portsmouth, M. J., *J. Chromatogr.* 1993, 641, 147-153.
- [64] Altria, K. D., *Chromatographia* 1993, 35, 177-182.
- [65] *Operational Performance Manual*, Hewlett Packard, Waldbronn, Germany 1994, pp. 96-97.
- [66] Frenz, J., Wu, S. L., Hancock, W. S., *J. Chromatogr.* 1989, 480, 379-391.
- [67] Dulfer, T., Herb, R., Herrmann, H., Kobold, U. *Chromatographia* 1990, 30, 675-685.
- [68] Wanders, B. J., Van de Goor, T. A. A. M., Everaerts, F. M., *J. Chromatogr. A* 1993, 652, 291-294.
- [69] Altria, K. D., Campi, F., *LC.GC* 1999, 17, 237-243.
- [70] Kenndler, E., Seawer, C., *Anal. Chem.* 1991, 63, 1801-1807.
- [71] Chen, N., Wang, L., Zhang, R., *J. Liq. Chromatogr.* 1993, 16, 3609-3622.
- [72] Zhang, Y. K., Chen, N. Wang, L., *J. Liq. Chromatogr.* 1993, 16, 3689-3697.
- [73] Jumppanen, J. H., Riekkola, M. L., *Anal. Chem.* 1995, 67, 1060-1066.
- [74] Penn, S. G., Goodall, D. M., Loran, J. S., *J. Chromatogr.* 1993, 636, 149-152.
- [75] Gomez, F. A., Avila, L. Z., Chu, Y. H., Whitesides, G. M. *Anal. Chem.* 1994, 66, 1785-1791.
- [76] Siren, H., Jumppanen, J. H., Manninen, K., Reikkola, M. L., *Electrophoresis* 1994, 15, 779-784.
- [77] Dose, E. V., Guiochon, G. A., *Anal. Chem.* 1991, 63, 1154-1158.
- [78] Holland, R. D., Sepaniak, M. J., *Anal. Chem.* 1993, 65, 1140-1146.

- [79] Mayer, B. X., *J. Chromatogr. A* 2001, 907, 21-37.
- [80] Cohen, N., Grushka, E., *J. Chromatogr. A* 1994, 684, 323-328.
- [81] Weinberger, R., Stevenson, R., Neue, U., *Am. Lab.* 1997, 29, 22-29.
- [82] *Understanding Your HP ChemStation*, Hewlett Packard, Waldbronn, Germany 1998, pp. 106-108.
- [83] Rogan, M., Altria, K. D., Goodall, D. *Chirality* 1994, 6, 25-40.
- [84] Kuhn, R., Hofstetter-Kuhn, S. *Chromatographia* 1992, 34, 505-512.
- [85] Wistuba, D., Diebold, H., Schurig, V. *J. Microcol. Sep.* 1995, 7, 17-22.
- [86] Sun, P., Barker, G., Mariano, G., Hartwick, R. *Electrophoresis* 1994, 15, 93-798.
- [87] Kuhn, R., Stoecklin, F., Erni, F. *Chromatographia* 1992, 33, 32-36.
- [88] Verleysen, K., Sandra, P. *J. Microcol. Sep.* 1999, 11, 37-43.
- [89] Kang, J., Yang, Y., You, J., Ou, Q. *J. Chromatogr. A* 1998, 825, 81-87.
- [90] Vespalec, R., Billiet, H., Frank, J., Böcek, P. *Electrophoresis* 1996, 17, 1214-1221.
- [91] Schaeper, J. P., Sepaniak, M. J. *Electrophoresis* 2000, 21, 1421-1429.
- [92] Ueda, T., Mitchell, R., Kitamura, F., Metcalf, T., Kuwana, T., Nakamoto, A. *J. Chromatogr.* 1992, 593, 265-274.
- [93] DeSilva, K., Kuwana, T. *Biomed. Chromatogr.* 1997, 11, 230-235.
- [94] Chan, K., Muschik, G., Issaq, H. *Electrophoresis* 1995, 16, 504-509.
- [95] Wan, H., Blomberg, L. *J. Chromatogr. Sci.* 1996, 34, 540-546.
- [96] Wan, H., Engstrom, A., Blomberg, L. *J. Chromatogr. A* 1996, 731, 283-292.
- [97] Terabe, S., Miyashita, Y., Ishihama, Y., Shibata, O. *J. Chromatogr.* 1993, 636, 47-55.
- [98] Valko, I., Siren, H., Riekkola, M. *Electrophoresis* 1997, 18, 919-923.
- [99] Valko, I., Siren, H., Riekkola, M. *J. Chromatogr. A* 1996, 737, 263-272.

- [100] Verleysen, K., Van den Bosch, T., Sandra, P. *Electrophoresis* 1999, 20, 2650-2655.
- [101] Zhu, W., Vigh, G. *Anal. Chem.* 2000, 72, 310-317.
- [102] Rizzi, A., Kremser, L. *Electrophoresis* 1999, 20, 2715-2722.
- [103] Lee, Y., Lin, T. *J. Chromatogr.* 1995, 716, 335-346.
- [104] Lindner, W., Bohs, B., Seidel, V. *J. Chromatogr. A* 1995, 697, 549-560.
- [105] Lin, B., Zhu, X., Jakob, A., Epperlein, U., Koppenhoefer, B. *J. High Resol. Chromatogr.* 1999, 22, 449-453.
- [106] Tanaka, M., Yoshinaga, M., Asano, S., Yamashoji, Y., Kawaguchi, Y. *Fresenius J. Anal. Chem.* 1992, 343, 896-900.
- [107] Yoshinaga, M., Tanaka, M. *J. Chromatogr. A* 1994, 679, 359-365.
- [108] Corradini, R., Buccella, G., Galaverna, G., Dossena, A., Marchelli, R. *Tetrahedron Letters* 1999, 40, 3025-3028.
- [109] Tanaka, Y., Terabe, S. *J. Chromatogr. A* 1997, 781, 151-160.
- [110] Galaverna, G., Corradini, R., Dossena, A., Marchelli, R., Vecchio, G. *Electrophoresis* 1997, 18, 905-911.
- [111] Fanali, S., Aturki, Z. *J. Chromatogr.* 1995, 694, 297-305.
- [112] Guttman, A., Paulus, A., Cohen, A., Grinberg, N., Karger, B. *J. Chromatogr.* 1988, 448, 41-53.
- [113] Bechet, I., Paques, P., Fillet, M., Hubert, P., Crommen, J. *Electrophoresis* 1994, 15, 818-823.
- [114] Nishi, H., Fukuyama, T., Terabe, S. *J. Chromatogr. A* 1991, 553, 503-516.
- [115] Fanali, S., Flieger, M., Steinerova, N., Nardi, A. *Electrophoresis* 1992, 13, 39-45.
- [116] Copper, C., Cole, R., Sepaniak, M. J. *Electrophoresis* 1994, 15, 785-792.
- [117] Fillet, M., Chankvetadze, B., Crommen, J., Blaschke, G. *Electrophoresis* 1999, 20, 2691-2697.

- [118] Fillet, M., Hubert, P., Crommen, J. *Electrophoresis* 1998, 19, 2834-2840.
- [119] Fillet, M., Bechet, I., Schomburg, G., Hubert, P., Crommen, J. *J. High Resol. Chromatogr.* 1996, 19, 669-673.
- [120] Kranack, A., Bowser, M., Britz-McKibbin, P., Chen, D. *Electrophoresis* 1998, 19, 388-396.
- [121] Culha, M., Fox, S., Betts, T., Green, T., Sepaniak, M. J. *J. Microcol. Sep.*, submitted.
- [122] SYBYL 6.6, Tripos Inc., 1699 South Hanley Rd., St. Louis, Missouri, 63144, USA.
- [123] Fox, S., Culha, M., Sepaniak, M. J. *J. Liq. Chromatogr.*, 2001, 24, 1209-1228.
- [124] Betteridge, D., Wade, A., Howard, A. Reflections on the modified simplex II. *Talanta* 1985, 32, 723-734.
- [125] *User's Guide to MultiSimplex Lite*, MultiSimplex, Karlskrona, Sweden, 1999, pp. 7-11.
- [126] Wren, S., Rowe, R. *J. Chromatogr.* 1992, 603, 235-241.
- [127] Devault, G. L., Sepaniak, M. J.. *J. Microcol. Sep.* 2000, 12, 419-428.
- [128] Carlson, R. *Design and Optimization in Organic Synthesis*, Elsevier, Amsterdam, 1992.
- [129] Davis, J., Clark, B., Stebbins, M., Sepaniak, M. J. *J. Microcol. Sep.* 1996, 8, 485-494.
- [130] Howard, A., Boenicke, I. *Anal. Chim. Acta* 1989, 223, 411-418.
- [131] Castagnola, M., Rossetti, D., Cassiano, L., Rabino, R., Nocca, G., Giardina, B. *J. Chromatogr.* 1993, 638, 327-334.
- [132] Foulon, C., Goossens, J. F., Fourmaintraux, E., Bonte, J. P., Vaccher, C. *Electrophoresis*, 2002, 23, 1121-1128.
- [133] Matthijs, N., Perrin, C., Maftouh, M., Massart, D. L., Vander Heyden, Y. J. *Pharmaceut. Biomed.* 2002, 27, 515-529.
- [134] Zhou, L. L., Thompson, R., Song, S., Ellison, D., Wyvratt, J. M. *J. Pharmaceut. Biomed.* 2002, 27, 541-553.

- [135] Maynard, D. X., Vigh, G. *Electrophoresis* 2001, 22, 3152-3162.
- [136] Perrin, C., Vander Heyden, Y., Maftouh, M., Massart, D. L. *Electrophoresis*, 2001, 22, 3203-3215.
- [137] Chen, F. T. A., Shen, G., Evangelista, R. A. *J. Chromatogr. A* 2001, 924, 523-532.
- [138] Zhu, W. H., Vigh, G. *Electrophoresis* 2001, 22, 1394-1398.
- [139] Yanes, E. G., Gratz, S. R., Sutton, R. M. C., Stalcup, A. M. *Fresen. J. Anal. Chem.* 2001, 369, 412-417.
- [140] Kuwahara, Y., Izumoto, S., Nishi, H. *Bunseki Kagaku* 2001, 50, 69-77.
- [141] Zu, W. H., Li, W. S., Raushel, F. M., *Electrophoresis* 2000, 21, 3249-3256.
- [142] Zhu, W. H., Vigh, G. *Electroporesis* 2000, 21, 2016-2024.
- [143] Nussbaum, M. A. *Electrophoresis* 1999, 20, 2664-2669.
- [144] Aboul-Enein H. Y., Efstatiade, M. D., Baiulescu, G. E. *Electrophoresis* 1999, 20, 2686-2690.
- [145] Verleysen, K., Sabah, S., Scriba, G. *J. Chromatogr. A* 1998, 824, 91-97.
- [146] Cai, H., Nguyen, T. V., Vigh, G. *Anal. Chem.* 1998, 70, 580-589.
- [147] Rousseau, D. L. *Optical Techniques in Biological Research*, Academic Press Inc., Orlando, FL 1984, pp. 66-69, 72-75.
- [148] Schrader, B. *Infrared and Raman Spectroscopy*, VCH Publishers Inc., New York, 1995, pp. 135-138, 489-495.
- [149] Gale, R. J., *Spectroelectrochemistry Theory and Practice*, Plenum Press, New York, 1988, pp. 263-266, 272-273, 301, 307-312, 321-327.
- [150] Frushour, B. G., Koenig, J. U. *Advances in Infrared and Raman Spectroscopy*, R. J. H. Clark and R. E. Hester Eds., London, 1975, pp. 35-97.
- [151] Sugeta, H., Go, A., Miyazawa, T. *Chem. Lett.* 1972,1, 83-86.
- [152] Erfurth, S. C., Kiser, E. J., Peticolas, W. L. *Proc. Natl. Acad. Sci.* 1972, 69, 938-941.

- [153] Oseroff, A. R., Callender, R. H., *Biochemistry* 1974, 13, 4243-4248.
- [154] Spiro, T. G. *Biochim. Biophys. Acta* 1975, 416, 169-189.
- [155] Spaulding, L. D., Chang, C. C., Yu, N. T., Felton, R. H. *J. Am. Chem. Soc.* 1975, 97, 2517-2525.
- [156] Lutz, M., Brenton, J. *Biochem. Biophys. Res. Comm.* 1973, 53, 413-418.
- [157] Fleischmann, M., Hendra, P. J., McQuillan, A. J. *Chem Phys. Lett.* 1974, 26, 163-166.
- [158] Jeanmaire, D. L., Van Duyne, R. P. *J. Electroanal. Chem.* 1977, 84, 1-20.
- [159] Albrecht, M. G., Creighton, J. A. *J. Am. Chem. Soc.* 1977, 99, 5215-5217.
- [160] Garcia-Vidal, F. J., Pendry, J. B., *Phys. Rev. Lett.* 1996, 77, 1163-1166.
- [161] Sergeev, B. M., Sergeev, G. B., Kasaikin, V. A., Litmanovich, E. A., Prusov, A. N., *Molecular Crystals and Liquid Crystals*, 2001, 356, 121-129.
- [162] Stockle, R. M., Deckert, V., Fokas, C., Zenobi, R. *Appl. Spectrosc.* 2000, 54, 1577-1583.
- [163] Kok, S. J., Velthorst, N. H., Gooijer, C., Brinkman, U. A. T. *Electrophoresis*, 1998, 19, 2753-2776.
- [164] Vo-Dinh, T., Stokes, D. L., Griffin, G. D., Volkan, M., Kim, U. J., Simon, M. I. *J. Raman Spectrosc.* 1999, 30, 785-793.
- [165] Walker, P. A., Morris, M. D., Burns, M. A., Johnson, B. N. *Anal. Chem.* 1998, 70, 3766-3769.
- [166] Kowalchuk, W. K., Walker, P. A., Morris, M. D. *Appl. Spectrosc.* 1995, 49, 1183-1188.
- [167] Ruddick, A., Batchelder, D. N., Bartle, K. D., Gilby, A. C., Pitt, G. D. *Appl. Spectrosc.* 2000, 54, 1857-1863.
- [168] Li, Z., Wang, Y. J., Liu, G. Q., Chen, Y. *Chinese Chemical Letters*, 2001, 12, 265-266.
- [169] Nirode, W. F., DeVault, G. L., Sepaniak, M. J. *Anal. Chem.* 2000, 72, 1866-1871.

[170] He, L., Natan, M. J., Keating, C. D. *Anal. Chem.* 2000, 72, 5348-5355.

[171] Weimer, W. A., Dyer, M. J. *Appl. Phys. Lett.* 2001, 79, 3164-3166.

135

Vita

Jim Schaeper was born in Cincinnati, Ohio and graduated from Xavier University with a bachelor's degree in chemistry in 1993. Next, he worked at Procter & Gamble in the hair and skin care department with separating components of skin care formulations by HPLC. In 1996, he obtained a Master's degree in chemistry from Miami University in Oxford, Ohio. The research involved the separation of phosphorylated sugars and phospholipids by capillary electrophoresis with indirect photometric detection. He started doctoral work in chemistry at the University of Tennessee in 1997 and worked under the guidance of Dr. Sepaniak. After graduation, he is headed to Furman University for a postdoctoral position that involves research and teaching. The research involves the interaction of DNA with chiral inorganic complexes and has potential for the production of cancer drugs.